NASA CR-134554

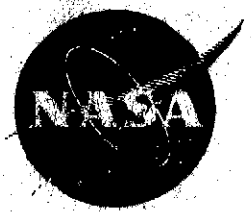

Volume II Final Report Appendixes

Vacuum Jacketed Composite Propulsion Feedlines for Cryogenic Launch and Space Vehicles

by

D. E. Spond, D. J. Laintz, C. A. Hall and D. E. Dulaigh

MARTIN MARIETTA CORPORATION

Prepared for

NATIONAL AERONAUTICS AND SPACE ADMINISTRATION

NASA Lewis Research Center

Contract NAS3-16762

Joseph Notardonato, Project Manager

1. Report No.	2. Government Accession No.	3. Recipient's Catalog No.
NASA CR-134554		

4. Title and Subtitle	5. Report Date
Vacuum Jacketed Composite Propulsion Feedlines for Cryogenic Launch and Space Vehicles	March 1974
	6. Performing Organization Code: 04236

7. Author(s)	8. Performing Organization Report No.
D. E. Spond, D. J. Laintz, C. A. Hall, D. E. Dulaigh	
	10. Work Unit No.

9. Performing Organization Name and Address	11. Contract or Grant No.
Martin Marietta Corporation P. O. Box 179 Denver, Colorado 80201	NAS3-16762
	13. Type of Report and Period Covered: Final Report, June 1972 to August 1973

12. Sponsoring Agency Name and Address	14. Sponsoring Agency Code
National Aeronautics and Space Administration Lewis Research Center Cleveland, Ohio 44135	

15. Supplementary Notes

16. Abstract

Thin metallic liners that provide leak-free service in cryogenic propulsion systems are overwrapped with a glass-fiber composite that provides strength and protection from handling damage. The resultant tube is lightweight, strong, and has a low thermal flux. The inside commodity flow line and the outside vacuum jacket were fabricated using this method. Several types of vacuum jackets were fabricated and tested at operating temperatures from 294 to 21 K (+70 to -423°F) and operating pressures up to 69 N/cm^2 (100 psi). The primary objective of the program was to develop vacuum jacket concepts, using previously developed concepts for the inner line. All major program objectives were met resulting in a design concept that is adaptable to a wide range of aerospace vehicle requirements. Major items of development included convolution of thin metallic sections up to 46 cm (18 in.) in diameter, design and fabrication of an extremely lightweight tension membrane concept for the vacuum jacket, and analytical tools that predict the failure mode and levels. An attempt to bond the vacuum jacket liner to the composite overwrap was unsuccessful resulting in the premature failure of several lines. A redesign, which is not dependent upon bonding, was successful. Weight savings of over 50% are attainable for vacuum jacketed composite feedlines when compared to conventional configurations and materials of construction.

17. Key Words (Suggested by Author(s))	18. Distribution Statement
Composite Cryogenic Feedline Overwrap Vacuum Jacketed Lines	Unclassified - Unlimited

19. Security Classif. (of this report)	20. Security Classif. (of this page)
Unclassified	Unclassified

FOREWORD

The work described herein was conducted by Martin Marietta Corporation, Denver Division, under NASA Contract NAS3-16762, under the management of the NASA Project Manager, Mr. Joseph Notardonato, Propulsion Systems Branch, NASA-Lewis Research Center, Cleveland, Ohio.

This final report is published in two volumes: Volume I describes the results of the program and Volume II contains related appendixes.

In addition to the stated authors, the following persons provided major assistance: Messrs. Clifford S. Foster, John R. Lager, Gary E. Wilson, Stanley R. Tomer, Walter L. McKenna, William E. Mohr, Timothy P. Quinn, Connie E. Lynch, and Donald A. Stang. Major contributors at the Grumman Aerospace Corporation included Messrs. Michael J. Martin, Benjamin Aleck, and Carlos Cacho-Negrete.

TABLE OF CONTENTS

Vol II

SYMBOLS

A	Area, cm^2 ($in.^2$)
A_L	Cross-sectional liner area, cm^2 ($in.^2$)
A_o	Cross-sectional overwrap area, cm^2 ($in.^2$)
a	Membrane width, cm (in.)
b	Membrane length, cm (in.)
b	Base, cm (in.)
C	Circumference, cm (in.)
C_p	Specific heat, cal/g/°K (Btu/lb/°F)
D	Diameter, cm (in.)
d	Resonant frequency, Hz
dB	Decibel
ε	Emittance
E_c	Composite modulus of elasticity (metal liner plus overwrap), N/cm^2 (psi)
E_L	Modulus of elasticity (liner), N/cm^2 (psi)
E_o	Modulus of elasticity (overwrap), N/cm^2 (psi)
E_θ	Circumferential modulus of elasticity, N/cm^2 (psi)
E_ϕ	Meridional modulus of elasticity, N/cm^2 (psi)
e	Strain, cm/cm (in./in.)
e_L	Strain in liner, cm/cm (in./in.)
e_o	Strain in overwrap, cm/cm (in./in.)
e_x	Strain in x direction (along tube centerline), cm/cm (in./in.)
e_h	Strain in hoop direction, cm/cm (in./in.)
F	Force, N (lb)
F_L	Force in liner, N (lb)

F_o	Force in overwrap, N (lb)
F_S	Factor of safety
f_{mn}	Frequency for mode shape, Hz
G	Acceleration (number of g's)
g	Acceleration of gravity, cm/sec^2 ($in./sec^2$)
g_o	Acceleration spectral density, g^2/Hz
Hz	Frequency in Hertz
h	Height, cm (in.)
I	Moment of inertia, cm^4 ($in.^4$)
i	Current, amperes
L	Length, cm (in.)
γ	Hottel gray body factor
M	Molecular weight, moles
m	Bending moment, cm-N (in.-lb)
mn	Mode shape
n	Number of cycles
P	Pressure, N/cm^2 (psi)
P_N	Load per unit length, N/cm (lb/in.)
P_L	Load in liner, N/cm (lb/in.)
P_o	Load in overwrap N/cm (lb/in.)
P_u	Uniform load intensity
ΔP	Pressure drop N/cm^2 (psi or microns)
Q	Flow rate
Q_F	Magnification factor
q	Radiation heat transfer, W/m (Btu/hr-ft)
R	Ring radius, cm (in.)

R	Ideal gas constant, J $°K^{-1}$ mol^{-1} (lb-mole °F)
R	Resistances, ohms
r_1	Radius of curvature, cm (in.)
r	Radius, cm (in.)
s	Time, seconds
S	Stress, N/cm^2 ($lb/in.^2$)
S_h	Stress in hoop direction, N/cm^2 ($lb/in.^2$)
S_L	Stress in liner, N/cm^2 ($lb/in.^2$)
S_o	Stress in overwrap, N/cm^2 ($lb/in.^2$)
S_x	Stress in x direction, N/cm^2 ($lb/in.^2$)
S_y	Yield stress, N/cm^2 ($lb/in.^2$)
S_z	Stress in z direction, N/cm^2 ($lb/in.^2$)
S_ϕ	Meridional stress, N/cm^2 ($lb/in.^2$)
T	Temperature, °K (°F)
T	Torque, cm-N (in.-lb)
t	Thickness, cm (in.)
ΔT_L	Change in liner temperature, °K (°R)
ΔT_o	Change in overwrap temperature, °K (°R)
V	Volume, liters ($in.^3$)
W	Weight, kg (lb)
w	Weight/unit area, kg/cm^2 ($lb/in.^2$)
X	Deflection ratio
Y	Distance from neutral axis to extreme fiber, cm (in.)
Z	Stefan-Boltzmann constant, W/m^2-K^4 ($Btu/ft^2-hr\ °R^4$)
Z_L	Uniform tension per unit length, N/cm (lb/in.)
σ	Sigma (statistical)

δ	Damping ratio
ϕ	Fluctuating pressure spectral density, $\frac{(N/cm^2)^2}{Hz}$ $\left(\frac{psi^2}{Hz}\right)$
μ	Microns of Hg
Δ	Deflection, cm (in.)
α	Coefficient of thermal expansion, cm/cm/°K (in./in./°F)
α_L	Liner coefficient of thermal expansion in axial direction, cm/cm/°K (in./in./°F)
α_o	Overwrap coefficient of thermal expansion in axial direction, cm/cm/°K (in./in./°F)
ν	Poisson's ratio
ρ	Density, kg/cm^3 $(lb/in.^3)$

Subscripts

AT	Axial tension
B	Bending
BL	Bending in liner
c	Composite
c	Curved section
DTC	Differential thermal contraction
IP	Internal pressure
i	Outside surface of inner line
L	Liner
o	Overwrap, or the inside surface of the vacuum jacket
rms	Random
st	Shear stress due to torsion
s	Straight section
T	Total
TC	Tensile stress in inner line liner
x	Longitudinal Direction

DEFINITION OF TERMS

A listing of commonly used terms and their definitions follows. Familiarity with these terms should help the reader to understand the technical aspects of this document.

Inner Line	Line carrying the commodity.
Vacuum Jacket	Outer line.
Composite Vacuum Jacket	A vacuum jacket concept that incorporates a thin metallic liner and composite material to provide strength and handling damage resistance. A typical composite vacuum jacket is shown in the sketch.

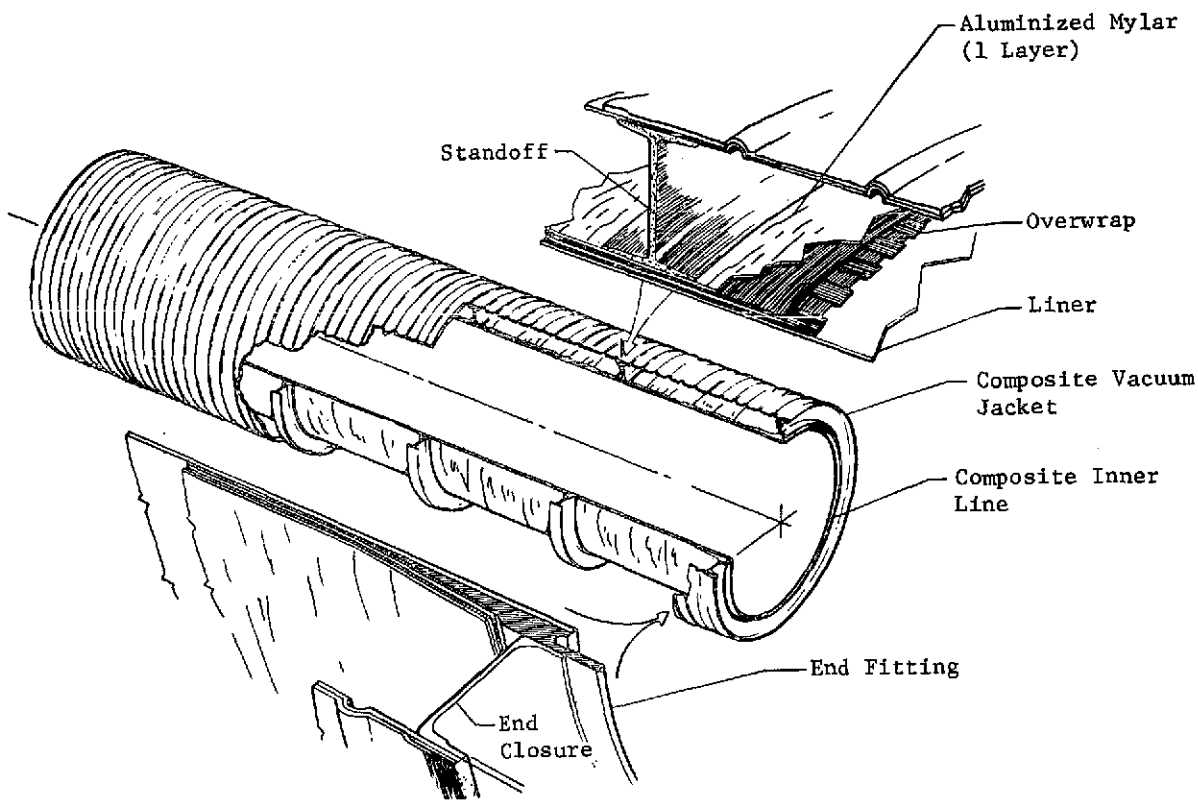

Tension Membrane Vacuum Jacket	A vacuum jacket concept that relies on tension in the metallic structure for load carrying. This concept has the appearance of a suspension bridge and, because the structure is in tension it can be loaded heavily without loss of reliability. It is a very lightweight concept. A tension membrane vacuum jacket is shown in the sketch.

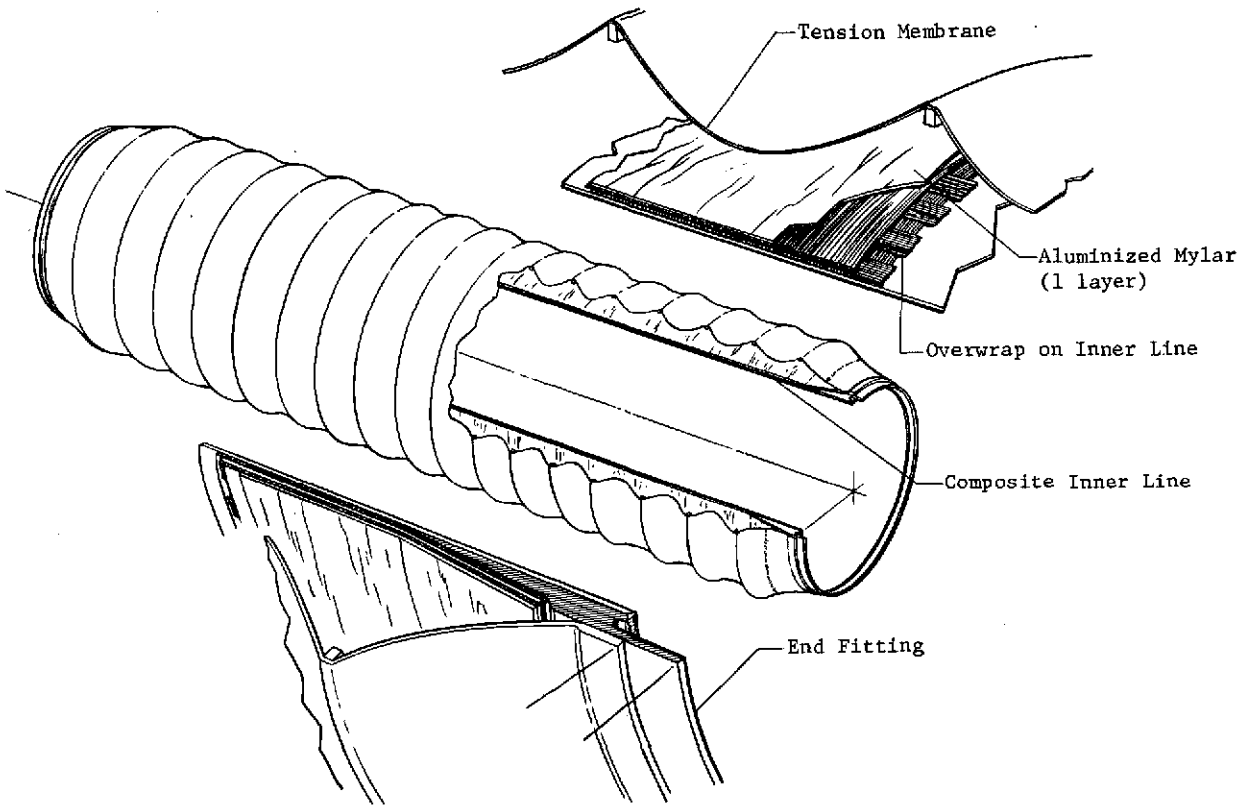

Overwrap	Total fiberglass composite thickness 0.05 cm (0.020 in.) consisting of 2 layers of hoop wrap and a ½ layer of axial cloth or 2 layers of hoop wrap applied in a criss-cross pattern.
Liner	Thin wall metal tube under the overwrap.

Standoff	Support between the vacuum jacket and the inner line.
End Closure	Metal membrane that seals the vacuum annulus between the inner line and the vacuum jacket.
Stiff End Closure	End closure capable of transferring all the loading due to thermal contraction of the inner line to the vacuum jacket and the load caused by external pressure to the inner line.
Flexible End Closure	End closure incapable of transferring the loading caused by thermal contraction of the inner line to the vacuum jacket; divides the load caused by external pressure between the inner line and the vacuum jacket.
End Fitting	Metal ring welded to the ends of the liner providing a surface for welding the end closure and a butt weld end for attaching one tube to another.
Solid State Bonding	Explosive bonding technique used to join two dissimilar metals such as aluminum to Inconel or stainless steel.

SUMMARY

This is the final report of a 14-month program that was conducted under Contract NAS3-16762. The objective of the program was to develop lightweight vacuum jacketed composite tubing for use as cryogenic plumbing on launch and space vehicles. Twelve tubes of two different inside diameters [13 and 38 cm (5 and 15 in.)] were fabricated in 3 different types of each size. Each tube was 61 cm (24 in.) long. The tubes were joined together in sets of two for testing.

The tubing in this program was intended to be representative of flight configuration for cryogenic feedlines for LH_2 service where vacuum jackets are mandatory. The sizes are representative of the Shuttle main propulsion and the Space Tug feedlines.

An analysis program assessed thermal, structural, weight, and fabrication parameters, and formed the basis for the tubing design. Ultimately, thin metallic liners 0.008 to 0.013 cm (0.003 to 0.005 in.) thick were selected as the primary load-carrying member. Ten of these liners were overwrapped with glass-fibers impregnated with a resin matrix suitable for cryogenic service for the inner line. A resin matrix suitable for ambient and slightly elevated temperatures was used for the outer jacket. The overwrapped composite was used to strengthen the liners and protect them from handling damage. Two of the tubes were of the tension membrane type consisting of a composite overwrapped inner line and a nonoverwrapped vacuum jacket. Concurrent with the analysis effort, preliminary tests were performed to aid in selecting materials and methods of construction.

The 12 tubes required for test were designed, fabricated, and verified ready for test. Tube fabrication included liner welding, joining of the liners to end fittings, instrumentation installation, overwrapping and curing, and a series of in-process leak checks and other quality determinations. After these individual subassembly steps were completed, the inner line and the vacuum jacket were joined by welding. Vacuum outgassing and vacuum acquisition completed the fabrication.

The tubes were subjected to a series of tests including leakage, pressure cycling, temperature cycling, pressure surge, acoustics, and burst. One of the tubes failed during the first vacuum acquisition test. It was subsequently determined that the bond between the jacket liner and overwrap failed because of atmospheric pressure acting between the overwrap and the liner.

A temporary fix, installed to permit testing to continue, proved capable of protecting the tubes and transferring the loading to the overwrap from the liner, but it was rather complex and had a low reliability. During subsequent testing several other lines became separated from the overwrap and immediately failed.

A single tube of a modified vacuum jacket design using a metal liner 0.030 cm (0.012 in.) thick was fabricated. This liner was capable of carrying external pressure but was still susceptible to handling damage. The vacuum jacket was overwrapped, in the same manner as the other test specimens, to provide protection from damage during handling. This tube passed all tests, was damage-resistant and of lighter weight than conventional all-metal vacuum jacketed lines.

The tension membrane concept, designed and fabricated by Grumman Aerospace Corporation, passed all tests and becomes a very strong candidate for vacuum jacketed feedlines. Its two main advantages are the very lightweight construction and the metal is in the predictable tensile stress mode instead of being subjected to the less predictable compressive buckling mode. The tension membrane concept was tested and evaluated by Martin Marietta Corporation concurrently with the composite vacuum jacket concepts. Complete design and fabrication details of the tension membrane concept are included in Appendix E, *Vacuum Jacketed Composite Lines, Final Report*, by the Grumman Aerospace Corporation.

The results of this and earlier programs clearly verify the advantages of using glass-fiber composite tubing in cryogenic propellant service for vacuum jacketed feedlines. Some of the advantages include low thermal flux, lightweight construction, low-heat-soakback from engines, rapid chilldown, resistance to damage, and high strength. This can be accomplished with a moderate increase in cost--in many cases for less than $60 per kg ($25 per lb) of weight reduced.

Additional work is needed to more fully develop the bonding concept, and eliminate the leakage and outgassing problems in some designs. The leakage and outgassing problems can be solved through process control since several tubes have exhibited successful properties in both areas of concern. The bonding development will only be required if optimum weight savings are to be realized.

APPENDIX A

STRUCTURAL ANALYSES

INTRODUCTION

A series of structural analyses was performed to provide an analytical basis for making a design decision for such questions as:

- Should the vacuum jacket inner line liners be heat treated or annealed?

- Is minimum gage adequate to withstand predicted tensile and torsional loading?

- Is it necessary to bond the glass fiber overwrap to the inner line liners?

These analyses are presented in the following paragraphs.

REQUIREMENTS FOR HEAT TREATING THE INNER LINE LINERS

Assuming that the inner liner material is 0.008 cm (0.003 in.) thick Inconel 718 for the 13 cm (5 in.) diameter inner line, with a safety factor of 2.5, and an operating pressure of 41 N/cm^2 (60 psia), the axial and hoop stresses are given by

$$S_{IP\ (axial)} = \frac{2.5\ Pr}{2t} = \frac{2.5 \times 41 \times 6.35}{2 \times 0.008} = 40{,}679\ N/cm^2\ (59{,}000\ psi)$$

$$S_{IP\ (hoop)} = \frac{2.5\ Pr}{t} = \frac{2.5 \times 41 \times 6.35}{0.008} = 81{,}359\ N/cm^2\ (118{,}000\ psi)$$

where

S_{IP} = stress (N/cm^2);

P = operating pressure (N/cm^2);

r = line radius (cm);

t = liner thickness (cm).

To provide an adequate safety factor in hoop loading caused by internal pressure, heat treating the Inconel 718 inner liners is required. In addition, analysis performed on the NAS3-14370 contract showed that if the nonheat treated inner liner is chilled to liquid hydrogen temperatures rapidly (in two seconds or less), the liner will buckle plastically because of restraint by the glass-fiber overwrap, which does not cool at the same rate. Thus, it was concluded that the inner line liners should be heat treated to a yield strength of 106,000 N/cm^2 (153,000 psi).

INNER LINE COMBINED STRESS ANALYSIS

The total axial stress in the inner line liner will be a function of: (1) internal pressure, (2) tension resulting from cryogenic cooling with the thermal shrinkage limited and constrained by the jacket, (3) loads caused by differential thermal contraction between the liner and overwrap, and (4) bending loads. A summation of these stresses is given by

$$S_{AT} = S_{IP} + S_{TC} + S_{DTC} + S_{BL}$$

where

S_{AT} = stress in the liner in the axial direction, tensile only, N/cm^2 (psi);

S_{IP} = stress in the liner in the axial direction because of internal pressure, N/cm^2 (psi);

S_{TC} = stress in the liner in the axial direction because of restraint from the jacket during a cryogenic cooldown or operation, N/cm^2 (psi)

S_{DTC} = stress in the liner in the axial driection because of differential thermal contraction between the overwrap and the liner. N/cm^2 (psi)

S_{BL} = stress in the liner in the axial direction because of bending, tensile only N/cm^2 (psi)

Solution of the equation is performed by knowing S_{AT} allowable, S_{IP} from standard equations, S_{TC} and S_{DTC} from limiting equations and permitting S_{BL} to be the remaining allowable. This solution is actually to calculate allowable bending loads given all other conditions. The feedline installation in a vehicle propulsion system can then be designed to limit bending loads to allowable levels. Development of equations for each component part of the total combined tensile stress follows:

1. Internal pressure: stress caused by internal pressure is expressed as

$$S_{IP} = \frac{Pr}{2t}$$

While empirical data indicates the overwrap will carry a portion of the axial load, especially if it is bonded to the liner, this effect is ignored. As an approximation of the conservatism resulting from this assumption, load sharing can be calculated, given

Equal strains $e_L = e_o$

where

e_L = liner strain

e_o = overwrap strain

and

$$E_L = \frac{S_L}{e_L} = \text{and } E_o = \frac{S_o}{e_o}$$

and stress in the materials is

$$S_L = \frac{P_L}{A_L} \text{ and } S_o = \frac{P_o}{A_o}$$

where

P_L and P_o are the loads carried by the respective members and,

$A_L = 2\pi\ r_L\ t_L$; $A_o = 2\pi\ r_o t_o$

with $r_L = r_o$ for simplification.

Finally, substituting

$$\frac{P_L}{E_L\ t_L} = \frac{P_o}{E_o t_o}$$

and clearing,

$$P_o = \frac{P_L E_o t_o}{E_L t_L}$$

For the inner line design used in this program, when r = 2.5 to 13 cm (1 to 5 in.)

$$P_o = \frac{P_L\ (1.103 \times 10^6)(0.0508)}{(21 \times 10^6)(0.008)}$$

$$P_o = 0.33\ P_L$$

and for r = 13 cm (5 in.) to 25.4 cm (10 in.)

$$P_o = \frac{P_L\ (1.103 \times 10^6)(0.0508)}{(21 \times 10^6)(0.013)}$$

$$P_o = 0.21\ P_L$$

These loads will be checked for overwrap allowables after calculating the liner stresses.

The overwrap configuration is assumed to be as shown in Figure A1, consisting of H, 1/2L, H in the abbreviated form.

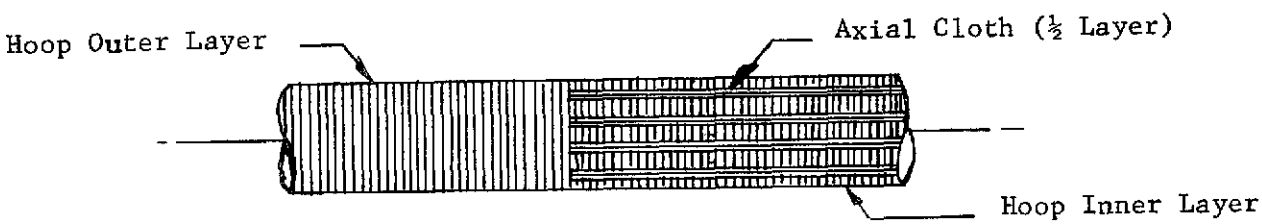

Figure A1. - Overwrap Pattern

Neglecting the resin, the axial strength in the overwrap is the tensile strength of the cloth. The cross-sectional area of the cloth will be

$$A_o = \frac{2\pi rt}{2} = \pi rt;$$

and the load at failure will be

$$P_L = S_L A_o$$

where S_L is the ultimate tensile stress that was empirically determined to be 51,700 N/cm^2 (75,000 psi). Substituting the equation for allowable axial load at failure in the glass-fiber overwrap, P_o for the 13 cm (5 in.) diameter lines is calculated as follows:

$$P_o = (51{,}700)\pi rt$$

$$P_o = (51{,}700)\pi r(0.02)$$

The pressure in the 13 cm (5 in.) diameter tubes at failure will be a function of load sharing, where

$$P_o = \frac{0.33\ PrA}{2\ t}$$

$$P = \left[(51{,}700)\pi r(0.02) \quad \frac{2t}{0.33(r)\ 2\pi rt} \right]$$

$$P = \frac{51{,}700\ (0.02)}{0.33r(6.35)}$$

$$P = 493\ N/cm^2\ (716\ psi)$$

The pressure in the 38 cm (15 in.) diameter tubes at failure will be

$$P = \frac{51{,}700\ (0.02)}{0.21(19)}$$

$$P = 259\ N/cm^2\ (376\ psi).$$

Using the above analyses and applying a 2.5 safety factor, the resultant pressure allowables are as follows

Tube Size	P
26 cm (10 in.) diameter	251 N/cm^2 (364 psi)
51 cm (20 in.) diameter	197 N/cm^2 (285 psi)

When the bending loads are calculated, they should be checked to determine if the axial overwrap is critical.

2. Thermal contraction restraint: When the inner line is cooled to LH_2 temperature while the jacket is at ambient temperature, the interaction between the two results in axial tensile loads in the inner liner. Lower limits on this stress are set where a flexible end closure exists (or a very flexible convolute is added to the jacket), in which no restraint exists and therefore $S_{TC} \rightarrow 0$. Upper limits on this stress are set with a very rigid end closure in which the vacuum jacket is infinitely rigid when compared to the inner line and

   $S_{TC} = E_L e_L$,

   where $e_L = \alpha_L \Delta T$,

   resulting in $S_{TC} = E_L \alpha_L \Delta T_L$.

   For the above application with E_L = 21,400,000 N/cm^2 (31,000,000 psi), $\alpha = 8.7 \times 10^{-6}$ cm/cm/°K ($4.82 \times {}^{-6}$ in/in/°F) average, and ΔT = 273°K (493°F), the resultant tensile stress will be

   $S_{TC} = 21{,}400{,}000\ (8.7 \times 10^{-6})\ (273)$

   $S_{TC} = 50{,}800\ N/cm^2\ (73{,}700\ psi)$.

The limits then are

$$o \leq S_{TC} \leq 50{,}800 \text{ N/cm}^2 \text{ (73,700 psi)},$$

and the actual stress will be a relationship between the relative stiffness of the inner and outer line, as transferred through the end closure. The solution then becomes one of evaluating the loads carried by each of the two component parts (the jacket and the inner line).

Reviewing deflections for a convoluted line (jacket) and a nonconvoluted line (inner line), each under a (unit) load

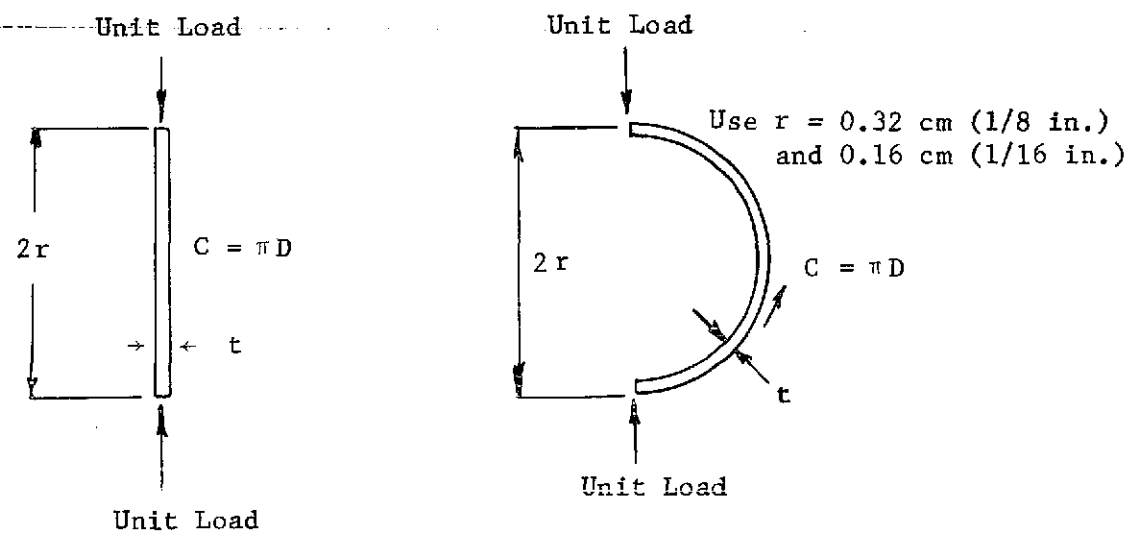

$$E = \frac{P_L L}{A\Delta L}$$

$$\Delta L_c = \frac{\pi r^3}{2EI} \text{ with } I = \frac{bh^3}{12} = \frac{\pi D t^3}{12}$$

$$\Delta \quad \Delta L_s = \frac{P_L L}{AE} = \frac{2r}{\pi DAE}$$

$$\Delta L_c = \frac{\pi r^3 \, 12}{2E\pi Dt^3} = \frac{6r}{EDt}\left(\frac{r}{t}\right)^2$$

$$\Delta L_s = \frac{r}{ED}\left(\frac{2}{\pi}\right) \text{ and, comparing length changes}$$

$$\frac{\Delta L_c}{\Delta L_s} = \frac{\dfrac{\dfrac{6r_c^2}{t_c}}{E_c D_c t_c}}{\dfrac{2}{\pi E_s D_s t_s}} = \frac{\dfrac{3\pi r_c^2}{t_c} \quad E_s D_s t_s}{E_c D_c t_c}$$

where ΔL is deflection under load and subscript c represents the curved section and s the straight section. Calculations for representative radii (r_c) of 0.32 cm (1/8 in.) and 0.16 cm (1/16 in.) using the various proposed configurations of inner lines and jackets are shown in Table A1.

TABLE A1.- DEFLECTION RATIOS FOR INNER LINE AND OUTER LINE (JACKET) UNDER LOAD DUE TO INNER LINE THERMAL CONTRACTION

Inner Line Configuration	Jacket Configuration	Jacket Diameter, cm (in.)							
		13 (5)		25.4 (10)		25.4 (10)		50.8 (20)	
		Convolute Radius, cm (in.)							
		0.32 (0.13)	0.16 (0.06)	0.32 (0.13)	0.16 (0.06)	0.32 (0.13)	0.16 (0.06)	0.32 (0.13)	0.16 (0.06)
0.008 cm (0.003 in.) Inconel	0.008 cm (0.003 in.) Inconel	6527	1632	12533	3138				
0.008 cm (0.003 in.) Inconel	0.008 cm (0.003 in.) Inconel - Bonded 0.050 cm (0.020 in.)	81	20	156	39				
0.008 cm (0.003 in.) Inconel - Bonded 0.050 cm (0.020 in.)	0.008 cm (0.003 in.) Inconel - Bonded 0.050 cm (0.020 in.)	111	28	214	54				
0.012 cm (0.005 in.) Inconel	0.012 cm (0.005 in.) Inconel					4519	1130	5109	1277
0.012 cm (0.005 in.) Inconel	0.012 cm (0.005 in.) Inconel - Bonded 0.050 cm (0.020 in.)					260	65	243	73
0.012 cm (0.005 in.) Inconel - Bonded 0.050 cm (0.020 in.)	0.012 cm (0.005 in.) Inconel - Bonded 0.050 cm (0.020 in.)					181	45	204	51
0.008 cm (0.003 in.) Inconel	0.015 cm (0.006 in.) Aluminum	2372	593	4562	1141				
0.008 cm (0.003 in.) Inconel	0.015 cm (0.006 in.) Aluminum Bonded 0.050 cm (0.020 in.)	83	21	160	40				
0.008 cm (0.003 in.) Inconel	0.015 cm (0.006 in.) Aluminum - Bonded 0.050 cm (0.020 in.)	115	29	220	45				
0.012 cm (0.005 in.) Inconel	0.015 cm (0.006 in.) Aluminum					5850	1462	6612	1650
0.012 cm (0.005 in.) Inconel	0.015 cm (0.006 in.) Aluminum - Bonded 0.050 cm (0.020 in.)					267	67	302	75
0.012 cm (0.005 in.) Inconel - Bonded 0.05 cm (0.020 in.)	0.015 cm (0.006 in.) Aluminum - Bonded 0.050 cm (0.020 in.)					327	82	370	92

Given a radius in the jacket convolute, and a configuration for both lines the residual tensile force in the inner line can be calculated:

$$S_{TC} = \frac{E_L \alpha_L \Delta T_L}{(X)}$$

where X is the deflection ratio calculated above and presented in Table A1.

3) Differential thermal contraction: In the usual case where the overwrap coefficient of thermal contraction is less than that of the metal and the overwrap temperature is warmer, a differential tensile stress is added to the liner.

The liner stresses can be calculated as follows:

$$S_{DTC} = \frac{\Delta T_o \alpha_o - \Delta T_L \alpha_L}{\frac{A_L}{E_o A_o} + \frac{1}{E_L}}$$

where

S_{DTC} = axial liner stress caused by thermal expansion (positive indicates tension; negative indicates compression), N/cm^2

ΔT_o = change in overwrap temperature, ^oK (negative if temperature is lowered; positive if temperature rises)

ΔT_L = change in liner temperature, ^oK

α_o = overwrap coefficient of thermal expansion, in axial direction, $cm/cm/^oK$

α_L = liner coefficient of thermal expansion, in axial direction, $cm/cm/^oK$

A_L = cross-sectional liner area, cm^2

A_o = cross-sectional overwrap area, cm^2

E_o = overwrap modulus of elasticity, cm^2

E_L = liner modulus of elasticity, cm^2

This stress will be very low in this design for two reasons: (1) with a layer of multilayer insulation on the outside of the inner line the differential temperature will be very low; (2) with the chosen wrap orientation, the coefficients of thermal expansion are

$$\alpha_{L_{AVE}} = 0.00000868 \text{ cm/cm/}^{o}\text{K } (0.00000482 \text{ in./in./}^{o}\text{F})$$

$$\alpha_{O_{AVE}} = 0.00000936 \text{ cm/cm/}^{o}\text{K } (0.00000520 \text{ in./in./}^{o}\text{F})$$

which actually results in a slight compressive stress in the liner. A null load or stress would result when

$$\alpha_L \Delta T_L = \alpha_o \Delta T_o$$

which will occur when the overwrap is 20°K (36°R) warmer than the liner. While the α for Inconel is fairly well known, the α for the overwrap is very much a function of resin content and wrap configuration and may vary considerably. The differential temperature will be a function of chilldown time.

As very low stress levels are expected from the differential thermal contraction, they will be ignored.

Actual test data indicates a 25°K (45°R) temperature difference at stable liquid hydrogen temperature and therefore a stress of 3555 N/cm^2 (5160 psi). This is still small compared to a yield stress of 106,000 N/cm^2 (153,000 psi) for the liner.

4) Bending stress: The stresses caused by internal pressure and thermal contraction can then be added algebraically (ignoring compressive values) to determine resulting axial stresses in the liner at operating conditions. This resultant axial stress can then be subtracted from the maximum allowable axial stress determined from the WEATOPT program to determine the amount of bending stresses that can be tolerated in the liner. The maximum allowable bending moment or side load for a given feedline length can then be determined.

$$\text{Since } S_{BL} = S_{AT} - (S_{IP} + S_{TC} + S_{DTC})$$

$$\text{and } S_{BL} = E_L e_L \text{ and } S_{BO} = E_o e_o$$

where

S_{BL} = bending stress in liner,

e_L = strain in liner because of bending,

e_o = strain in overwrap because of bending,

S_{BO} = bending stress in the overwrap.

Since the overwrap and liner must deflect together,

$$e_L = e_o = e_c$$

where e_c = strain in the composite feedline and the bending stress in the composite feedling is

$$S_B = \frac{my}{I} = E_c e_c$$

where

m = bending moment,

y = distance from neutral axis to extreme fiber,

I = cross-section moment of inertia,

E_c = composite modulus of elasticity.

E_c can be calculated as follows

$$E_c = \frac{t_o}{t_o + t_L}(E_o) + \frac{t_L}{t_o + t_L}(E_L)$$

where

t_o = thickness of overwrap,

t_L = thickness of liner.

Knowing the allowable bending stress in the liner (S_{BL}), the strain (e_c) can be calculated, then the composite bending stress (S_B) can be calculated from $S_B = E_c e_c$. The bending moment (m) can be calculated as

$m = \frac{S_B I}{Sy}$ and for a given feedline section length (L) the allowable side load force (F) can be determined as $F = \frac{m}{L}$.

This analysis will determine the bending loads that the feedline can withstand without exceeding the liner stresses allowable in the axial direction, i.e.,

$$S_{AT} = S_{IP} + S_{TC} + S_{DTC} + S_{BL}$$

As a check of the overwrap's ability to withstand this additional tensile force, the two components of the bending stress can be separated, knowing total (S_B) and the liner allowable (S_{BL}) so that

$$S_o = S_B - S_{BL}$$

This stress should be added to the tensile stress caused by internal pressure.

INNER LINE TORSION ANALYSIS

The maximum allowable torque that can be applied to the inner line can be determined by

$$T = 2\pi r^2 t S_{st}$$

where

T = allowable torque,

r = liner radius or overwrap radius,

t = liner thickness or overwrap thickness,

S_{st} = shear stress caused by torsion,

and S_{st} will be calculated based on the $\frac{L}{r}$ values for the feedline section being considered using formulas from Roark* (page 353, case 28) where L is length of the tube. For almost all applications of interest,

$$S_{st} = E\left(\frac{t}{L}\right)^2 \left[3.0 + \sqrt{3.4 + 0.240\left(\frac{L}{\sqrt{tr}}\right)^3}\right]$$

where

E = Young's modulus,

L = length.

This analysis can be performed using only the liner characteristics, or if the liner and overwrap are bonded together, composite properties will be required with the changes being to E and t.

$t_c = t_L + t_o$ and

*Roark, R. J.: *Formulas for Stress and Strain.* 4th Edition, McGraw-Hill, 1954

$$E_c = \frac{E_L t_L + E_o t_o}{t_L + t_o}$$

where

E_c = composite modulus

E_L = liner Young's modulus

E_o = shear modulus of overwrap

Holston, Feldman and Stang* determined the shear modulus of an pseudo - orthotropic glass-fiber cylinder with 75% hoop wrap (which is close to the 80% hoop wrap used in this program) to be 1.03×10^6 N/cm^2 (1.5×10^6 psi).

This analysis will prove conservative because the resistance of the vacuum jacket is ignored. In fact, when a jacket is used, with a stiff end closure to the inner line, the above calculations can be applied to the jacket instead of the inner line.

VACUUM JACKET AXIAL LOAD CAPABILITY

The capability of vacuum jacket design concepts #1, #3, and #4 to withstand combined external pressure and axial compression loading is shown in Figure A2. The 20 cm (8 in.) diameter and 46 cm (18 in.) diameter jackets will each withstand 25 N/cm^2 (36.8 psi) collapse pressure if they are not subjected to axial compression loading. However, if the external pressure is only 10 N/cm^2 (14.7 psi), the 20 cm (8 in.) and 46 cm (18 in.) jackets will withstand 1450 kg (3200 lb) and 2840 kg (6260 lb) axial compressive load, respectively. The amount of axial compressive force that the jacket must resist depends upon the jacket structural concept and the end closure design.

Thermal contraction of the inner line could load the vacuum jacket in axial compression if the end closure and vacuum jacket are rigid. The load level can be approximated by assuming that the metal in the inner line and vacuum jacket contributes most to axial stiffness and coefficient of thermal expansion. Using this assumption, axial compressive loads of 1012 kg (2230 lb) and 2869 kg (8530 lb) can be expected in the 20 cm (8 in.) and 46 cm (18 in.) vacuum jackets, respectively. It is obvious that it would be desirable to select a structural concept that allows

*Holston, Jr., A., Feldman, A. and Stang, D. A.: *Stability of Filament Wound Cylinders under Combined Loading.* AFFDL Report TR-67-55, 1967.

only minimal transfer of load to the vacuum jacket because of inner line thermal contraction. This can be done by either using a flexible end closure design or by including at least one low stiffness convolute in the vacuum jacket wall.

INNER LINE AXIAL COMPRESSION LOADING AND BONDING REQUIREMENTS

Pressure on the vacuum jacket end closure must be reacted by either inner line or the vacuum jacket and inner line together. If the vacuum jacket concept is flexible (contains at least one convolute) and the end closure is rigid, nearly all of the end pressure load will be transferred directly to the inner line. If the glass/epoxy overwrap on the inner line is not bonded directly to the liner, all of the end pressure compressive load would have to be reacted by the thin inner line liner. The axial load carrying capability of the unpressurized 13 cm (5 in.) diameter and 38 cm (15 in.) diameter inner line for various Inconel or 304L Stainless Steel liner thicknesses and various unsupported lengths are shown in Figures A3 and A4. These results indicate that the existing inner line thickness would not be adequate to resist all of the end pressure loading if not bonded. However, they are capable of withstanding half of the end pressure loading. The end pressure can be distributed between the inner line and vacuum jacket if the vacuum jacket concept is rigid (does not contain convolutes). This would result in approximately 644 and 2977 kg (1420 and 5460 lb) axial compression in each of the inner line and vacuum jacket for the 20 cm (8 in.) and 46 cm (18 in.) systems, respectively.

The above analysis is conservative in that empirical results by Kaufman-Johns, which show that overwrapping dramatically increases buckling allowables, are not considered. Another approach to improving axial load carrying capability from the overwrap is to knurl and overwrap the end fittings.

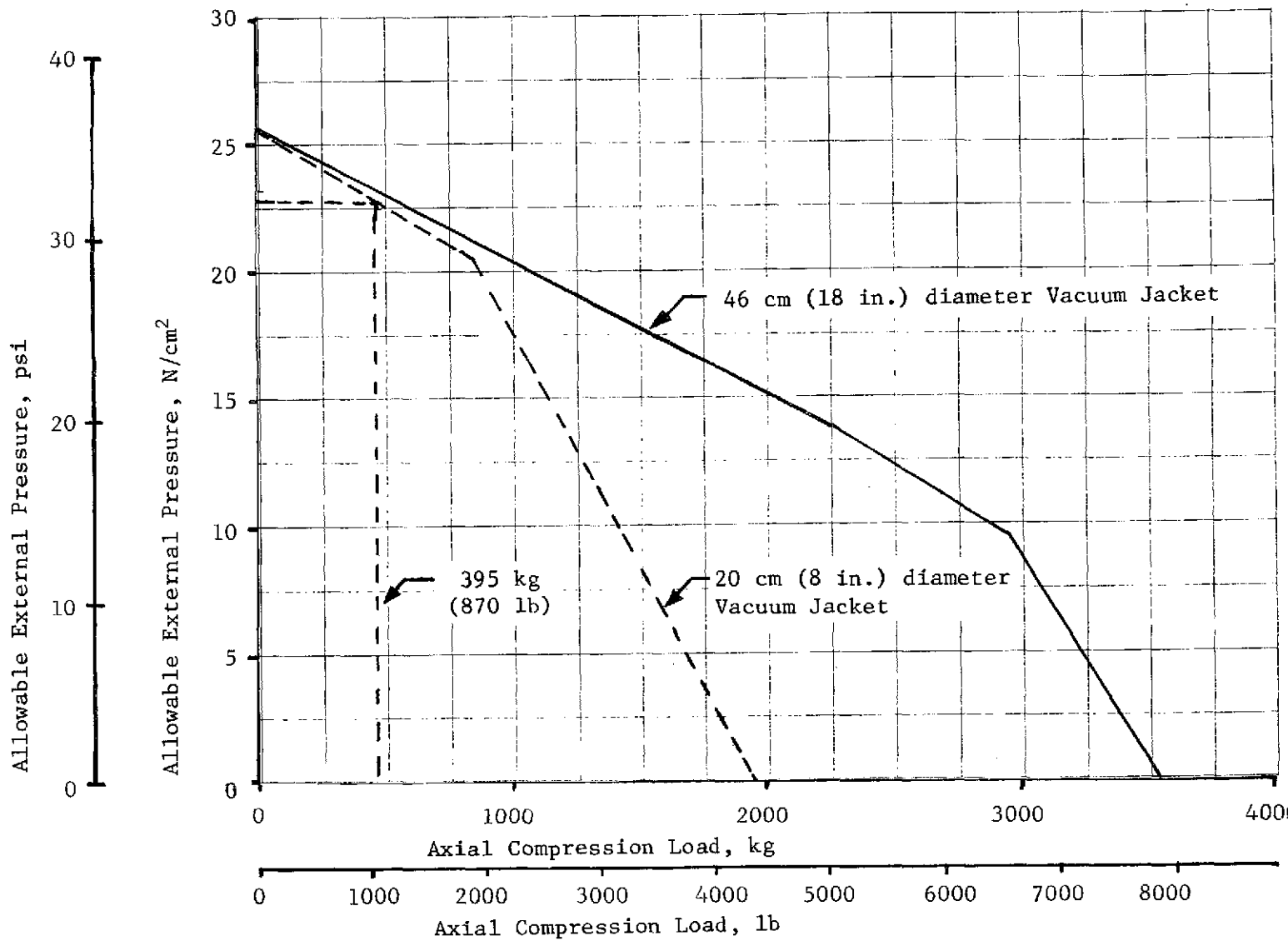

Figure A2. - Vacuum Jacket Axial Compression Loading Capability

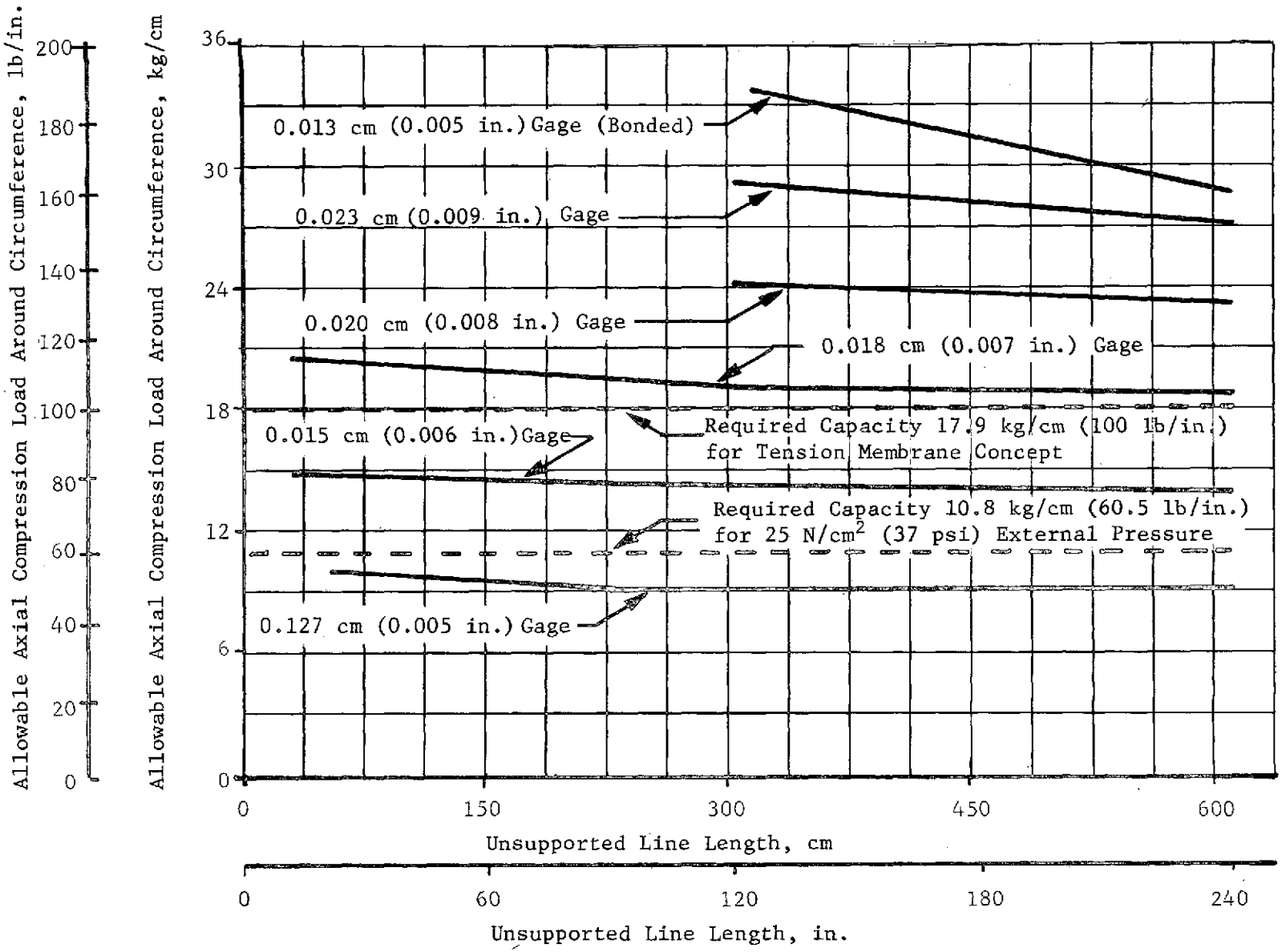

ASSUMPTION: ALL AXIAL LOAD DUE TO EXTERNAL PRESSURE GOES INTO INNER LINE

Figure A4. - 38 cm (15 in.) Diameter Inner Line Axial Compression Capability Versus Material Thickness

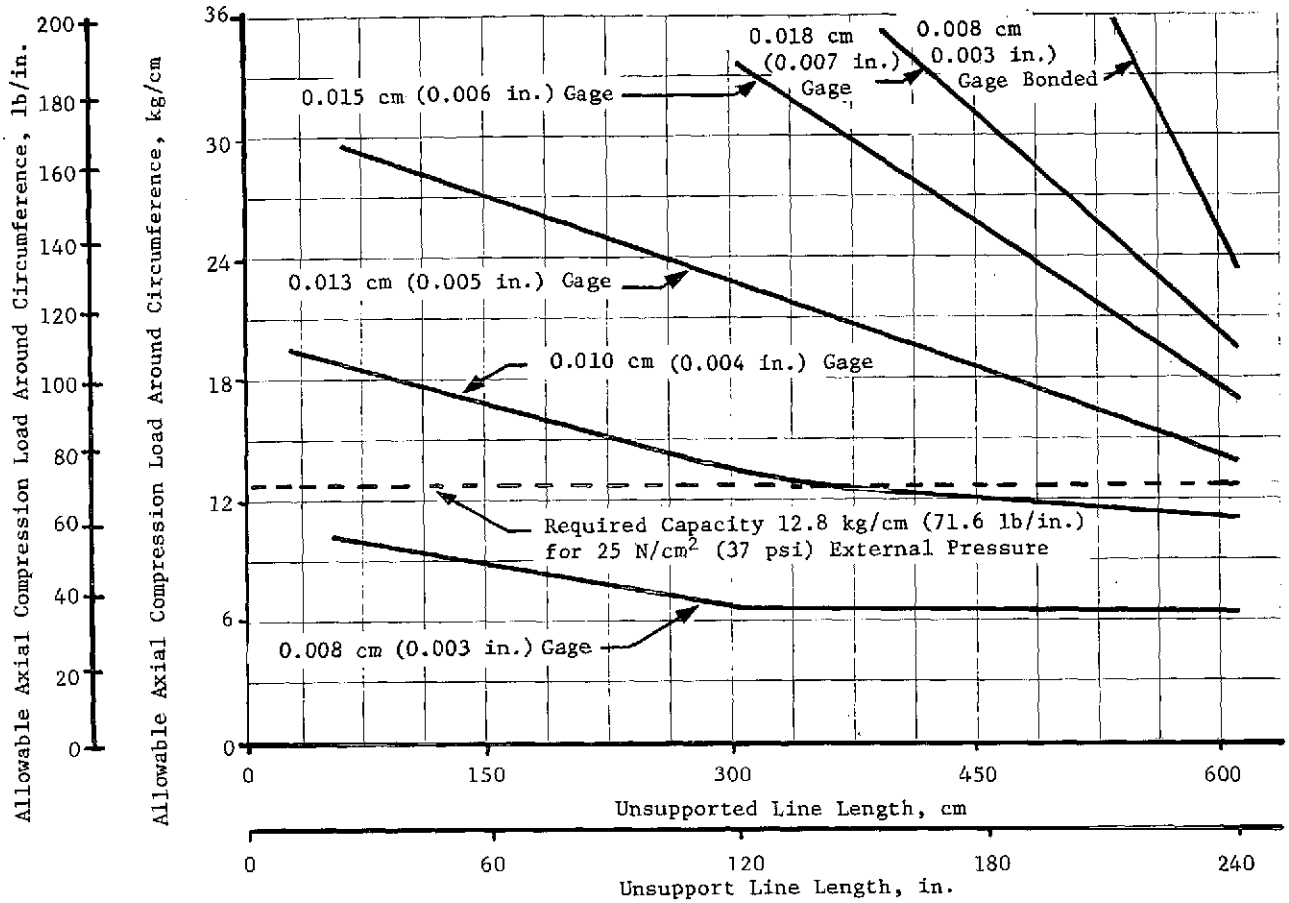

ASSUMPTION: ALL AXIAL LOAD DUE TO EXTERNAL PRESSURE GOES INTO INNER LINE

Figure A3. - 13 cm (5 in.) Diameter Inner Line Axial Compression Capability Versus Material Thickness

INTRODUCTION

The thermal performance of three all-metal and four composite configurations of vacuum jacketed lines was evaluated. Only one of the composite configurations (aluminum vacuum jacket liner) compares favorably with the all-metal configurations without modification of the outside of the inner line.

With a modification of the outside of the inner line to reduce its emittance to 0.035 or less, all of the composite structures can be made to perform as well or better than the best all-metal configuration. Two methods whereby this modification can be effected are suggested. The anticipated thermal parameters of these methods are given.

THERMAL MODEL

A thermal model was developed using the following assumptions:

1) Only radiation heat transfer is considered.

2) Line diameters of 5 cm (2 in.) through 51 cm (20 in.) are considered.

3) For any line size, the vacuum annulus is assumed to be 3.8 cm (1.5 in.) on the radius.

4) The inner line is assumed to have a temperature equal to 21°K (-423°F). Temperatures of 294°K (70°F) and 422°K (300°F) are assumed for the outer line.

5) Temperature gradients exist in the radial direction only. Temperature gradients along the longitudinal axis or around the circumference of both lines are not considered.

Assumption 5) enables treatment of this problem as one of infinite concentric cylinders and considers the heat transfer to the inner line per running foot of line as the performance evaluation parameter of the various configurations. Proceeding on this basis the thermal model has an exact solution as follows:

NOMENCLATURE:

A - area, m^2

D - diameter, cm

ε - emittance

γ - Hottel gray body factor

q - radiation heat transfer to the inner line per running meter of line, W/m

Z - Stefan-Boltzmann constant, $W/m^2\text{-}°K^4$

T - temperature, °K

Subscripts: i - outside surface of the inner line

o - inside surface of the vacuum jacket

$$q = ZA_i \gamma_{io} \left(T_o^4 - T_i^4\right)$$

(See Page 227 of reference B4.)

where: $$A_i \gamma_{io} = \frac{1}{\frac{1 - \varepsilon_i}{A_i \varepsilon_i} + \frac{1}{A_i} + \frac{1 - \varepsilon_o}{A_o \varepsilon_o}}$$

and: $A_i = \pi D_i$ $\qquad A_o = \pi\left(D_i + 7.62\right)$

EMITTANCE VALUES

Successful application of the thermal model equations requires the proper selection of emittance of the various surfaces under consideration. Emittance value of a surface is a function of material, surface finish (mechanical), surface condition (cleanliness), and degree of degradation during service life. In order to account for the interaction of all of these items, it is reasonable to assume a nominal emittance value centered between a clean, polished surface value and a clean, oxidized surface value. This has been done and the results are shown in Table B1. The nominal values shown in Table B1 are the values used for the comparisons made in this study.

TABLE B1. - EMITTANCE VALUES

Material	Surface condition	EMITTANCE at 21°K(-423°F)	EMITTANCE at 294°K(70°F)	EMITTANCE at 422°K(300°F)	Reference
Aluminum (6061-T6)	Polished	0.02	0.031	0.034	B2,B3,B4
	Oxidized	0.09	0.106	0.110	
	Nominal	0.055	0.068	0.072	
Stainless steel (304)	Polished	0.14	0.16	0.17	B1
	Oxidized	0.40	0.60	0.65	
	Nominal	0.27	0.38	0.41	
Inconel	Polished	0.20	0.25	0.26	B1
	Oxidized	0.60	0.63	0.66	
Inconel X	Polished	0.09	0.11	0.12	
	Oxidized	0.86	0.88	0.885	
	Nominal	0.44	0.47	0.48	
Titanium	Polished	0.10	0.16	0.18	B1
	Oxidized	0.63	0.66	0.665	
	Nominal	0.37	0.41	0.43	
Cloth composite		0.80	0.85	0.87	B4*

*These values are based on test data developed at NASA-LeRC.

PERFORMANCE EVALUATION

The nominal emittance values shown in Table B1 have been used in the thermal model equations with the results shown in Figures B1 and B2. The thermal performance of three all-metal (both inner and outer lines) and four composite (each line composed of a metal inner liner and S-Glass overwrap) lines have been shown. Of the composite structures examined, only the one using aluminum inner liner is thermally competitive with the all-metal lines, and even this composite has reduced thermal performance compared to an all-aluminum line. The primary parameter contributing to the reduced performance of the composites is the high emittance of the overwrap over the inner line. A lowering, in value, of this parameter can make the composite structures thermally competitive.

In Figure B3, the radiation heat transfer to the inner line as a function of the emittance of the inner line has been plotted for the four composite lines under consideration in the 25 cm (10 in.) size. As indicated, emittances of 0.035 and less will make all four of the composite lines thermally competitive with an all-aluminum line. This same result will be true of all line sizes. For emittance values of 0.02 and less, the thermal performance of the composite lines surpasses that of an all-aluminum line. Emittance values of 0.035 or less can probably be achieved by vacuum depositing pure metal (silver, gold, aluminum, copper) films on the overwrap. They most certainly can be achieved by covering the overwrap on the inner line with metalized Mylar (Appendix B1). Of the two methods, the use of metalized Mylar is the least expensive.

REFERENCES

B1 *Thermal Radiative Properties of Selected Materials.* Defense Metals Information Center Battelle Memorial Institute, Columbus, Ohio, DMC Report 177, Vol 1, November 15, 1962, RL39159.

B2 *Manned Space Vehicles Environmental Controls.* Report II Preliminary Data, Analysis of Heat Rejection by Radiation in Space Applications. Hamilton Standard, Windsor Locks, Connecticut, March, 1961.

B3 *Thermal Properties Handbook.* ER 13997, December 1965, Martin Marietta Corporation.

B4 Frank Kreith: *Principles of Heat Transfer.* International Textbook Company, Scranton, Pennsylvania, January 1966.

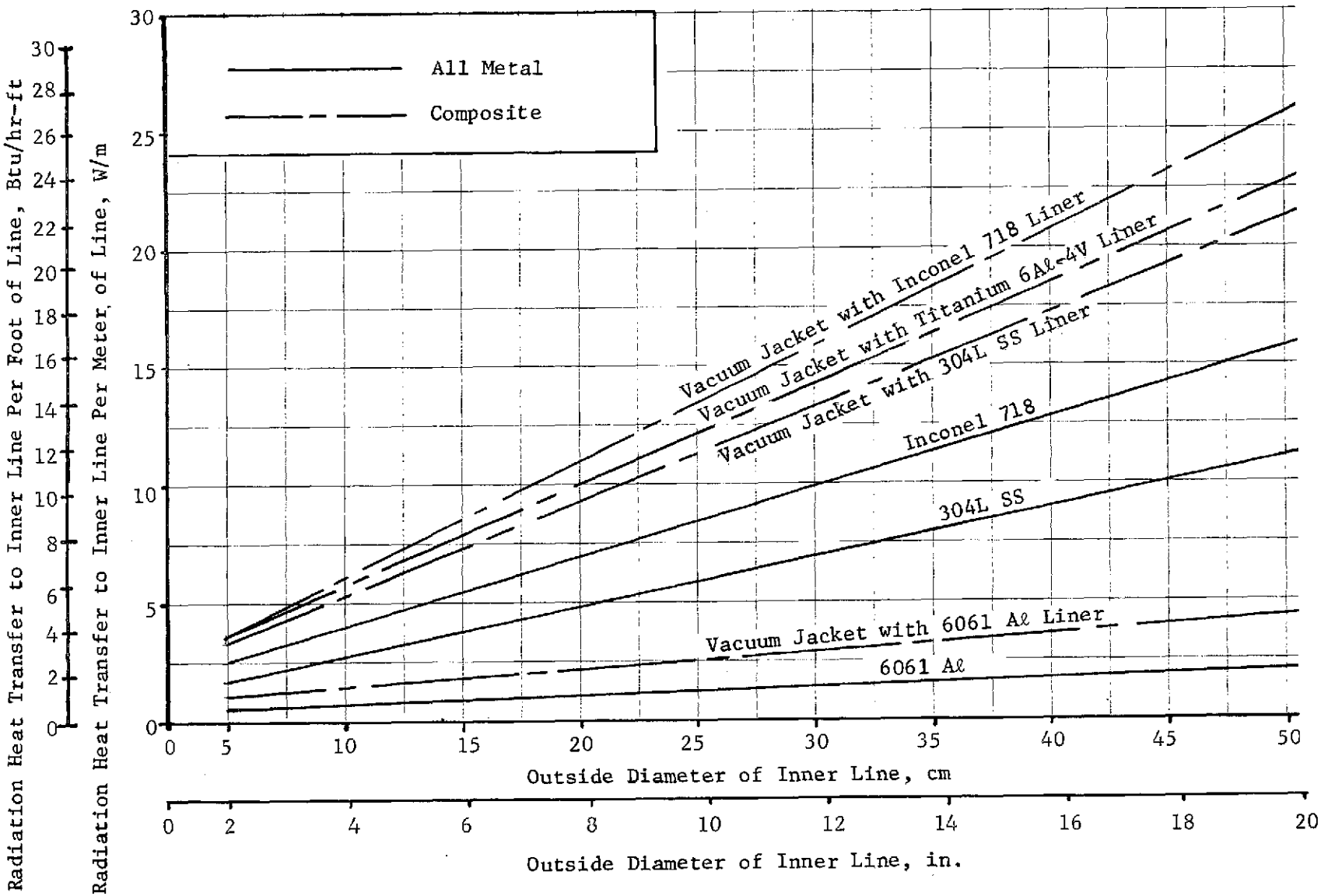

Figure B1.- Vacuum Jacketed Feedline Radiation Heat Transfer for Inner Line Temperature of 21°K (-423°F) and Outer Line Temperature of 294°K (70°F)

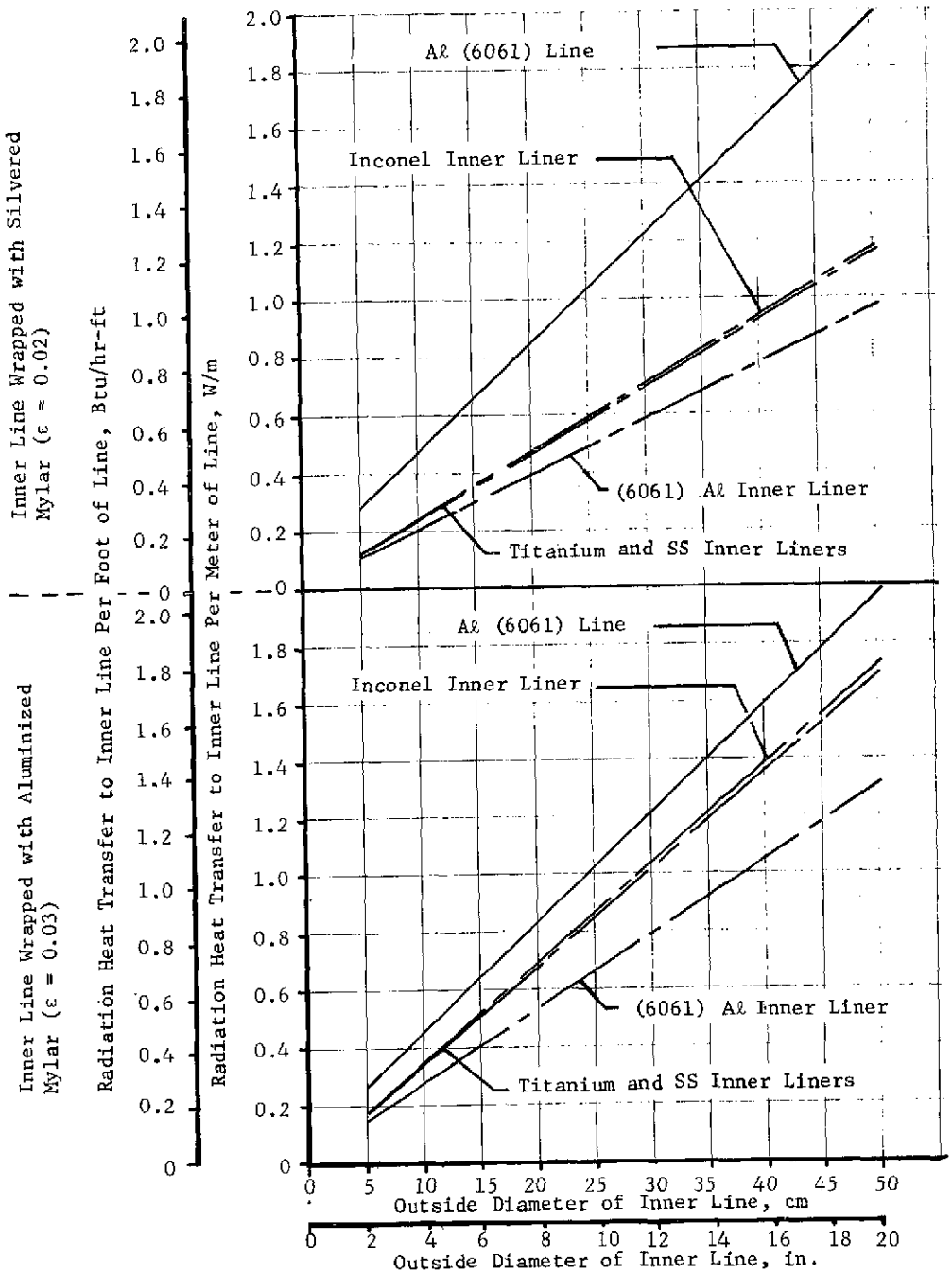

Figure B2.- Vacuum Jacketed Feedline Radiation Heat Transfer for Metallized Mylar Wrapped Inner Lines, Inner Line Temperature 21°K (-423°F), Outer Line Temperature 294°K (70°F)

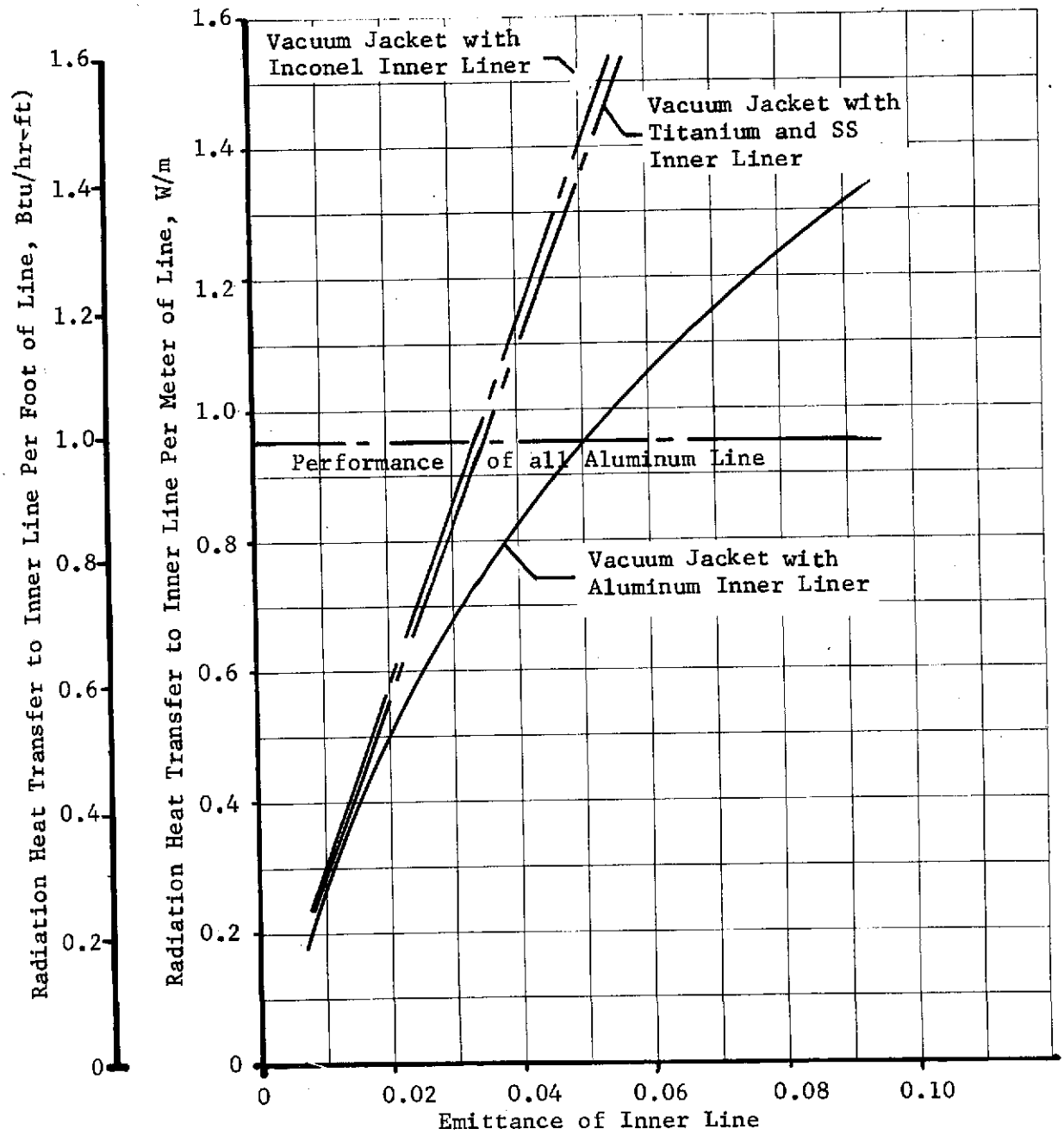

Figure B3.- Radiation Heat Transfer Versus Emittance of 25.4 cm (10 in.) Diameter Composite Lines, Inner Line at 21°K (-423°F), Outer Line at 294°K (70°F)

APPENDIX B1

THE SURFACE EMITTANCE OF VACUUM-METALLIZED POLYESTER FILM

Taken in whole from a paper of the same title by F. E. Ruccia and R. B. Hinckley in ADVANCES IN CRYOGENIC ENGINEERING, Volume 12.

Proceedings of the 1966 Cryogenic Engineering Conference
K. D. Timnerhaus, Editor
Plenum Press, New York, 1967

Thickness Effects. - Data relating to coating thickness and surface emittance for aluminum, gold, silver, copper, SiO/silver, and SiO/copper coatings are summarized in Figure B1-1. The actual data points have been omitted for the purposes of clarity. However, each curve represents an average of available data.

It is apparent from Figure B1-1 that initially the surface emittance decreases as the coating thickness increases. The emittance of aluminum and silver reach asymptotic values at 750-1000 A. The emittance of gold achieves its asymptote at about 1500 A thickness. Data for copper are insufficient to establish its thickness at the emittance asymptote. The reverse slope of the curve for copper can also be attributed to the smaller number of data points rather than to any real trend in the emittance at low thickness values.

The data on Figure B1-1 indicate that for any given thickness, silver gives the lowest emittance surface. Although emittance data for copper is available over a limited range, it appears to have the next lowest emittance; gold and aluminum follow next in order. Further, the data indicate that significant lowering of the emittance value is obtained as the coating thicknesses are increased from 250 to 1000 A. A thickness of about 250 A is that normally available from commercial suppliers of metallized polyester film.

The protective coatings of silicon monoxide applied over the silver and copper coatings result in degrading the emittance of the basic surfaces by approximately 40%. Therefore, these composite coatings have emittance values generally comparable to that of gold. The results obtained for gold and aluminum protective coatings (about 100 A thick) applied to silver are not shown in Figure B1-1. However, these coatings were not successful since they seriously degraded the basic emittance of the silver.

Environmental Effects. - The emittance results obtained with samples after exposure to four different environments are presented in Table B1-1. The results obtained with the scotch-tape test are also shown in Table B1-1. In this test a qualitative measure of the coating adherence to the film is established by the amount of coating retained on scotch-tape when a small amount is applied and removed from the metallized film. The numbers reported are the estimated percentages of removed coating.

The emittances of the aluminum coatings appear to be stable for all environments tested except one; the commercial sample exhibited significant deterioration after 100 hr in the 95% relative humidity environment. The aluminum coatings adhered acceptably through all environments.

The emittance of the gold coatings appear to be generally less than that of the aluminum coating for all environments tested. Increases in the emittance ranging from 10-30% of one or more samples was noted at the end of 100 hr in the 95% relative humidity,

CO_2, and salt environments. One sample in each of the 95% relative humidity and salt environments resulted in significant coating liftoff.

Since 45% and 95% relative humidity environments degrade both the emittance and adherence of the silver coatings, no additional samples were subjected to further testing in the CO_2 and salt environments. The SiO/silver coatings were tested in all environments and either the emittance or adherence was degraded in all but the 45% relative humidity environment.

The 45% and 95% relative humidity environments seriously degrade the emittance of the copper coatings. The adherence of the coatings remains acceptable. The silicon monoxide coatings over the copper significantly improve the emittance stability of the coatings. The 95% relative humidity environment degrades both the coating emittance and adherence. No degradation occurs with these composite coatings in other environments.

TABLE B1-1 EMITTANCE OF VACUUM-METALLIZED POLYESTER FILM AT 307°K (93°F) FOR VARIOUS METAL COATINGS AND MATERIAL THICKNESS

Environment	Film	Source	Sample No.	Thickness, Å	Start	Tape test, %	50 hr	Tape test, %	100 hr	Tape test, %
Air atm, 45% rel humidity, 95°F	Aℓ	ADL	48	790	0.021	0	0.021	0	0.0195	0
	Au	ADL	35-2	783	0.015	0	0.0159	0	0.0148	0
	Ag	ADL	36	762	0.0133	0	0.0181	10	0.016	10
	SiO/Ag	ADL	42	75/745	0.0160	0	0.0152	1	0.0165	0
	Cu	ADL	58	675	0.013	0	0.0167	0	0.0174	0
	SiO/Cu	ADL	52	75/761	0.0179	0	0.0178	0	0.0173	0
	Aℓ°	NRC	305	376	0.0136†	0	0.025	0	0.0291	0
	Au°	Hastings	304-A	1000	0.025	0	0.025	0	0.0234	0
	Au°	Nat. Met.	308	240	0.0214	0	0.0211	0	0.0235	0
Air arm, 95% rel humidity, 95°F	Aℓ	ADL	49	862	0.0184	0	0.0225	0	0.0206	0
	Au	ADL	35-1	940	0.0140	0	0.0145	0	0.014	0
	Ag	ADL	37	762	0.0111	0	0.0144	20	0.0147	40
	SiO/Ag	ADL	43	75/745	0.0141	0	0.0199	20	0.0175	20
	Cu	ADL	59	675	0.0121	0	0.0437	0	0.0713	0
	SiO/Cu	ADL	53	75/761	0.0174	0	0.0212	10	0.0254	10
	Aℓ	NRC	321	435	0.0225	0	0.0229	0	0.243	0
	Au	Hastings	304B	825	0.021	0	0.023	2	0.0225	30
	Au	Nat. Met.	322	212	0.0211	0	0.027	0	0.0271	0
CO_2 atm, 95°F	Aℓ	ADL	50	862	0.0203	0	0.0192	0	0.0184	0
	Au	ADL	34-1	1020	0.0152	0	0.0148	0	0.0187	0
	SiO/Ag	ADL	44	75/745	0.0150	0	0.0142	0	0.0207	0
	ClO/Cu	ADL	54	75/761	0.0170	0	0.018	0	0.0166	0
	Au	Hastings	333	953	0.0259	0	0.0273	0	0.0299	--
	Au	Hastings	330A	1840	0.0146	0	0.0146	0	0.0153	0
Salt atm, 95°F	Aℓ	ADL	51	862	0.0191	0	0.0187	0	0.0200	0
	Au	ADL	35-2	455	0.0154	0	0.0153	0	0.0152	0
	SiO/Ag	ADL	45	75/745	0.0198	0	0.0179	50	0.0165	100
	SiO/Cu	ADL	55	75/761	0.0228	0	0.0248	0	0.0255	0
	Au	Hastings	336	1050	0.0228	0	0.0225	0	0.0202	40
	Au	Hastings	3308	2072	0.0127	0	0.0160	0	0.0144	0

Purchased samples are coated on both sides.
†Questionable value; previous measurements indicate this value has a range of 0.023 to 0.027.

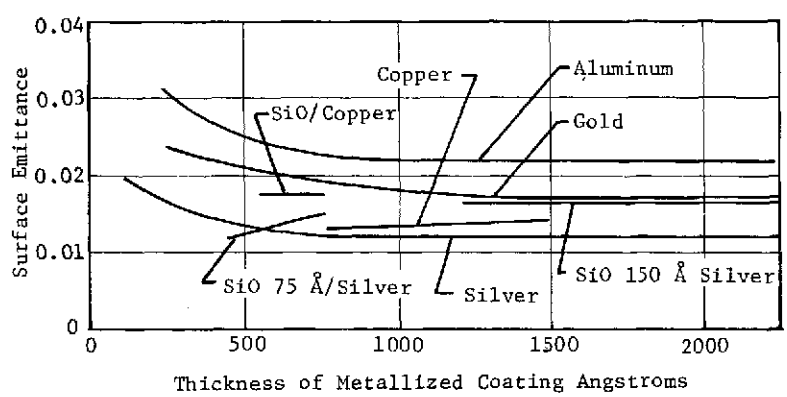

Figure B1-1 Emittance of Vacuum Metallized Polyester Film at 307°K (93°F) for Various Metal Coating Materials and Thickness.

APPENDIX C

HEAT TRANSFER PERFORMANCE
VACUUM END CLOSURES FOR VACUUM JACKETED COMPOSITE LINES

THERMAL MODEL

To develop a thermal model of the vacuum end closure, the following assumptions were made:

1) The radiation heat transfer between the inner and outer jacket is small compared to the end closure heat transfer and can be omitted in this study.

2) The metallic inner liner in contact with the liquid hydrogen is at the liquid hydrogen temperature 21°K (-423°F). That portion of the inner adapter ring in contact with the metallic inner liner is also at this temperature.

3) The line is completely enclosed at 294°K (70°F). The area of the enclosure is large compared to the area of the line; thus radiation from the line to the enclosure is a function only of the line area and emittance ($\varepsilon = 0.85$). The line also has convective heat transfer to the enclosure based on the line area and a convective coefficient of 2.6 $W/m^2-°K$ (1.5 $Btu/hr-ft^2-°F$).

4) That part of the end closure in contact with the foam insulation is an adiabatic surface (i.e., no heat transfers to the foam).

5) If a given length of feedline with end closures on both ends is divided into two equal length segments, then one segment is a mirror image, thermally, of the other segment. Therefore, only half of the line and one end closure need be modeled.

6) Because of the cryogenic temperatures involved, thermal conductivity of the various materials used must be evaluated as a function of temperature. Therefore, a thermal conductivity survey has been made with the results shown in Figures C1.a and C1.b. Where necessary, data has been extrapolated (dashed lines on Figures C1.a and C1.b; the Inconel line is not extropolated). The values shown on these figures were taken from the references listed at the end of this Appendix.

7) Condensation on the line outer jacket was not considered. Further in-depth analysis should allow for this parameter.

CONFIGURATION

Based upon the previously stated assumptions, the line was thermally modeled as shown in the Figures C2 and C3. Most of the conductors shown in Figure C3 have values that are functions of line size, line length, and material, or combinations of all three. For these reasons their values are calculated by the computer program as it analyzes the thermal model. Details of how this is accomplished are available but have not been included herein.

SUMMARY

The relative heat leak through the vacuum jacketed composite line end closure has been evaluated for different materials, two line lengths, four inner line materials, and four line sizes. A summary showing the end closure configuration and the thermal performance is given in Figure C2 and Tables C1 and C2. An effort was made to set up the thermal models in sufficient detail to give realistic results. However, the simplifying assumptions may have made the results quite conservative (i.e., heat transfer reported is too large). In any case, the assumptions were applied in a consistent manner to all configurations. Therefore, the relative performance between the configurations is valid.

As indicated in Table C1, the Inconel and stainless steel configurations have the smallest, and nearly identical, heat leaks for all line sizes and lengths. The all-aluminum end closure exhibits the largest heat leak for all line sizes and lengths. This is a result of the high thermal conductivity of aluminum and the increased conductive path made necessary by structural considerations. The titanium has a heat leak approximately 25% larger than Inconel and stainless steel in the 61 cm (24 in.) line length and approximately 50% larger in the 610 cm (240 in.) line length. The aluminum/S-Glass end closure is slightly worse than the titanium in the 61 cm (24 in.) line length, and comparable (slightly better) in the 610 cm (240 in.) line length. The 304L/S-Glass is the superior configuration from a heat transfer standpoint.

TABLE C1.- VACUUM JACKETED LINE END CLOSURE HEAT TRANSFER PERFORMANCE FOR 61 CM (24 IN.) LINE LENGTH

O.D. of Jacket, cm (in.)	Inner liner and closure material	Inner liner thickness, cm (in.)	End closure thickness, cm (in.)	Adapter ring thickness, cm (in.)	Heat transfer through end closure, W (Btu/hr)
5 (2)	6061 Aluminum	0.015 (0.006)	0.198 (0.078)	0.635 (0.250)	59 (203)
	Titanium	0.008 (0.003)	0.094 (0.037)	0.318 (0.125)	13 (43)
	Inconel	0.008 (0.003)	0.094 (0.037)	0.318 (0.125)	9 (32)
	304L SS	0.008 (0.003)	0.109 (0.043)	0.318 (0.125)	9 (32)
	Aℓ/S-Glass *	0.015 (0.006)	*0.008 (0.003)	0.635 (0.250)	15 (50)
	SS/S-Glass **	0.008 (0.003)	**0.008 (0.003)	0.318 (0.125)	2 (7)
25 (10)	6061 Aluminum	0.015 (0.006)	0.098 (0.078)	0.635 (0.250)	167 (571)
	Titanium	0.008 (0.003)	0.094 (0.037)	0.318 (0.125)	41 (139)
	Inconel	0.008 (0.003)	0.094 (0.037)	0.318 (0.125)	31 (107)
	304L SS	0.008 (0.003)	0.109 (0.043)	0.318 (0.125)	31 (106)
	Aℓ/S-Glass*	0.008 (0.003)	*0.008 (0.003)	0.635 (0.250)	50 (171)
	SS/S-Glass**	0.008 (0.003)	**0.008 (0.003)	0.318 (0.125)	9 (29)
28 (11)	Titanium	0.013 (0.005)	0.094 (0.037)	0.318 (0.125)	46 (156)
	Inconel	0.013 (0.005)	0.094 (0.037)	0.318 (0.125)	35 (118)
	304L SS	0.013 (0.005)	0.109 (0.043)	0.318 (0.125)	35 (118)
	SS/S-Glass**	0.013 (0.005)	**0.008 (0.003)	0.318 (0.125)	9 (32)
51 (20)	6061 Aluminum	0.015 (0.006)	0.198 (0.078)	0.635 (0.250)	299 (1021)
	Titanium	0.013 (0.005)	0.094 (0.037)	0.318 (0.125)	78 (266)
	Inconel	0.013 (0.005)	0.094 (0.037)	0.318 (0.125)	60 (204)
	304L SS	0.013 (0.005)	0.109 (0.043)	0.318 (0.125)	59 (202)
	Aℓ/S-Glass*	0.015 (0.006)	*0.008 (0.003)	0.635 (0.250)	93 (317)
	SS/S-Glass**	0.013 (0.005)	**0.008 (0.003)	0.318 (0.125)	16 (55)

*End closure of 0.008 cm (0.003 in.) aluminum bonded on both sides with 0.040 cm (0.016 in.) S-Glass.

**End closure of 0.008 cm (0.003 in.) stainless steel bonded on both sides with 0.040 cm (0.016 in.) S-Glass.

TABLE C2.- VACUUM JACKETED LINE END CLOSURE HEAT TRANSFER PERFORMANCE FOR 610 CM (240 IN.) LINE LENGTH

O.D. of inside jacket, cm (in.)	Inner liner and closure material	Inner liner thickness, cm (in.)	End closure thickness, cm (in.)	Adapter ring thickness, cm (in.)	Heat transfer through end closure, (Btu/hr)
5 (2)	6061 Aluminum	0.015 (0.006)	0.198 (0.078)	0.635 (0.250)	135 (462)
	Titanium	0.008 (0.003)	0.094 (0.037)	0.318 (0.125)	18 (61)
	Inconel	0.008 (0.003)	0.094 (0.037)	0.318 (0.125)	12 (42)
	304L SS	0.008 (0.003)	0.109 (0.043)	0.318 (0.125)	13 (43)
	Aℓ/S-Glass*	0.015 (0.006)	*0.008 (0.003)	0.635 (0.250)	17 (58)
	SS/S-Glass**	0.008 (0.003)	0.008 (0.003)	0.318 (0.125)	2 (7)
25 (10)	6061 Aluminum	0.015 (0.006)	0.198 (0.078)	0.635 (0.250)	425 (1450)
	Titanium	0.008 (0.003)	0.094 (0.037)	0.318 (0.125)	65 (222)
	Inconel	0.008 (0.003)	0.094 (0.037)	0.318 (0.125)	45 (154)
	304L SS	0.008 (0.003)	0.109 (0.043)	0.318 (0.125)	46 (158)
	Aℓ/S-Glass	0.015 (0.006)	*0.008 (0.003)	0.635 (0.250)	61 (209)
	SS/S-Glass	0.008 (0.003)	0.008 (0.003)	0.318 (0.125)	9 (29)
28 (11)	Titanium	0.013 (0.005)	0.094 (0.037)	0.318 (0.125)	71 (242)
	Inconel	0.013 (0.005)	0.094 (0.037)	0.318 (0.125)	49 (168)
	304L SS	0.013 (0.005)	0.109 (0.043)	0.318 (0.125)	51 (173)
	SS/S-Glass	0.013 (0.005)	0.008 (0.003)	0.318 (0.125)	9 (32)
51 (20)	6061 Aluminum	0.015 (0.006)	0.198 (0.078)	0.635 (0.250)	772 (2635)
	Titanium	0.013 (0.005)	0.094 (0.037)	0.318 (0.125)	122 (417)
	Inconel	0.013 (0.005)	0.094 (0.037)	0.318 (0.125)	85 (289)
	304L SS	0.013 (0.005)	0.109 (0.043)	0.318 (0.125)	87 (298)
	Aℓ/S-Glass	0.015 (0.006)	*0.008 (0.003)	0.635 (0.250)	85 (291)
	SS/S-Glass	0.013 (0.005)	0.008 (0.003)	0.318 (0.125)	16 (55)

*End closure of 0.008 cm (0.003 in.) aluminum bonded on both sides with 0.040 cm (0.016 in.) S-Glass.

**End closure of 0.008 cm (0.003 in.) stainless steel bonded on both sides with 0.040 cm (0.016 in.) S-Glass.

REFERENCES

C1. Russel B. Scott: *Cryogenic Engineering*. D. Van Nostrand Company, Inc., New York, 1959.

C2. E. G. Eckert: *Heat and Mass Transfer*. McGraw-Hill Book Company, Inc., New York, 1959.

C3. *The Experimental Measure of Thermal Conductivities, Specific Heats and Densities of Metallic, Transparent, and Protective Materials*, Part 1. AF Technical Report 6145.

C4. *Cryogenic Engineering Data Book and Buyers Guide/1969*. Business Communications, Inc., Cleveland, Ohio.

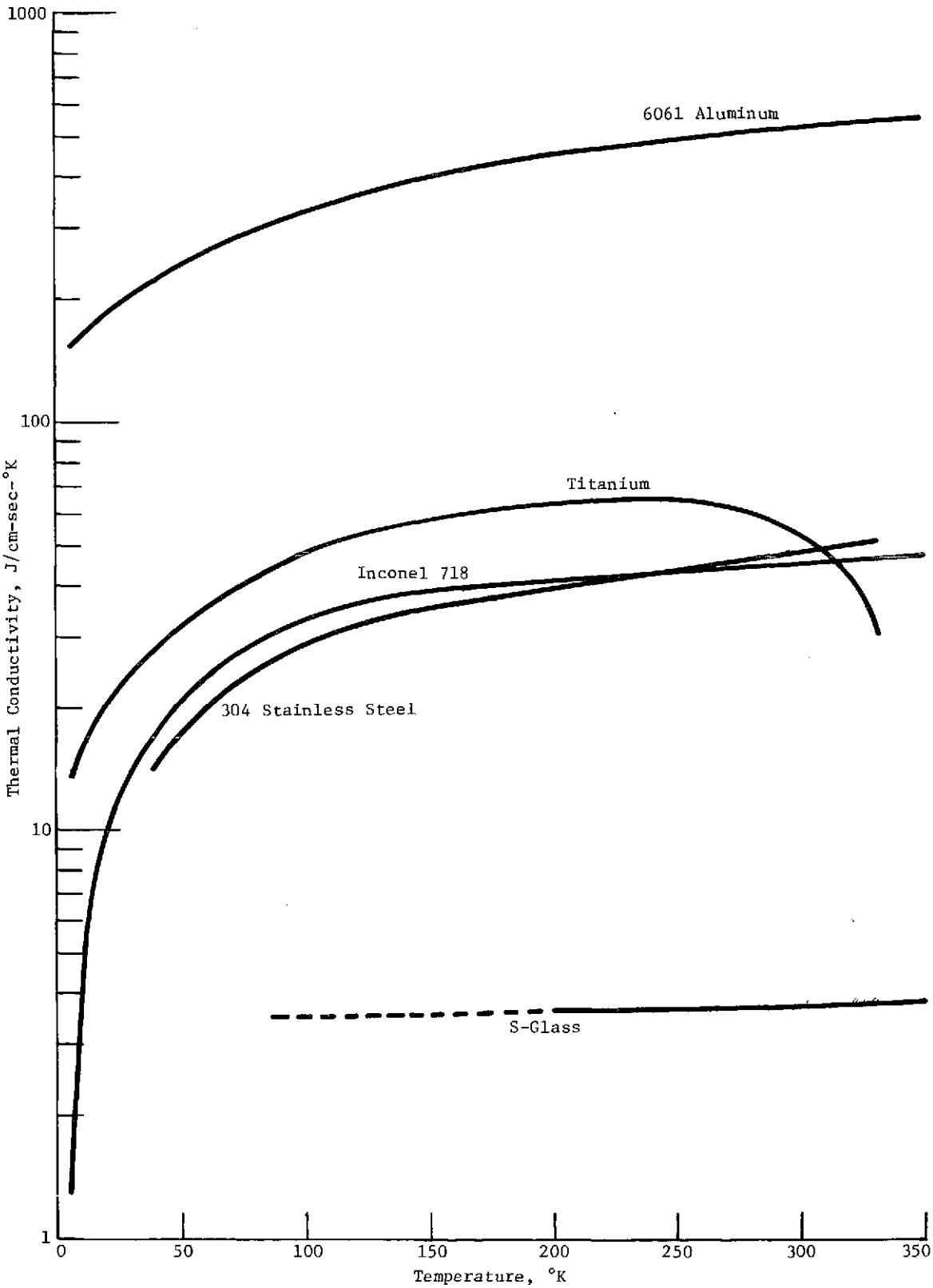

Figure C1.a.- Thermal Conductivity of Candidate Materials for Vacuum End Closures

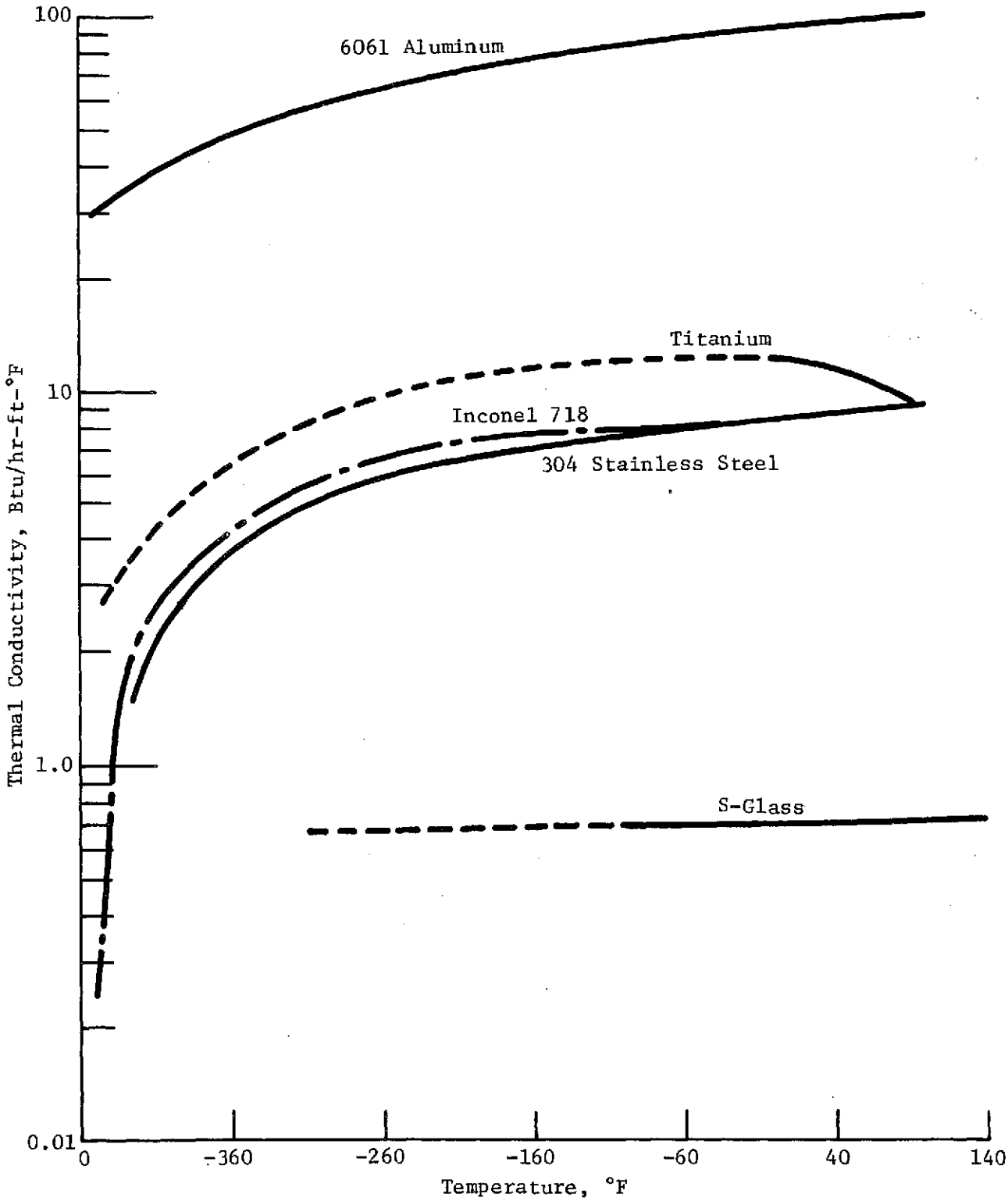

Figure C1.b.- Thermal Conductivity of Candidate Materials for Vacuum End Closures

- Vacuum Line Details:

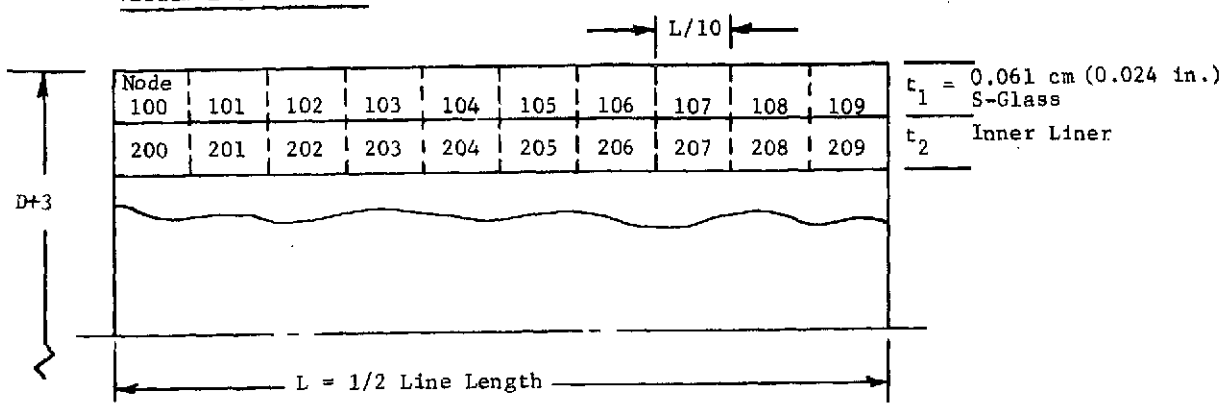

- End Closure (Except Aℓ/S-Glass Composite):

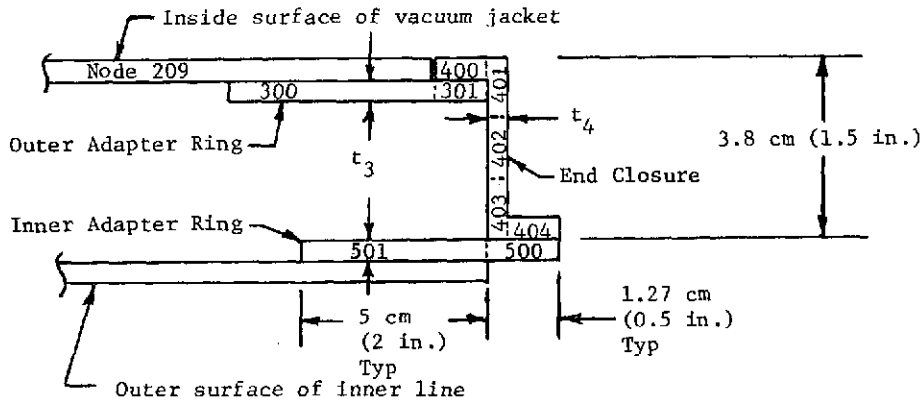

- End Closure Modification for Aℓ/S-Glass Composite:

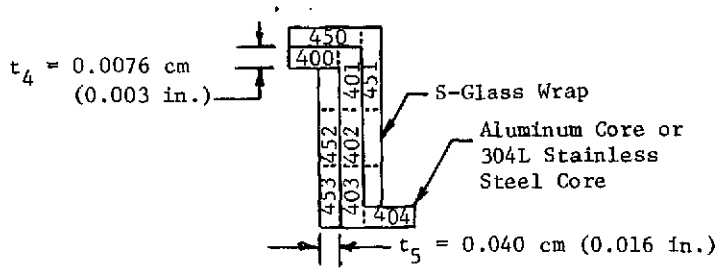

Figure C2.- Details of Thermal Model

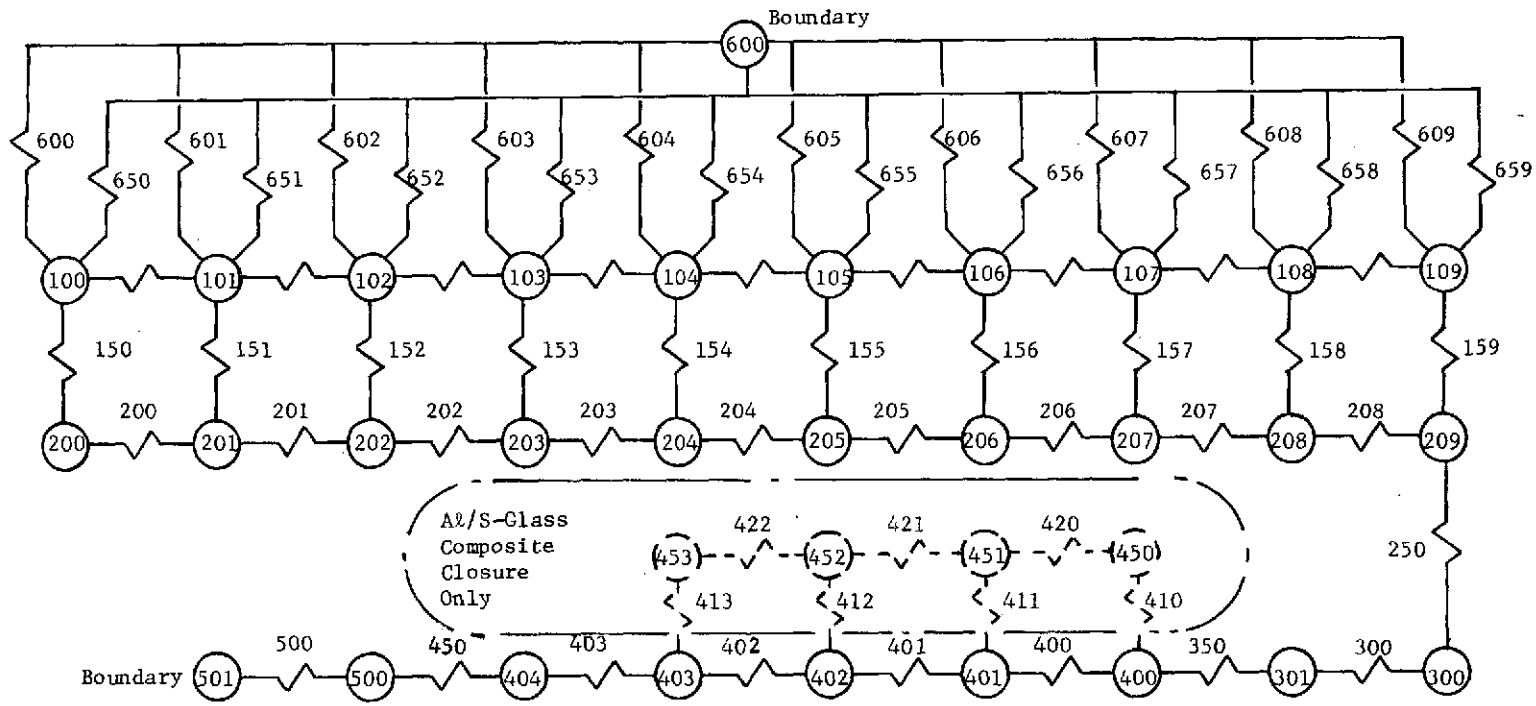

Nodes:

100-109	S-Glass
200-209	Inner Liner
300-301	Outer Adapter Ring
400-404	End Closure
500-501	Inner Adapter Ring
600	Enclosure

Conductors:

100-108	S-Glass Conduction
150-159	S-Glass/Inner Liner Conduction
200-208	Inner Liner Conduction
250	Inner Liner/Adapter Ring Conduction
300	Adapter Ring Conduction
350	Adapter Ring/End Closure Conduction
400-403	End Closure Conduction
450	End Closure/Adapter Ring Conduction
500	Adapter Ring Conduction
600-609	S-Glass Radiation
650-659	S-Glass Convection

Figure C3.- Thermal Model Node and Conductor Diagram

APPENDIX D

FAILURE ANALYSES - VACUUM JACKETED COMPOSITE LINES COLLAPSE FAILURE

INTRODUCTION

On the 7th of June, 1973, during evacuation of the two 20-cm (8-in.) diameter externally convoluted vacuum jacketed lines, one of the jackets experienced an external pressure collapse failure. The two lines were manifolded together so they were evacuated concurrently from the same vacuum source (Figure D1). The failure occurred shortly after start of evacuation. Provisions were made to monitor strain and vacuum intermittently during evacuation. The failure occurred, however, before any data was obtained. One strain gage was being monitored and the lines were under visual surveillance during evacuation. There was no warning or indication that a failure was about to occur.

The purpose of this analysis is to determine the cause of failure and to perform sufficient evaluation to provide a basis for redesign and rework of the remaining vacuum jacketed lines.

The analysis included (1) performing a visual inspection of the failed vacuum jacket and the other vacuum jackets that had not yet been evacuated, (2) reviewing the structural analysis and preliminary testing for any anomalies, (3) evaluating the bonding strength of the overwrap to the metal liner when subjected to a peel-type loading and determining the effects of flaws in the bond, (4) reviewing the bonding procedures, (5) evaluating the effect of a flaw in the vacuum jacket that had been repaired before the failure, (6) measuring the roundness of the remaining vacuum jackets to determine if an out-of-roundness condition could have caused structural instability, (7) reviewing the test specimen configuration to determine if buckling loads could have been induced into the jacket by the way in which the vacuum tubes and instrumentation tubes were supported, and (8) evaluating a vacuum jacket external seal technique that could be installed on the remaining vacuum jackets, which would allow the test program to proceed.

INSPECTION OF VACUUM JACKETS

A visual inspection of the failed vacuum jacket was performed. The overwrap was cut off and photographed (Figure D2). The following conditions were noted:

1) The vacuum jacket liner was totally collapsed around the inner line.

2) The overwrap was badly cracked but returned to a round shape after removal.

3) The metal liner surface was clean, indicating good composite-to-metal contact.

4) The burn hole in the jacket that had been repaired still maintained a seal.

5) Overwrap porosity was clearly evident.

All of the remaining vacuum jackets were inspected for evidence of disbond or other irregularities. The following was noted:

1) All of the vacuum jackets have separation between the overwrap and the liner where the instrumentation and vacuum tubes are welded to the end closures. This separation extends approximately 0.47 cm (0.186 in.) into the overwrap and 2.54 cm (1 in.) around the circumference, as shown in Figure D3. The separation was caused by warpage of the end closure during welding.

2) The mate to the failed vacuum jacket 20 cm (8 in.) diameter, H-assembly has a disbond area at each end as shown by the photograph in Figure D4. The failed tube had a similar disbond area before evacuation. Small marks or dimples were also noted on the convolutes. These marks were not noted previously and may be evidence of start of collapse. It is also possible that they are tool marks on the liner. The same type of marks, however, are not visible on any of the other tubes.

3) One 46 cm (18 in.) diameter vacuum jacket (internal hoop support design, G-assembly) has a large disbond area at one end and small disbonds near the center as shown in Figures D5 and D6, respectively.

4) All vacuum jackets have evidence of small disbonds along the metal liner seam weld similar to that shown in Figure D6.

5) All vacuum jackets of the external convolute design have uneven overwrap on the convolutes. There are a few places where the liner can be seen through the overwrap.

It is concluded from this inspection that all the vacuum jackets have some disbonds. The overwrap being porous will result in the bond being loaded in peel as opposed to tension loading, which was the design intent. The cause of the disbonds is discussed elsewhere in this report.

STRUCTURAL ANALYSIS AND PRELIMINARY TESTING REVIEW

The vacuum jacketed line structural analysis was reviewed to assure that the design and the line configurations agree. No discrepancies were found. The analysis shows a theoretical external pressure capability of 25 N/cm^2 (36.7 psia). The analysis treats the metal liner and overwrap as a composite structure. Thus, a bond between the two materials is required for structural integrity. Without overwrap support, the 0.013 cm (0.005 in.) thick Inconel liner will fail at a differential pressure of 3.4 N/cm^2 (5 psi) over a 3.8 cm (1.5 in.) unsupported span [distance between convolutes is 3.8 cm (1.5 in.)].

Two vacuum jacketed lines were tested in Task II, Preliminary Testing, to verify structural analytical models. A comparison of these lines to the failed vacuum jacket is provided in Table D1. Failure of the two preliminary vacuum jackets at 82% of theoretical indicated that analytical techniques were consistent and acceptable. The fact that one tube was bonded and the other tube was not tended to de-emphasize the importance of the bond. A significant difference between the preliminary test items and the failed line is the welding that was done on the failed line after overwrap. The bond was degraded on the failed vacuum jacket during welding, as was previously discussed.

BONDING EVALUATION

An evaluation was made to determine the cause of the premature disbonds, the effect of the disbond on the strength of the line, and to develop repair techniques that could be applied to the remaining lines. The first part of the evaluation consisted of performing bond peel tests on composite material samples that had been exposed to environments of heat, cold, and moisture. The second part of the evaluation tested composite material samples with controlled flaw sizes and techniques of repairing the flaws.

Peel tests - Composite material samples were made by overwrapping 2.54 cm (1 in.) wide by 15 cm (6 in.) long strips of Inconel 718, on a 46 cm (18 in.) diameter mandrel. The surface preparation procedure for bonding, overwrap materials, wrap tension and pattern, and cure cycle was the same as for the vacuum jacketed lines. Figure D7 is a photograph of the overwrap in process.

TABLE D1.- COMPARISON OF FAILED VACUUM JACKET TO PRELIMINARY TEST SPECIMEN

First preliminary test vacuum jacket	Failed vacuum jacket	Second preliminary test vacuum jacket
Style: External Convolutes	Style: External Convolutes	Style: Internal Hoop Supports
Liner not bonded	Liner bonded	Liner bonded
S-Glass in 58-68R	S-Glass in Epon 828 mpda	S-Glass in Epon 828 mpda
321 SS, 0.025 cm (0.10 in.) thick	Inconel 718, 0.013 cm (0.005 in.) thick	Inconel 718, 0.025 cm (0.010 in.)
Convolute spacing = 3.18 cm (1.25 in.)	= 3.81 cm (1.5 in.)	Support Spacing = 3.81 cm (1.5 in.)
Convolute radius = 0.20 cm (0.08 in.)	= 0.28 cm (0.11 in.)	N/A
Outside diameter = 30 cm (12 in.)	= 20 cm (8 in.)	= 26 cm (10.25 in.)
Overwrap: 1 layer hoop	2 layers, $\pm 5^{o}$ hoop	2 layers, $\pm 5^{o}$ hoop
Length = 32 cm (12.5 in.)	= 57 cm (22.25 in.)	= 38 cm (15 in.)
Calculated Collapse Pressure = 24 N/cm^2 (35 psid)	= 25 N/cm^2 (36.7 psid)	= 55 N/cm^2 (80 psid)
Test Collapse Failure = 20 N/cm^2 (28.7 psid)	= less than 8 N/cm^2 (11.7 psid)	= 45 N/cm^2 (65.7 psid)
Failed at 82% of theoretical	= less than 32% of theoretical	= 82% of theoretical
No welding done on tube after overwrap	Vacuum jacket was welded to inner line and instrumentation ports welded after overwrap	No welding

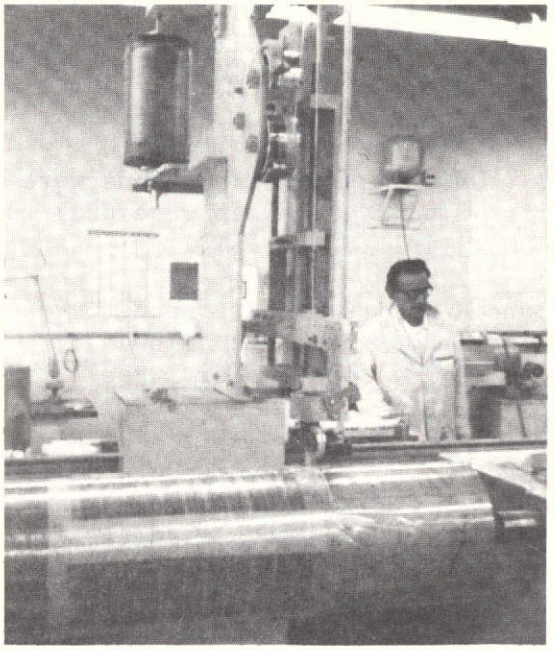

Figure D7.- Peel Test Specimens Being Overwrapped

1) Test Method - Peel tests were performed on 2.54 cm (1 in.) wide Inconel strips overwrapped with glass-fiber to duplicate the outer shell of the vacuum jacketed lines. Weights were added until a steady peel rate was observed. The Inconel was allowed to assume its natural shape as it was pulled. A photograph of the test setup is provided in Figure D8.

2) Tare Tests - The test coupons (no environmental exposure) were peeled as described in test methods. Tare peel forces were 500 to 600 g (1.1 to 1.3 lb).

3) Weld Burn Hole - The Inconel was exposed to the arc of a heli-arc welder to the extent that a small hole was burned in the liner. The liner holes, 0.16 cm (1/16 in.) diameter, caused disbonds of 0.64 cm to 1.9 cm (1/4 to 3/4 in.) diameter. Peel strengths were 250 to 350 g (0.5 to 0.7 lb) in the area of disbond and 500 g (1.1 lb) between disbonds.

4) Hot Water - After submersion in 355°K (180°F) water for 7 minutes, peel strengths deviated considerably from 140 g (0.3 lb) to 450 g (1 lb) between coupons.

5) Weld Temperature - One end of the Inconel of each coupon was heated to 366°K (200°F) and then subjected to the peel test. Peel strengths were 400 to 450 g (0.9 to 1 lb) at the thermocouple location and 500 to 700 g (1.1 to 1.5 lb) at 2.54 cm (1 in.) from the thermocouple (cool direction).

6) 311°K (100°F) Soak - The coupons were soaked in a 311°K (100°F) oven for 2 hours and then were peel tested. Peel strengths were 500 to 700 g (1.1 to 1.5 lb).

7) Heat and Humidity - The coupons were soaked in a 311°K (100°F) oven for 1 hour and then allowed to cool in a horizontal attitude 7.6 cm (3 in.) over water. Peel strengths were 400 to 700 g (0.9 to 1.5 lb).

8) Heat and LN_2 - The coupons were heated as in the weld temperature test except LN_2 was impinged on the glass directly opposite the heat source. Peel strengths were 400 to 800 g (0.9 to 1.8 lb).

9) Drilled Flaw - A 0.24 cm (0.093 in.) hole was drilled through the Inconel only and a disbond of approximately 0.95 cm (0.375 in.) diameter resulted. Peel strength was 550 g (1.2 lb) in the area of disbond and 700 g (1.5 lb) elsewhere.

10) Cold Soak - Two weld temperature coupons and one heat and LN_2 coupon were soaked in 293°K (68°F) water for 1 hour and were then subjected to the peel test. Peel strength was reduced by approximately 30%.

11) Hot Peel - One 311°K (100°F) soak coupon and two heat and humidity coupons were peel tested while at 366°K (200°F). Peel strength was increased by 20% to 57%.

It was concluded from these tests that the peel strength is affected by disbonds (weld hole or artificially induced) to the extent that bond area is reduced. Peel strength is reduced only slightly by heat and is greatly reduced by exposure to moisture. The peel strength of all test samples was low, indicating the inability of the bond on the composite lines to survive peel-type loading. Any modifications proposed on the remaining lines must include provisions for eliminating peel-type loading. The bond strength on the composite lines may have been reduced by 30% due to the welding, which exposed the tubes to temperatures of 366°K (200°F), and to moisture. The reduction in bond strength caused by moisture may be a serious objection to the use of any design concepts that depend on a bond for structural integrity. This problem warrants further evaluation.

Controlled Flaw Size Test - The purpose of this test was to determine some relationship between size of flaw and composite strength, and to develop repair techniques.

Dish-shaped composite test samples of 18 cm (7 in.) diameter, some without flaws and some with flaws of controlled dimensions, were prepared using standard materials, surface preparation, and overwrap procedures. Disbond flaws were controlled by overwrapping 0.64 cm (0.25 in.) to 2.54 cm (1 in.) diameter precured glass-fiber disks on the Inconel lines.

The samples were placed in a flanged fixture with glass view ports, providing capability to evacuate the Inconel side and pressurize the overwrap side. A photograph of the test setup is provided in Figure D9.

Two flaw repair techniques were tested. They consisted of (1) rebonding by injecting epoxy into the disbond areas with a hypodermic needle, and (2) placing a nylon cover over the overwrap to the liner. The test results are summarized in Table D2.

The following conclusions were drawn from these tests:

1) There is no 1-to-1 correlation between this test and the vacuum jackets.

2) Tests demonstrate that the structural strength of the composite decreases as the disbond flaw size increases.

3) Repairing flaws by injecting epoxy into disbond areas approximately doubles the load carrying capability, but does not regain original strength.

4) Covering the overwrap with a nylon or PVC sheet improved the load carrying capability. This technique changes the loading characteristics in that the peel loading is eliminated.

5) A technique of covering the vacuum jacketed lines with an evacuated nonpermeable bag should successfully eliminate peel loading on the bond, and substantially increase the external pressure load carrying capability of the line.

TABLE D2.- TEST RESULTS, DISBOND REPAIR TECHNIQUES

Sample description	Differential pressure at time of disbond	
	Average	Spread
No flaw	100 N/cm^2 (145 psid)	91 to 112 N/cm^2 (132 to 162 psid)
0.64 cm (0.25 in.) flaw	54 N/cm^2 (78 psid)	58 to 60 N/cm^2 (70 to 87 psid)
1.9 cm (0.75 in.) flaw	39 N/cm^2 (57 psid)	38 to 41 N/cm^2 (55 to 59 psid)
1.9 cm (0.75 in.) flaw rebonded by injecting Epon 828 mpda into disbond area	76 N/cm^2 (110 psid)	63 to 91 N/cm^2 (92 to 132 psid)
1.9 cm (0.75 in.) flaw rebonded by injecting Hysol 9309, structural adhesive, into the disbond area	73 N/cm^2 (106 psid)	69 to 77 N/cm^2 (100 to 112 psid)
1.9 and 2.54 cm (0.75 in. and 1 in.) flawed samples were covered by a sheet of nylon. Holes were drilled through the test sample to assure a vacuum under the nylon.	Samples were pressurized to 150 N/cm^2 (217 psid), the maximum allowable for the fixture. No disbond occurred during pressurization. The overwrap deformed with the lines when pressure was released.	
2.54 cm (1 in.) flawed samples covered by PVC bag in the as-cured condition.	Pressurized to maximum allowable, no failure, same results as with the nylon bag.	

General Notes:

1. Permeability of the nylon sheet was tested by measuring vacuum decay for 1 hour. No decay was detected.
2. Motion pictures of the disbond were taken during the failure of two samples, which provided capability to study the disbond taking place.
3. Flaw size on all samples was the disk diameter; actual flow was longer than the disk.
4. A backup plate with 10 cm (4 in.) I.D. hole was used in the test fixture.

BONDING PROCEDURE AND LITERATURE REVIEW

An investigation was made to determine what, if any, deviations were made to the bonding procedure as defined on the drawings.

The surface preparation procedure for bonding as defined on the drawings required removal of any surface deposits with nonmetallic agents (e.g., alumina grit paper) and degreasing in accordance with the following procedure:

1) Degrease with trichloroethylene.

2) Immerse in the following alkaline detergent solution for 10 minutes at 311°K to 344°K (100° to 160°F):

	Parts/Weight
Sodium Metasilicate	3.0
Tetrasodium Pyrophosphate	1.5
Sodium Hydroxide	1.5
Nacconol NR (Allied Chemical Company)	0.5
Distilled Water	134.0

3) Rinse thoroughly with cold, running tap water, followed by distilled or deionized water.

4) Dry in oven at 366°K (200°F).

5) Immediately after drying, install tube on overwrap fixture, pressurize, brush exterior surface with Pasa-Jell 105, set aside for 30 minutes and then rinse thoroughly with tap water. Follow manufacturer's instructions for application and safe handling procedures. Use extreme caution during the application of Pasa-Jell 105 to preclude buckling of the thin tube.

6) Apply overwrap within 2 hours after rinsing off the Pasa-Jell 105. If this is not possible, apply a thin coating of epoxy over the surface to be bonded within the 2-hour time limit.

Actual surface preparation procedure was in accordance with the drawings, with the following exceptions:

1) MEK and toluene were used for degreasing instead of trichloroethylene.

2) Specimen was thoroughly washed with alkaline detergent, instead of immersing in solution.

3) Air dry (ambient temperature) as noted by inspection, instead of 570°K (200°F) oven dry.

The exceptions made are acceptable and should not have resulted in a weaker bond than would have been obtained from the procedure specified on the drawings.

This bonding procedure was developed in Task II. Bonded test coupons were made and tested using this procedure. The coupons had a tensile strength of approximately 345 N/cm^2 (500 $lb/in.^2$). Peel tests were not performed in Task II because the potential for a peel-type loading was not anticipated. It was believed that 345 N/cm^2 (500 $lb/in.^2$) tensile capability was more than adequate.

Discussions were held with personnel at Martin Marietta having a background in composites, and literature on metal bonding was reviewed to determine if the bonding procedure was faulty or could be improved. The following data were obtained:

1) Use of solvents: the inability of solvents to escape between nonporous surfaces may result in porous bonds. Adhesives containing solvents can be used with metals if they are coated and left apart until most of the solvent has evaporated. MEK was present during preimpregnation as evidenced by the small blow holes in the overwrap surface. Performing the cure in a vacuum would increase evaporation of the solvents.

2) Residual stresses: residual stresses result from the differential thermal expansion between the adhesive and the metal. These can be minimized by using a thicker glue line, by altering the adhesive composition to make it more resilient, and by post-curing. The vacuum jacketed lines (metal to overwrap bond) have built-in residual stresses caused by curing temperature and pressure approximately equal to 23 N/cm^2 (34 $lb/in.^2$). When atmospheric pressure (external pressure on the vacuum jacket) is added to this, the minimum bond strength required is 34 N/cm^2 (48.7 $lb/in.^2$).

3) Elastomers such as nitrile rubber or nylon may be blended with the epoxy to increase resiliency of the adhesive. A resilient adhesive is better able to accommodate internal stresses and to resist failure by peeling than a hard or brittle adhesive.

4) Fitup tolerance: clearance between bonded surfaces should be uniform and somewhere between 0.013 to 0.025 cm (0.005 to 0.010 in.). The vacuum jacketed lines have an irregular surface at the weld seam line and at tool separation points. These surface irregularities could cause voids in the bond line if not filled with epoxy. It is suspected that these voids do exist, probably because of advanced preimpregnation. This can be minimized by coating the liner with epoxy or an adhesive before overwrap.

5) Surface cleanliness: adherend surfaces must be pretreated and kept clean until bonded. While due care was taken to maintain the vacuum jacket cleanliness before bonding, the jackets were not maintained in a controlled environment. An improved procedure would involve coating the line with the epoxy or adhesive as soon as possible after the Pasa-Jell and drying treatment. This would preserve the clean surface until bond.

6) Wetting the surface: any adhesive, to be effective, must wet the adherend surface. Another reason for coating the surface of the line is to assure 100% liner wetting.

7) Application of pressure during cure: when bonding with adhesives that release water, solvents, or other volatile substances during curing, it is often necessary to clamp the adherends to each other with pressures up to several hundred pounds per square inch. With 100% solids adhesives, such as epoxies, such curing pressures are not necessary. The vacuum jacketed lines were cured with approximately 2 N/cm^2 (3 psi) overwrap pressure on the liner. This was also true for the bonded test samples. This low pressure is probably responsible (at least in part) for low bond strengths. The cure pressure could easily be raised to about 10.3 N/cm^2 (15 psi) by placing the line in a vacuum bag during cure.

8) Peel strength to shear strength comparison:

Peel Strength: 45 to 130 N-cm/cm (10 to 30 in.-lb/in.) [2.54 cm (1 in.) wide specimen]

Shear Strength: 1520 N/cm^2 (2200 $lb/in.^2$)

Data on Nitride-Phenolic Adhesive

These values are about the same ratio as was obtained with the Inconel and S-Glass test samples, but are an order of magnitude higher.

9) Disbond repair: the technique of injecting an adhesive into the disbond area was suggested. The success of this technique, however, is questionable since the required surface condition for bonding has been lost.

10) Disbond inspection techniques: (1) visual examination, (2) tapping with a light metal rod or hammer, and (3) ultrasonic inspection. Martin Marietta has had excellent results in mapping disbond areas using ultrasonic inspection. The technique, however, is expensive and requires submerging the tubes in water.

11) Environmental effects: Bond strength tends to decrease with (1) high temperature, (2) age, and (3) exposure to moisture.

12) Epon 828 mpda as an adhesive: the general conclusion is that this epoxy is a good adhesive.

Conclusions - As a result of these discussions and the bonding literature review, it is concluded that the following changes to the bonding procedures used on the vacuum jacketed composite lines should improve bond strength:

1) Add pretreatment of metal surface with fine grit aluminum oxide before Pasa-Jell application.

2) Add 344°K (160°F) oven dry for 30 minutes immediately after the Pasa-Jell rinse.

3) Apply a coat of epoxy on the line immediately after oven cure, before removing from the area.

4) Cure the overwrap in vacuum bag to increase pressure between adherents and to assure complete evaporation of solvents.

5) Add 100% surveillance of surface preparation and overwrap.

References -

1. Dr. A. Feldman, Composite Structures, Martin Marietta Corporation.

2. John Lager, Structural Analysis, Martin Marietta Corporation.

3. Walter Batty, Composites Laboratory, Martin Marietta Corporation.

4. Tom Hay, Materials Engineering, Martin Marietta Corporation.

5. Ralph Tonge, American Cyanamid Company.

6. *Adhesive Bonding of Nickel and Nickel-Base Alloys*. NASA TMX-53428, October 1965.

7. *Handbook of Adhesives*. American Cyanamid Company.

8. *Graphite/Epoxy Compression Panels, Final Report.* MCR-73-40. Martin Marietta Corporation, February 1973.

9. *Pasa-Jell Technical Data Sheets.* Products Research and Chemical Corporation.

EFFECT OF PREVIOUSLY BURNED HOLE IN VACUUM JACKET

A gross analysis was performed to determine any effect that the burned hole in the vacuum jacket may have had on the failure. The hole was burned in the vacuum jacket during assembly welding and had been repaired.

Assumptions -

1) No real dissipation of heat during current flow.

2) Surfaces are considered flat.

Heat input = $i^2 R$

Temperature increase = $\frac{i^2 Rs}{WC_p}$

Resistance at L = $FK\left[\frac{dL}{2\pi Lt}\right]$

Weight at L = $2LdL\pi t\rho$

Temperature increase at = $\frac{i^2 Ks}{(2\pi)^2 t^2 L^2 \rho C_p}$

F = function of temperature
T = temperature
R = resistance
i = current
s = time
W = weight
C_p = specific heat
K = constant
L = distance from center
ρ = density of metal
t = thickness of metal
dL = differential length

When L = 0.317 cm (0.125 in.) and T = 1533°K (2300°F), then

$\frac{i^2 Ks}{(2\pi t)^2 \rho C_p}$; and

$L^2 T = 37.5$ from which L can be determined for assumed T:

L cm (in.)	T °K (°F)
4.9 (1.936)	261 (10)
1.6 (0.613)	311 (100)
1.1 (0.433)	366 (200)
0.9 (0.353)	422 (300)
0.8 (0.306)	477 (400)
0.7 (0.274)	533 (500)

The analysis plots the approximate temperature of the liner from the center of the burn hole.

If it is assumed that 422°K (300°F) will cause a disbond, then there would have been a 1.78 cm (0.7 in.) diameter disbond around the repaired hole. Recalling from the structural analysis, discussed earlier, that a 3.81 cm (1.5 in.) liner span with no overwrap support will fail at about 3.4 N/cm^2 (5 psi), the disbond could have been sufficient to start a failure. There were other larger disbonds at the ends of the tube, however.

CIRCUMFERENCE MEASUREMENT

All of the 20 cm (8 in.) diameter vacuum jackets were measured to determine if they are out-of-round to the extent that resistance to buckling loads is degraded. The measurement accuracy was about 0.08 cm (0.031 in.) because of taking the measurements with O.D. calipers on the composite surface. Three measurements were taken at each end and at the middle of the line. Variations in diameter of approximately 0.09 cm (0.035 in.) were recorded. This is not considered sufficient to cause degradation, considering the measurement accuracy.

TEST SPECIMEN CONFIGURATION

Analysis of the vacuum jacketed line test configuration showed that buckling loads could possibly be induced into the vacuum jacket if the instrumentation tubes are anchored. It was concluded that the instrumentation tubes should be free at all times except during handling and acoustic tests, at which time they should be guided only and not anchored.

VACUUM JACKET OUTER SEAL EVALUATION

As discussed earlier, it is desirable to eliminate peel loading on the bond between the liner and the overwrap. A technique was developed using an evacuated nylon cover over the overwrap, sealed at each end of the tube with Dux-seal. A photograph of this installation is shown in Figure D10. This installation can easily be incorporated for ground test purposes, but would not be acceptable for flight. The concept, however, may be further developed for flight hardware.

VACUUM TESTING

Two additional vacuum jacketed lines were vacuum tested (Assembly H, which is of the same design as the line that failed, and Assembly K, which is of external rib support design).

Assembly H had been evacuated previously in that the vacuum was manifolded with the failed tube at the time of failure. It is suspected, as discussed previously, that structural degradation had started during the initial evacuation. The barrel section of the line was wrapped with nylon and sealed at the ends with cement and Saran Wrap. All strain gages were connected to recorders and the end closure was instrumented with a dial indicator to measure axial deflection. The nylon bag was evacuated. The vacuum annulus was evacuated slowly to approximately 0.69 N/cm^2 (1 psia) at which time the vacuum jacketed imploded [differential pressure was 7.4 N/cm^2 10.7 psi)]. The implosion occured exactly as in the first line. There was in indication from the strain gages, which were being continuously monitored, that a failure was about to occure. The dial indicator showed 0.0025 cm (0.001 in.) deflection of the end closure at 1.4 N/cm^2 (2 psia). Immediately before the implosion, the dial indicator showed a movement of 0.14 cm (0.057 in.) and showed a permanent set of 0.11 cm (0.045 in.).

Assembly K was wrapped with a nylon bag and sealed at the ends with Dux-seal and tape. The bag was evacuated, strain gages were connected and the dial indicator was set on the end closure, as for Assembly H. The vacuum annulus was evacuated to 0 psia, as indicated by an absolute pressure gage, and maintained for approximately 5 minutes. The dial indicator showed no axial movement of the end closure and only strain gages S2 and S5 indicated strain of 60 and 120 μcm/cm (μin./in.), respectively. Posttest inspection revealed no damage or change to the vacuum jacketed line assembly.

FAILURE ANALYSIS CONCLUSIONS

Several factors contributed to the failure by reducing the structural capability of the vacuum jacketed lines. These factors included:

1) Metal liner imperfections mostly consisting of tool marks (slight indentations) on the convolutes.

2) Overwrap imperfections on the convolutes. The coverage was not 100%, or of uniform thickness, which reduced the convolute stiffness.

3) Significant bond degradation that occurred during welding. The overwrap was separated from the liner at each end of the line.

4) Overwrap porosity that resulted in pressure being applied directly to the metal liner, creating a peel-type loading on the liner to overwrap bond. This is especially severe in areas of disbond.

5) Since all of the remaining vacuum jacket lines had bond degradation, the probability of surviving the test program was low. The 46 cm (18 in.) diameter lines with external convolutes have the same liner and overwrap imperfections as existed on the 20 cm (8 in.) lines that failed. One of the 46 cm (18 in.) lines with internal hoop supports has a large disbond that will surely fail.

6) Rework possibilities are defined and evaluated in Table D3.

RECOMMENDATIONS

Repair all remaining vacuum jackets by methods a), b), and c) defined in Table D3. This approach has a low risk for further damage to the hardware and will build in a significant margin, assuring completion of the test program. The final test (external pressure collapse) can then be used to determine the amount of design margin.

INCORPORATION OF RECOMMENDED REWORK AND RESULTS

The failure analysis was reviewed with NASA-LeRC. It was concluded that the recommended rework be incorporated on one 46 cm (18 in.) diameter vacuum jacket and tested by exposure to a 15 cm (22 psi) differential. This action was successfully completed 9 July 1973. The rework was authorized for the remaining vacuum jackets.

TABLE D3. - EVALUATION OF REWORK POSSIBILITIES

Repair method	Discussion/evaluation
a) Repair disbonds using epoxy hypodermic needle approach.	Technique was proven effective in sample tests. Bond repair alone, however, is inadequate to assure success.
b) Cover tubes with evacuated nylon bag to preclude external pressure from acting directly on the liner causing further disbond by peel.	Technique was also proven effective in sample tests. One vacuum jacketed line was successfully evacuated using this technique, can be used in conjunction with a).
c) Apply additional layers of overwrap on the vacuum jackets thus increasing the overwrap load carrying capability.	Technique would essentially double the buckling strength of the glass overwrap and tend to reduce porosity. If used in conjunction with a) and b), success would be virtually assured.
d) Strip overwrap off of vacuum jackets and re-overwrap using improved bonding techniques.	Removing the overwrap without damage to the liners may be difficult. While improvements in bonding procedures are indicated by literature, additional testing is required to assure results.
e) Cut the vacuum jackets off of the inner lines and add internal hoop supports.	This technique would be very difficult, especially on the 46 cm (18 in.) diameter vacuum jackets. Instrumentation is likely to be damaged. Potential for inner line damage is high.

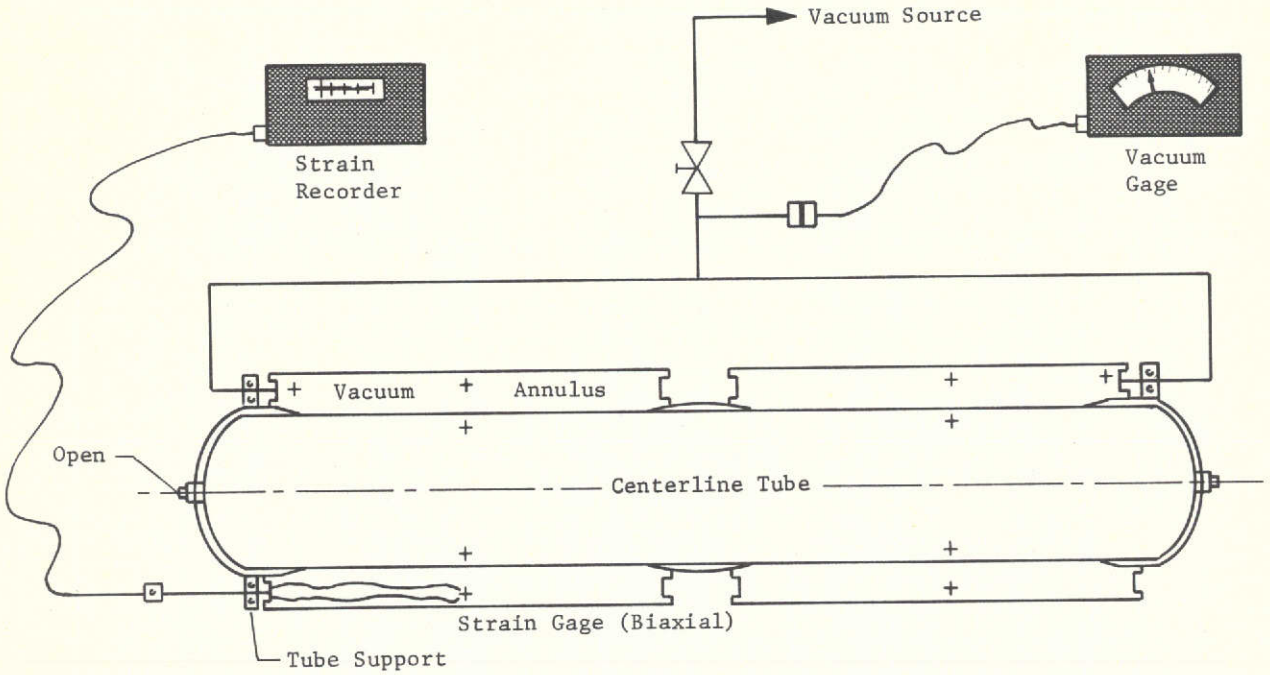

Figure D1.- Configuration of Test Specimen and Evacuation Facility

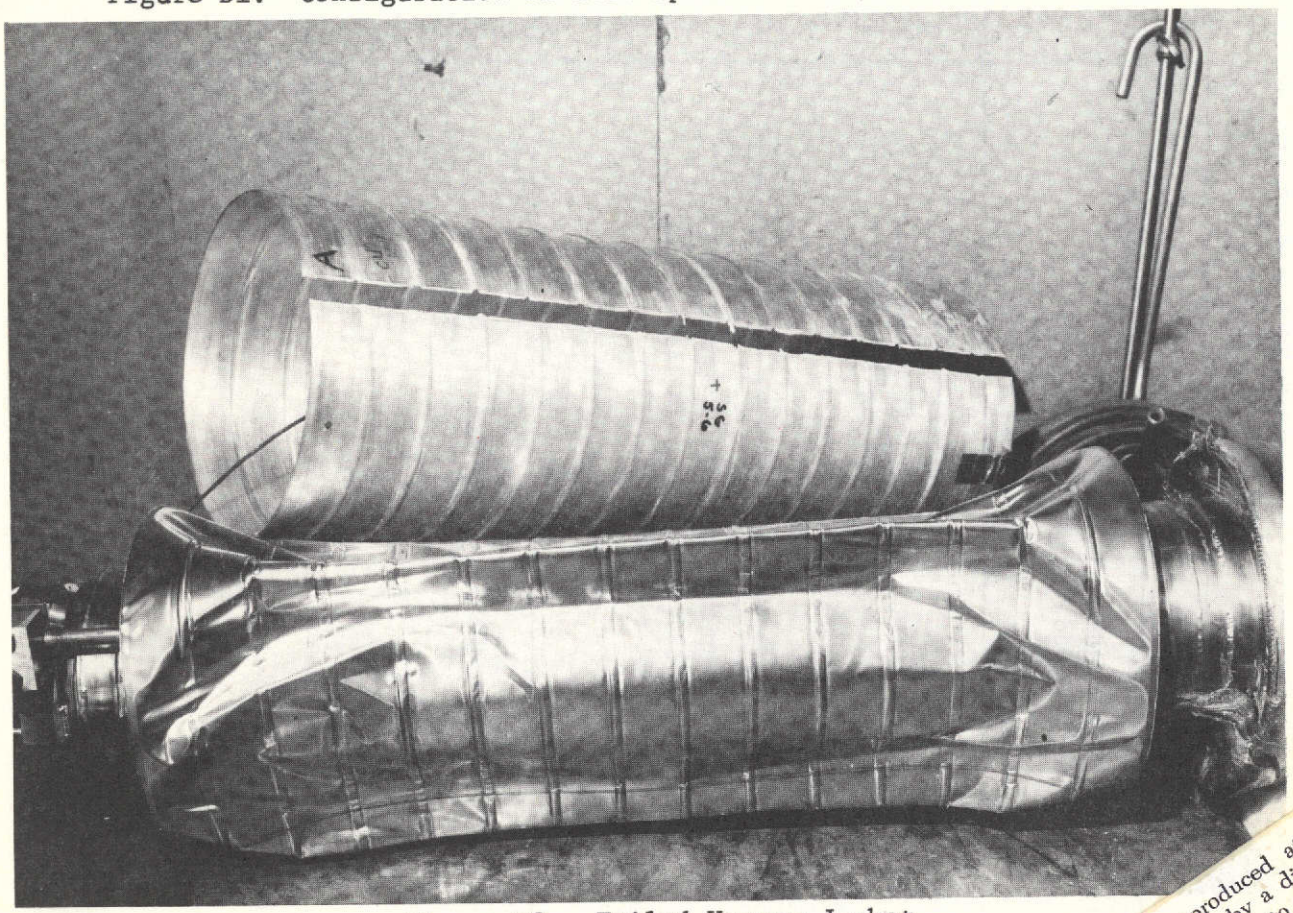

Figure D2.- Failed Vacuum Jacket

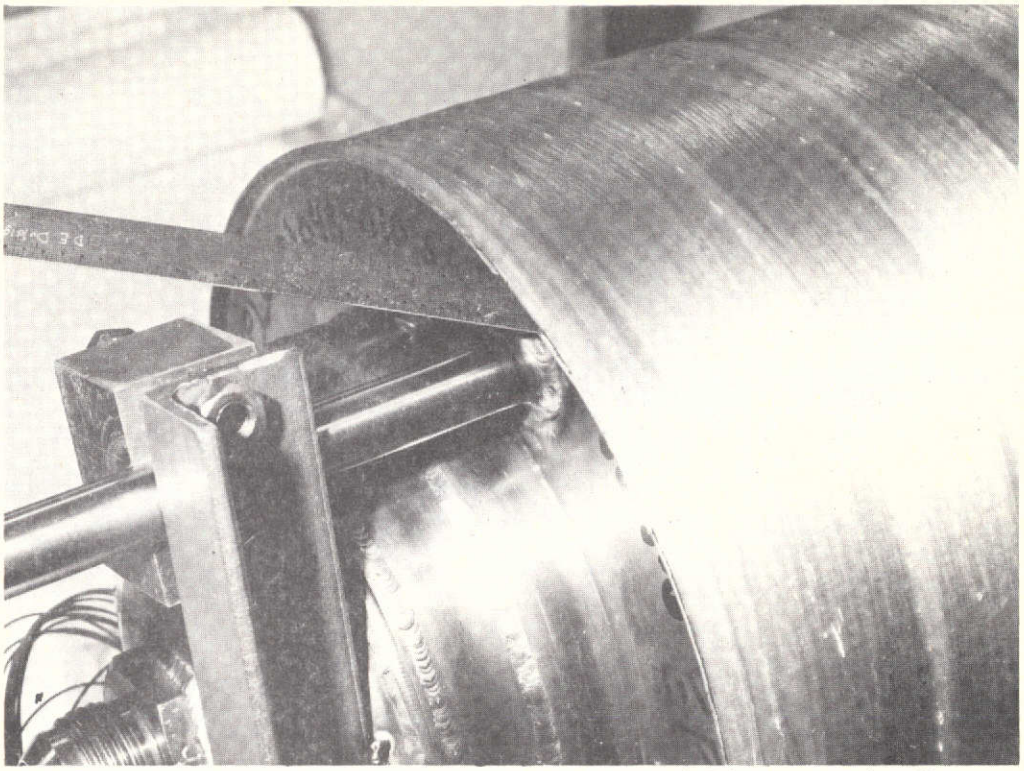

Figure D3.- Separation Between Overwrap and Liner at the Vacuum and Instrumentation Port

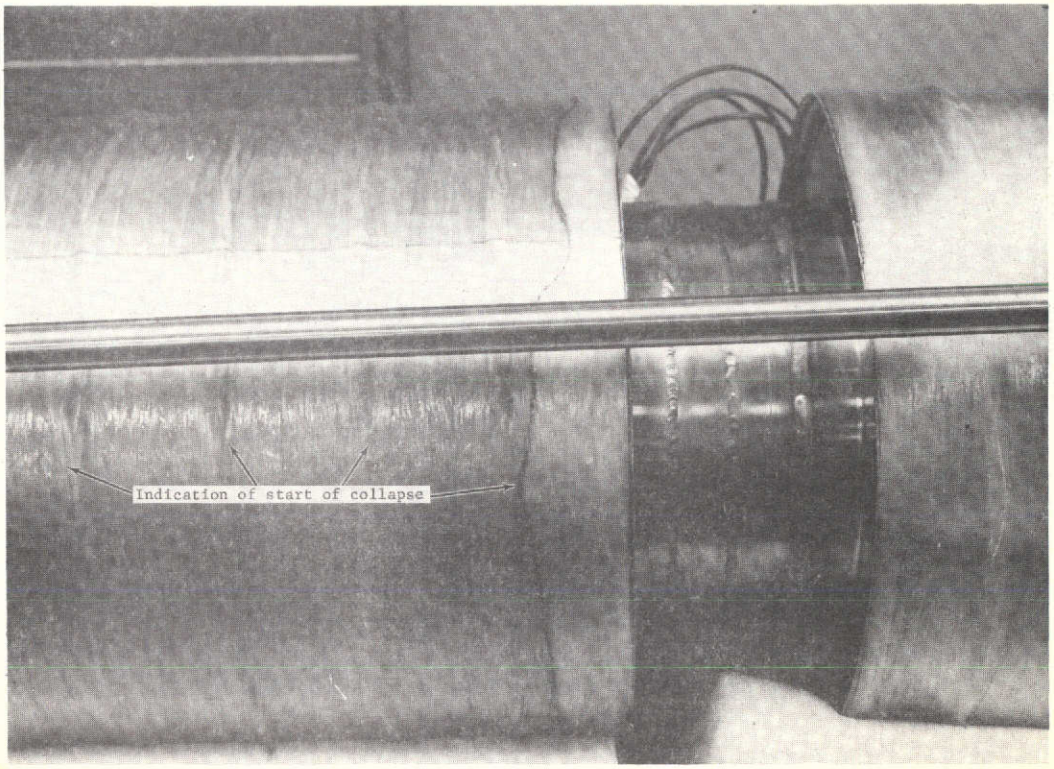

Figure D4.- Overwrap to Liner Disbond at End of 20 cm (8 in.) Vacuum Jacket (Mate to Failed Tube)

This page is reproduced at the back of the report by a different reproduction method to provide better detail.

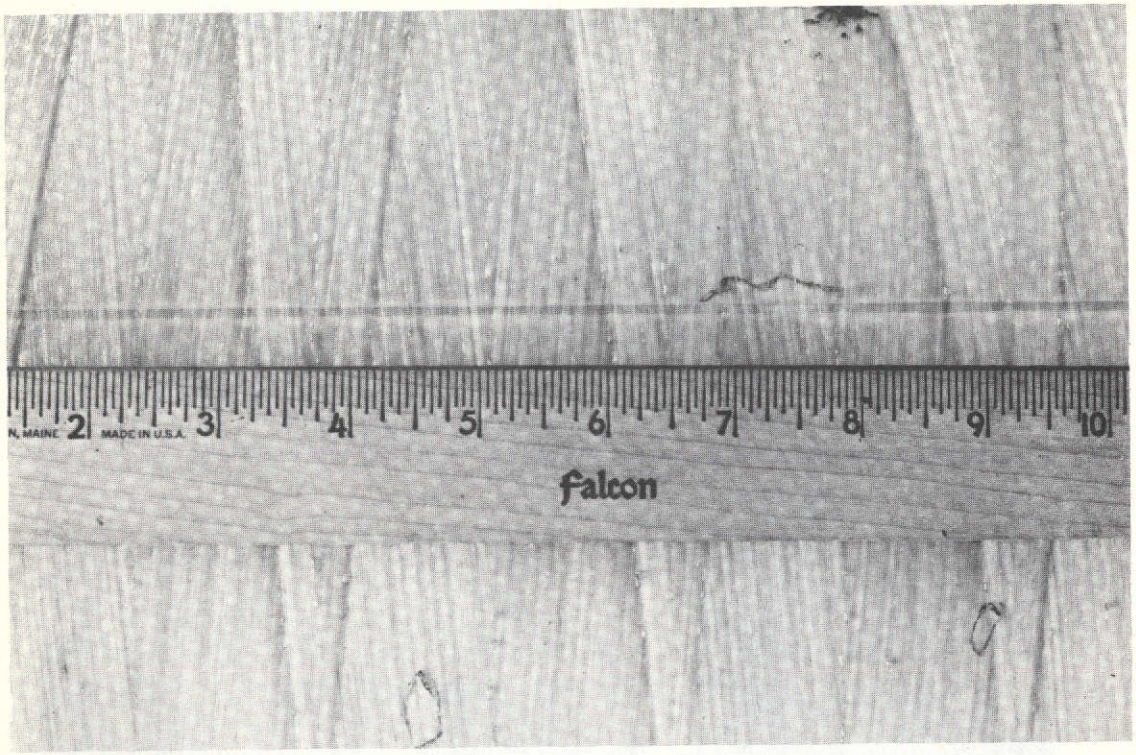

Figure D5.- Disbond Area on 46 cm (18 in.) Diameter Vacuum Jacket (G-Assembly)

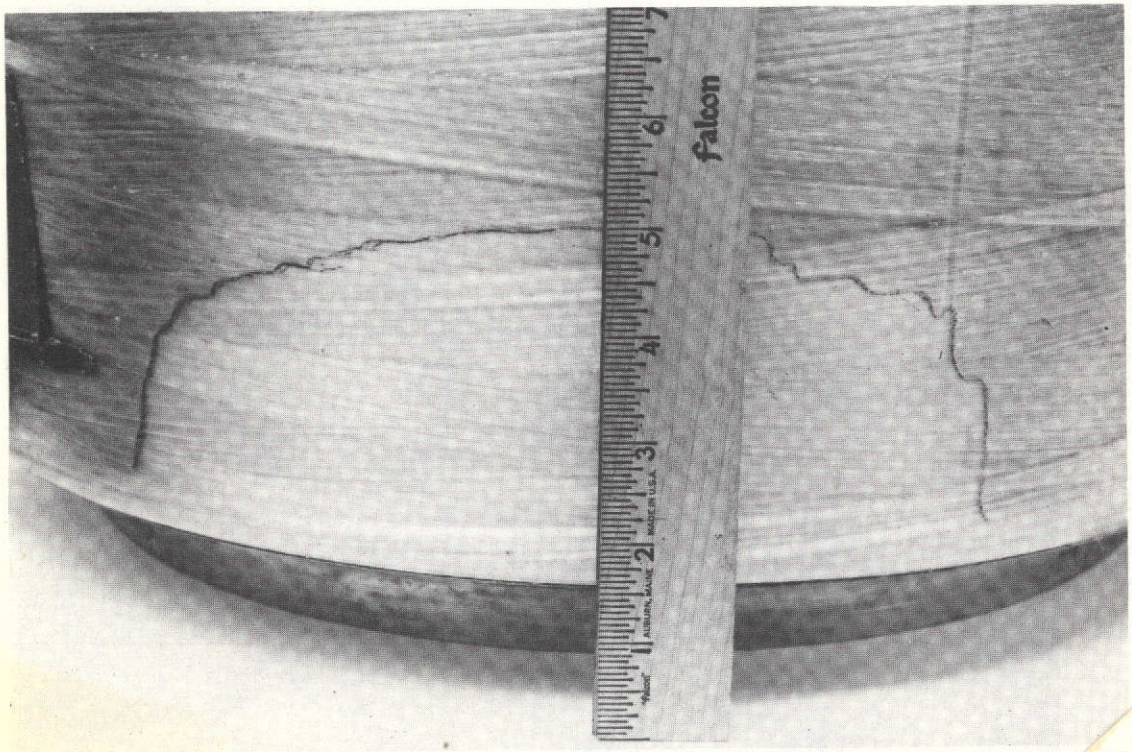

Figure D6.- Disbond Areas on 46 cm (18 in.) Diameter Vacuum Jacket (G-Assembly)

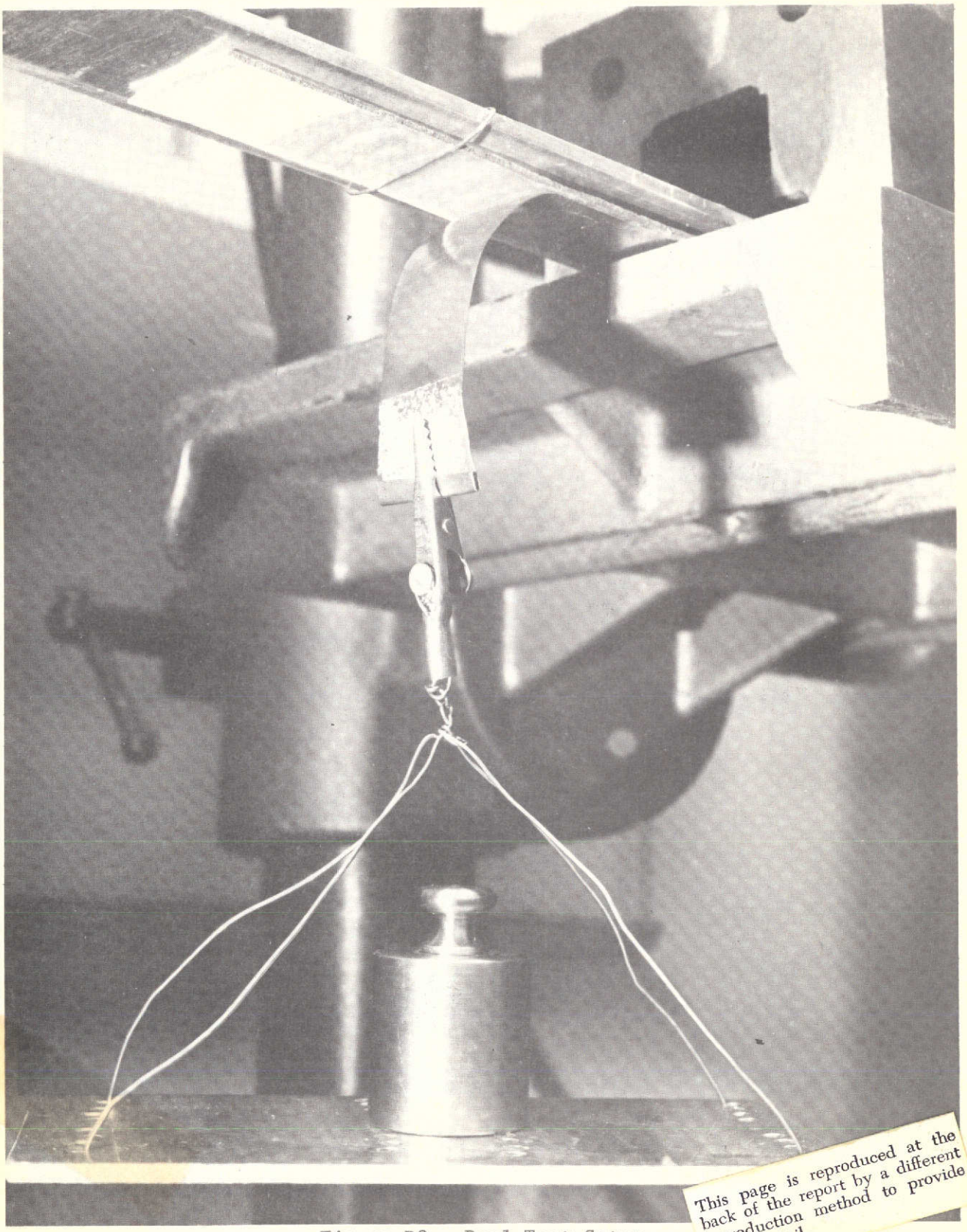

Figure D8.- Peel Test Setup

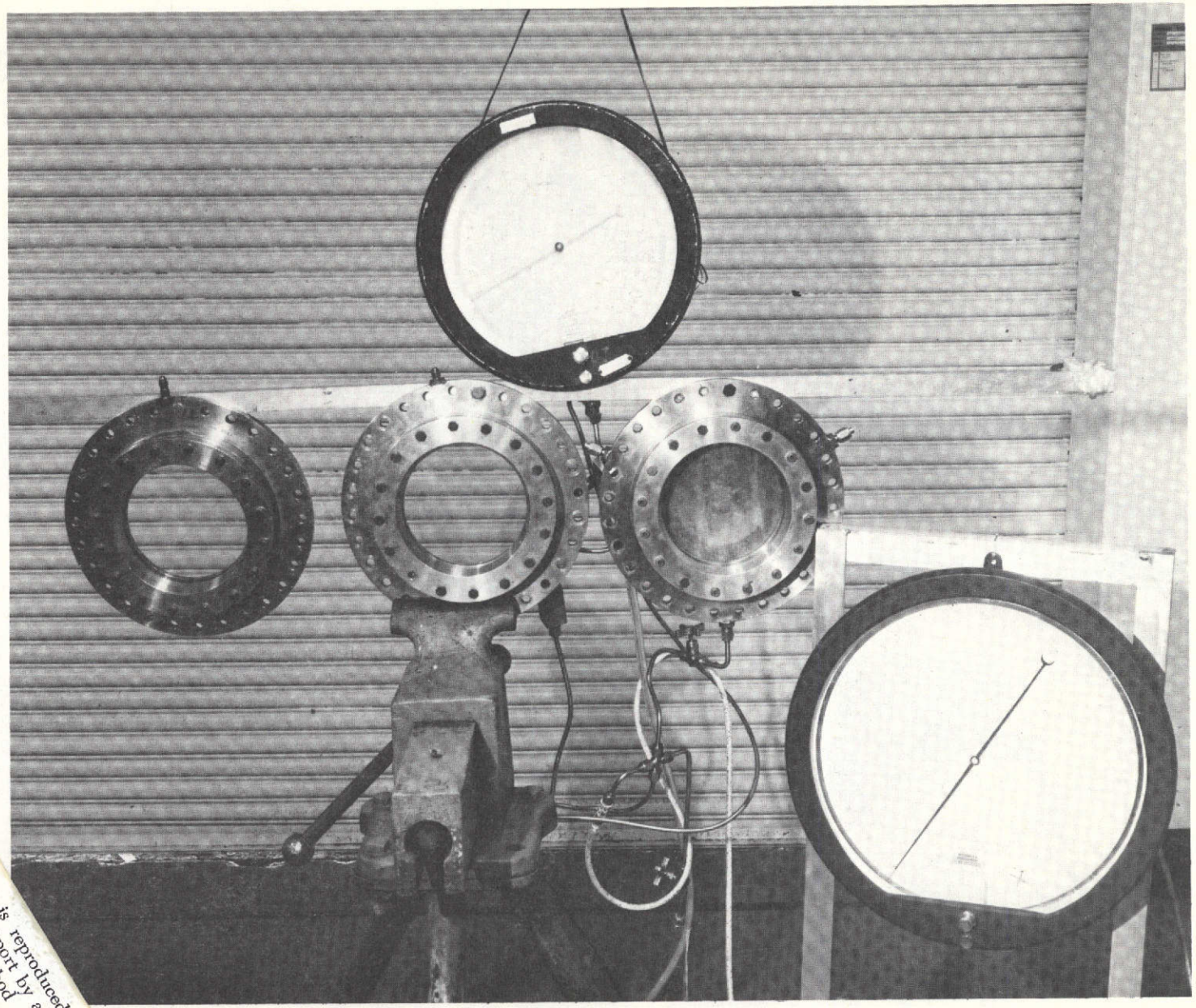

Figure D9.- Test Setup for Disbond Flaw Repair Development Test

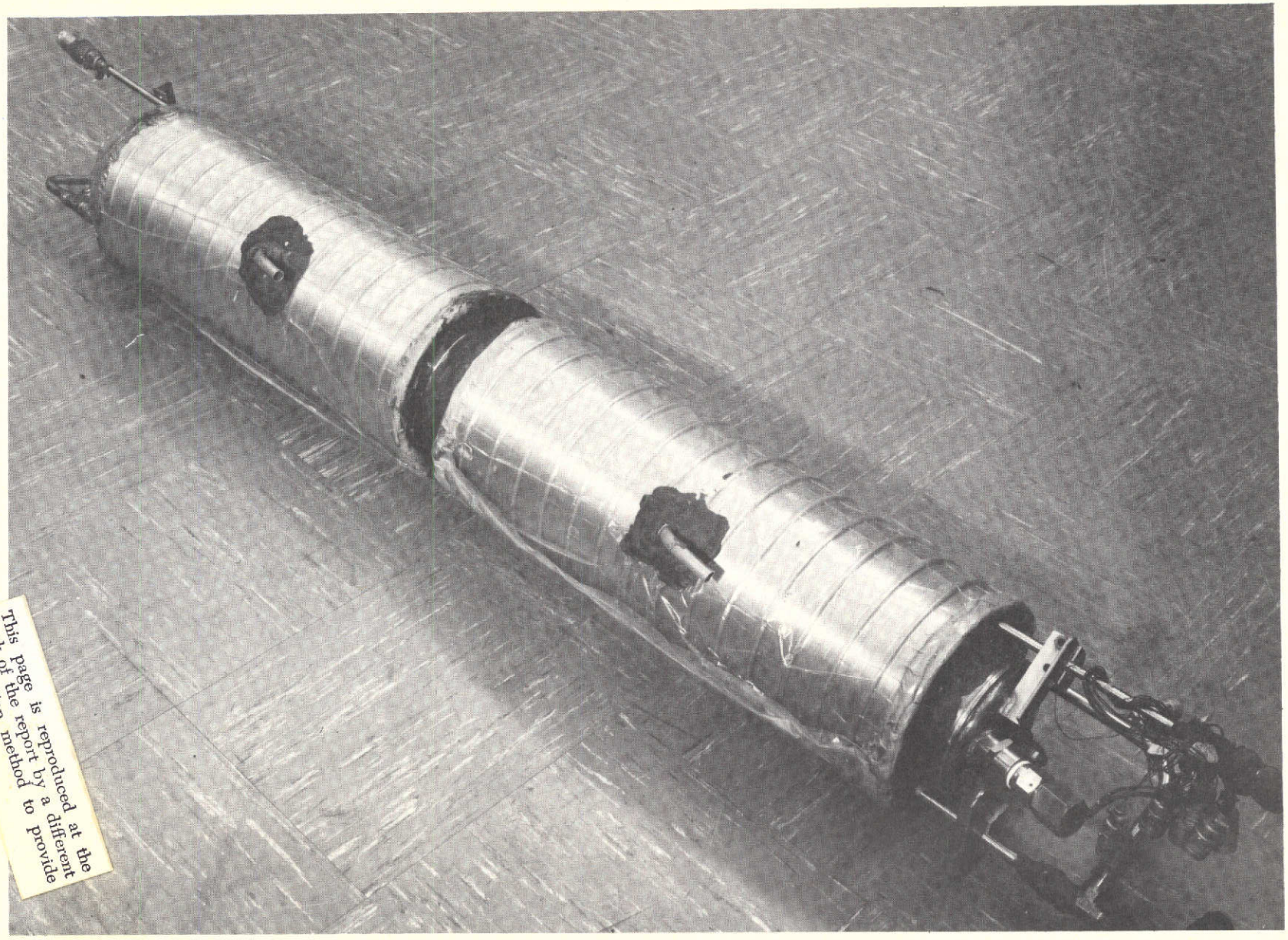

Figure D10.- Vacuum Jacketed Line Covered with Evacuated Nylon Bag

APPENDIX E

TENSION MEMBRANE - DETAILED INFORMATION

The detailed information presented herein was produced by Grumman Aerospace Corporation and was included in their *Final Report, Vacuum Jacketed Composite Lines*, June 7, 1973. Certain sections of the Grumman report that did not specifically discuss the tension membrane design concept are not included herein.

1. INTRODUCTION

This final report was prepared by Grumman Aerospace Corporation for Martin Marietta Corporation, Denver Division, in support of Martin Marietta's efforts on NASA Contract NAS 3-16762, *Vacuum Jacketed Composite Lines*. This report covers the period 18 July 1972 to 7 June 1973.

Vacuum jacketed lines are desirable for handling cryogenic fluids in space vehicles where reusability is required, where mission duration extends to several days and particularly from a safety standpoint, eliminating the hazard associated with having liquid air around a hydrogen system. In their present contract, Martin Marietta will apply composite overwrap techniques to the inner lines and vacuum jackets in an effort to achieve substantial weight reductions and to improve thermal performance.

Grumman Aerospace Corporation has developed a novel concept for a thermally efficient, lightweight vacuum jacket--the tension membrane concept. Under subcontract to Martin Marietta, Grumman has designed and fabricated test specimens which combine the Grumman tension membrane vacuum jacket and Martin Marietta composite reinforced inner line. These specimens were tested by Martin Marietta and evaluated with other program concepts.

Grumman's activities in this program were carried out under four main tasks: Conceptual Design, Preliminary Testing, Test Specimen Design, and Test Specimen Fabrication. Assistance in support of total program objectives was given in the analytical studies of Task I, Conceptual Design, and with respect to the Grumman tension membrane concept in other tasks.

Contributions of the following personnel are gratefully acknowledged: B. Aleck (Advanced Development), C. Cacho-Negrete (Design), Dr. H. Chau (Thermodynamics), Dr. R. Emerton (Structural Mechanics), L. Brown (Structural Analysis), R. Moebes (Tool Design), D. Bauer and W. McCormick (Welding), and E. Hall and R. Ewing (Vacuum Testing).

2. TASK I - CONCEPTUAL DESIGN

Method of Analysis and Assumptions.- The tension membrane shell consists of a series of toroidal segments that carry load to intermediate rings in suspension bridge fashion. Unlike sandwich and discrete stiffener cylinder designs, the membrane shell is loaded in tension and thus the material can operate at a stress close to its yield point. The compact intermediate compression rings carry the transverse component of the membrane load and are designed from overall and local instability considerations. Although material is used at a high efficiency in the membrane shell, it is not able to sustain longitudinal loads unless supported at its ends. In applications to lines it is convenient to use the inner line to support the tension membrane shell ends.

The key assumption in formulation of the tension membrane shell theory is that the membrane is permitted to buckle hoopwise with the pressure load being carried along the meridian direction. This expected physical behavior can be incorporated into the analysis in one of two ways: (1) assume that the hoop stress resultant, S_ϕ is equal to zero, or (2) analyze the membrane as an orthotropic shell with its circumferential modulus of elasticity, E_θ, small compared to its meridional modulus, E_ϕ.

By following the first approach, with the hoop stress resultant S_ϕ prescribed to be zero, and considering the membrane theory of shells, the equilibrium of forces in the normal direction yields:

$$S_\phi = Pr_1$$

where

S_ϕ = meridonal stress resultant

P = external pressure

r_1 = radius of curvature (Fig. 2-1).

The maximum radius of curvature, r_1 max, occurs at mid-bay and the required membrane thickness is determined from:

$$t \text{ reqd} = \frac{Pr_{1 \text{ max}}}{S_y}$$

where

t reqd = required membrane thickness

S_y = material yield stress.

The ring design is governed by the stability requirement:

$$I \text{ reqd} = \frac{P_u R^3}{3E}$$

where

$P_u = PL$ = uniform load intensity

L = ring spacing

R = ring radius

E = ring modulus of elasticity.

If the annulus between the vacuum jacket and the inner line is specified, then for a given membrane depth, a design exists for each ring spacing and weight-per-unit length of vacuum jacket may be computed. As the ring spacing decreases, r_1 max decreases and the required thickness is reduced. With the skin at minimum thickness, ring spacings have been further decreased beyond the minimum weight point to reduce the axial load produced by the membrane for reasons of compatibility with the inner line design.

Restriction on Longitudinal Load Exerted by Tension Membrane on LH_2 Line.- The Martin Marietta Corporation elected to restrict the maximum compressive limit load on the inner line to 175 N/cm (100 lb/in.) of circumference. This load can be achieved by holding the sag of the catenary constant while decreasing the ring spacing. From a dynamic (vibration) viewpoint, such designs of increased flexibility exhibit higher flexural stresses. To reduce the flexibility and flexural stresses of the design shown in Figure 2-2, the final design, Figure 2-3, maintains the same meridional radius of curvature (hence the same catenary tension) but reduces the sag by introducing flats over the rings.

Precise Membrane Definition.- A more precise definition of the shape of tension membrane, which conforms exactly to the design assumptions, can be obtained from the analysis of the Appendix. With this analysis which Grumman has programmed, the results of Table 2-1 were obtained.

TABLE 2-1. - TENSION MEMBRANE CONFIGURATION WEIGHTS

Ring Spacing		Membrane Area Per Unit Length		Membrane Weight per Unit Length								Ring Weight	
				kg/m t=0.0127	lb/ft t=0.005	kg/m t=0.0102	lb/ft t=0.004	kg/m t=0.0076	lb/ft t=0.003	kg/m t=0.0051	lb/ft t=0.002		
cm	in.	cm^2/m	$in.^2/ft$									kg/m	lb/ft
14.22	5.60	16.36×10^3	772.7	1.667	1.120	1.333	0.896	1.000	0.672	0.667	0.448	1.268	0.852
14.40	5.67	16.33	771.4	1.664	1.118	1.332	0.895	0.998	0.671	0.665	0.447	1.268	0.852
14.58	5.74	16.30	770.1	1.661	1.116	1.329	0.893	0.995	0.669	0.664	0.446	1.268	0.852
14.76	5.81	16.27	768.8	1.658	1.114	1.327	0.892	0.994	0.668	0.663	0.445	1.268	0.852
14.91	5.87	16.25	767.7	1.656	1.113	1.326	0.891	0.992	0.667	0.662	0.445	1.268	0.852
15.09	5.94	16.22	766.5	1.653	1.111	1.323	0.889	0.991	0.666	0.661	0.444	1.268	0.852
15.27	6.01	16.20	765.2	1.650	1.109	1.320	0.887	0.990	0.665	0.659	0.443	1.268	0.852
15.42	6.07	16.17	764.1	1.649	1.108	1.318	0.886	0.988	0.664	0.659	0.443	1.268	0.852
15.60	6.14	16.15	762.8	1.646	1.106	1.315	0.884	0.987	0.663	0.658	0.442	1.268	0.852
15.75	6.20	16.12×10^3	761.7	1.643	1.104	1.314	0.883	0.985	0.662	0.656	0.441	1.268	0.852

t = membrane thickness

To examine bending stresses at supports, membrane theory will not suffice and Grumman STARS program must be used. The bending stresses caused by pressure alone are small and will not be treated in this section. They are included in the lateral vibration analysis when they are coupled with stresses due to lateral acceleration.

Application of Analytic Relations to Proposed Design.-

Membrane Thickness: From Figure 2-3, the value of r_1, between rings is 10.95 cm (4.31 in.). The nominal skin thickness is 0.010 cm (0.004 in.). For one atmosphere pressure:

$$Pr_1 = (10.13\ N/cm^2)(10.95\ cm) = 110.9\ N/cm\ (63.5\ lb/in.)$$

$$\frac{Pr_1}{t} = \frac{110.9}{0.010} = 11{,}090\ N/cm^2\ (15{,}900\ psi)$$

indicating that 0.010 cm (0.004 in.) is an ultraconservative thickness from a membrane viewpoint.

Ring Section:

Ring area = 0.342 cm^2 (0.053 $in.^2$)

Ring mean radius = 25.4 cm (10 in.)

Ring moment of inertia = 0.283 cm^4 (0.0068 $in.^4$)

Ring spacing, d = 14.02 cm (4.42 in.)

Ring material modulus of elasticity = 6.89×10^6 N/cm^2 (10×10^6 psi)

$$PL < \frac{3EI}{R^3} \qquad (10.13)(14.02) = 142\ N/cm\ (81.2\ lb/in.)$$

$$\frac{(3)(6.89 \times 10^6)(0.283)}{(25.4)^3} = 358\ N/cm\ (204\ lb/in.)$$

$$142 < 358 \text{ or } FS = \frac{358}{142} = 2.52$$

Ring Stress:

$$S_{Hoop_{ULT}} = \frac{1.5\ pdR}{A} = \frac{(1.5)(10.13)(14.02)(25.4)}{(0.342)} =$$

$$14{,}700\ N/cm^2\ (23{,}000\ psi)$$

$$S_{Allowable} = 29{,}000\ N/cm^2\ (42{,}000\ psi)$$ (Method of Ref 2-1) (Aluminum Alloy 7075-T7351)

$$MS = \frac{29{,}000}{15{,}700} = -1 = +0.83$$

For the cone region, $r_1 = 14.66$ cm (5.77 in.), $t_{min} = 0.010$ cm (0.004 in.). At one atmosphere pressure

$$Pr_1 = (10.13)(14.66) = 148.3\ N/cm\ (85\ lb/in.)$$

$$S = \frac{Pr_1}{t} = \frac{(148.3)}{(0.010)} = 14{,}830\ N/cm^2\ (21{,}200\ psi)$$

which is less than the yield stress, 20,700 N/cm^2 (30,000 psi), for annealed 321 stainless steel.

If the tension load between adjacent meridians is assumed constant, because of the reduction in radius from 24.5 cm (9.65 in.) to 19.25 cm (7.58 in.) in the cone section, there is an increase in load per unit of circumference.

$$S_{\phi\ INNER} = \frac{24.5}{19.25}\ (148.3) = 188.7\ N/cm\ (108\ lb/in.)$$

At an angle of 0.42 rad (24°) to the longitudinal axis, the longitudinal component of this load is

$$(188.7)\ [\cos 0.42\ rad\ (24°)] = 172\ N/cm\ (98.5\ lb/in.)$$

which is less than the 175 N/cm (100 lb/in.) desired.

Acoustic Analysis.- Requirements for the tension membrane test specimen include withstanding an acoustic noise level of 160 dB applied for 450 seconds and 167 dB applied for 60 seconds. The method of analysis used is that of Ref. 2-2;

$$S_{rms} = \left(\frac{\pi\ d\ \phi_0}{4\delta}\right)^{\frac{1}{2}} S$$

where

S_{rms} = Random stress (rms), N/cm^2 (psi)

δ = Damping ratio, (% of critical damping)

d = Resonant frequency in the fundamental mode, Hz

ϕ_0 = Fluctuating pressure spectral density, $\frac{(N/cm^2)^2}{Hz}\left(\frac{psi^2}{Hz}\right)$

S_0 = Stress due to 1 psi uniform pressure, $\frac{N}{cm^2}$ (psi)

Frequency of the membrane will be calculated for a planar rectangular membrane. This will give a lower frequency than if curvature is considered, which will result in a higher calculated stress than in the actual case. The fundamental frequency will be calculated from:

$$f_{mn} = \tfrac{1}{2}\sqrt{\frac{gZ_L}{w}\left(\frac{m^2}{a^2} + \frac{n^2}{b^2}\right)} \quad \text{(Ref. 2-3)}$$

where

f_{mn} = frequency for mode shape, Hz

g = acceleration of gravity, cm/sec^2 ($in./sec^2$)

Z_L = uniform tension per unit length, N/cm (lb/in.)

w = weight of membrane per unit area, kg/cm^2 ($lb/in.^2$)

a = membrane width, cm (in.)

m,n = mode shapes, widthwise, lengthwise

b = membrane length, cm (in.)

The lowest (fundamental) mode of vibration will be obtained by m = 1, n = 1. Membrane width will be taken equal to the ring spacing and membrane length will be the developed length of the circumference of the outer jacket. Calculations are presented for a membrane thickness of 0.010 cm (0.004 in.), a ring spacing of 11.43 cm (4.5 in.), and a circumference of 155.2 cm (61.1 in.). A 11.43 cm (4.5 in.) ring spacing results in a longitudinal load of 77.0 N/cm (44.1 lb/in.) in the membrane shell under a one atmosphere external pressure. The weight of the 0.010 cm (0.004 in.) thick stainless steel membrane per unit area is 0.00008 kg/cm^2 (0.0011 $lb/in.^2$). The acceleration of gravity is taken as 980.7 cm/sec^2 (386.4 $in./sec^2$). The membrane fundamental frequency is calculated to be:

$$d = \frac{1}{2}\sqrt{\frac{(980.7)(77.0)}{(0.0000815)(9.807)}\left[\frac{1}{(11.43)^2}+\frac{1}{(155.2)^2}\right]} = 428 \text{ Hz}$$

The spectrum level which will be used in calculating the stress due to acoustic loading is calculated using data from Ref 2-4. Estimating the fundamental frequency as 430 Hz and using 167 dB as the overall level, the spectrum level is calculated to be:

$$\phi_0 = 0.000181 \frac{(N/cm^2)^2}{Hz} \quad (0.000381 \text{ (psi)}^2/Hz)$$

and for 160 dB:

$$\phi_0 = 0.0000385 \frac{(N/cm^2)^2}{Hz} \quad (0.000081 \text{ (psi)}^2/Hz)$$

The damping ratio is assumed to be 0.016. Stress at unit uniform pressure

$$S = \frac{Pr_1}{t}$$

where

S = stress due to a unit uniform pressure

r_1 = maximum membrane radius

t = membrane thickness.

For a ring spacing of 11.43 cm (4.5 in.), r_1 max = 7.62 cm (3.0 in.)

$$S = \frac{(1)(7.62)}{(0.010)} = 762 \text{ N/cm}^2 \quad (1105 \text{ psi})$$

The random stress at 167 dB is:

$$S_{rms} = \left[\frac{(\pi)(430)(0.000181)}{(4)(0.016)}\right]^{\frac{1}{2}} (762) = 1480 \text{ N/cm}^2 \quad (2120 \text{ psi})$$

If we conservatively assume that the peak stress occurs at the natural frequency, the peak stress will be:

$$S_{peak} = 3S_{rms} = 3(1480) = 4440 \text{ N/cm}^2 \quad (6360 \text{ psi})$$

The static stress due to one atmosphere external pressure is:

$$S = \frac{(10.13)(7.62)}{(0.010)} = 7719 \text{ N/cm}^2 \quad (11{,}197 \text{ psi})$$

Maximum dynamic stress will be:

$$S_{max} = 4440 + 7719 = 12{,}159 \text{ N/cm}^2 \text{ (17,637 psi)}$$

This level must be sustained for a number of cycles, n, equal to the fundamental frequency times the exposure time:

$$n = (430)(60) = 25{,}800 \text{ cycles}$$

Information from Ref 2-5 gives the endurance limit of annealed 321 stainless steel as 26,200 N/cm^2 (38,000 psi), indicating that the exposure planned is safe from a sonic fatigue viewpoint. The additional exposure at 160 dB for 450 seconds will now be checked.

$$S_{rms} = \left[\frac{\pi(430)\ (0.0000385)}{4(0.016)}\right]^{\frac{1}{2}} (762) = 687 \text{ N/cm}^2 \quad (980 \text{ psi})$$

$$S_{peak} = 3(687) = 2061 \text{ N/cm}^2 \quad (2940 \text{ psi})$$

Maximum dynamic stress is:

$$S_{max} = 2061 + 7719 = 9780 \text{ N/cm}^2 \text{ (14,186 psi)}$$

Number of cycles, exposure:

$$n = (430)(450) = 194{,}000 \text{ cycles}$$

Again the stress level and the number of cycles represent a safe exposure level when compared to the endurance limit of the annealed stainless steel sheet.

Lateral Structural Vibration of Full Tension Membrane.- A dynamic analysis of the tension membrane vacuum jacket was performed to determine its response to the acceleration spectral density given in Figure 2-4. The fundamental natural frequencies, G levels, and displacements were determined for several unsupported jacket lengths. The effective jacket flexural stiffness for the analysis was obtained using the Grumman STARS (shells of revolution) computer program. The analysis incorporated both isotropic and orthotropic behavior of the membrane. For orthotropic behavior, the modulus of elasticity in the hoop direction was assumed to be equal to 10% of the modulus in the axial direction. The geometry of a segment of the vacuum jacket is given in Figure 2-5.

The natural frequency of a simply supported beam is given (Ref 2-6) by the expression

$$d = \frac{\pi}{2}\sqrt{\frac{EIg}{wL^4}}$$

where

EI = effective flexural stiffness of beam, N/cm^2 ($lb/in.^2$)

g = gravitational acceleration, 980.7 cm/sec^2 (386 $in./sec^2$)

w = beam weight per unit span 0.0221 kg/cm, (0.124 lb/in.)

L = beam support spacing, cm (in.)

The peak response to a uniform spectral density is obtained (Ref 2-6) from

$$G = 3\left(\frac{Q_F 2\pi\ dg_0}{4}\right)^{\frac{1}{2}}$$

where

Q_F = magnification factor for light damping (assumed = 30)

d = fundamental natural frequency, Hz/sec

g_0 = acceleration spectral density obtained from Figure 2-4, g^2/Hz

G = acceleration, g.

The maximum deflection of uniformly loaded simply supported beam is

$$\Delta = \frac{5\bar{w}L^4}{384\ EI}$$

where $\bar{w}$ = G x w, N/cm (lb/in.) and the maximum bending moment

$$m = \frac{\bar{w}L^2}{8}$$

The above calculations are carried out in Table 2-2.

TABLE 2-2. - RESPONSE OF VACUUM JACKET

Behavior	Effective Stiffness		Support Spacing		Natural Frequency	Spectral Density	Peak Response	Dynamic Load		Jacket Deflection		Bending Moment		Bending Load Intensity	
	N/cm^2	$lb/in.^2$	m	ft	Hz	g^2/Hz	g	N/cm	lb/in.	cm	in.	cm-N	in.-lb	N/cm	lb/in.
Isotropic	$30.8x10^6$	$44.6x10^6$	1.52	5	162.6	0.340	153.3	33.3	19.0	0.183	0.072	$96.6x10^3$	8,550	48.3	27.6
	$30.8x10^6$	$44.6x10^6$	3.05	10	40.7	0.275	69.0	15.0	8.56	1.32	0.518	$174x10^3$	15,400	87.0	49.7
	$30.8x10^6$	$44.6x10^6$	6.10	20	10.2	0.074	17.9	3.89	2.22	5.49	2.16	$181x10^3$	16,000	92.1	52.6
Orthotropic	$5.74x10^6$	$8.32x10^6$	1.52	5	68.9	0.340	99.6	21.6	12.35	0.638	0.251	$62.9x10^3$	5,570	31.5	18.0
	$5.74x10^6$	$8.32x10^6$	3.05	10	17.2	0.120	29.6	6.43	3.67	3.02	1.19	$74.7x10^3$	6,610	37.3	21.3
	$5.74x10^6$	$8.32x10^6$	6.10	20	4.3	0.032	7.7	1.68	0.96	12.7	4.99	$78.2x10^3$	6,920	39.0	22.3

Calculations also show that the peak stress in the 0.010 cm (0.004 in.) steel membrane reaches 86,100 N/cm^2 (125,000 psi) at the edge of the ring for a 3.05 m (10 ft) support spacing and is somewhat lower for a 1.52 m (5 ft) spacing. A 6.10 m (20 ft) support spacing is unacceptable since the maximum deflection exceeds the clearance between the jacket and the inner line. For a 3.05 m (10 ft) support spacing and assuming an orthotropic membrane, a 3.02 cm (1.19 in.) jacket deflection coupled with a 0.203 cm (0.080 in.) line deflection leaves a sufficient gap remaining from a 3.80 cm (1.5 in.) initial gap.

If the strength of the steel membrane is not greater than the 86,100 N/cm^2 (125,000 psi) level, a small thickness increase will be required in the membrane in the vicinity of the rings.

It should be noted that the foregoing analysis takes no theoretical advantage of the longitudinal tension already existing to increase the stiffness of the membrane. At 6.10 m (20 ft) spans, this would be an important effect. However, $m/\pi R^2$ is generally less than the 111 N/cm (63.5 lb/in.) due to external pressure so that longitudinal buckling cannot occur during vibration.

Longitudinal Acceleration.- The effect of longitudinal acceleration is to produce a tensile loading in the outer jacket, similar to the loading produced by pressure. Combining pressure and axial acceleration will produce an increase in the maximum tensile stress in the outer jacket. The effect of longitudinal acceleration, however, is small compared to the effect of pressure. If we assume a jacket weight of 3.86 kg/m (2.6 lb/ft), the load due to a longitudinal acceleration of 4g on a 3.05 m (10 ft) long line segment is:

$$P_L = (4)(3.05)(3.86) = 47.1 \text{ kg } (104 \text{ lb}).$$

The load per unit length around the circumference of the jacket is:

$$P_L \text{ (Unit)} = \frac{(47.1)(9.807)}{\pi(45.7)} = 3.22 \text{ N/cm } (1.83 \text{ lb/in.})$$

Load due to pressure is in the order of 175 N/cm (100 lb/in.) so that the effect of longitudinal acceleration is relatively minor.

Tie Downs - Tension Membrane Concept.-

Tie Down (External): External tie downs will be located at support rings. To assure proper installation of the rings into the Tension Membrane jacket, they will be split rings, machined in three sections. Between each section there will be a locking

wedge (Fig. 2-6). The tie down fitting will attach to the wedge. The wedge can be made of the same material as the jacket to allow brazing of components to ensure leak tightness. Figure 2-7 shows the integral and nonintegral types of external support fittings that could be applied to this concept. The choice of the support type would be dependent on details which would be examined in a typical design study.

Tie Down (Internal): Internal tie downs will also be at the support ring locations. To minimize heat loss, fiberglass struts will be used (Fig. 2-8). Optimum support spacing will be determined in the dynamic analysis of the inner line and jacket.

End Fixture: Figure 2-9 shows the end fixture configuration for the Tension Membrane test specimen. Proper vacuum seal is achieved by welding or brazing the jacket end detail to the inner line end fitting.

Fittings and Joints - Tension Membrane Concept.-

Fittings: As with the external and internal supports, all required fittings (i.e., pressure gage, vacuum acquisition point, etc) will be located at support rings. The fittings will be located in the wedge sections, which may be made of stainless steel. This makes the fitting, outer jacket, and ring compatible for welding or brazing. Fittings will be incorporated in a manner similar to the support fittings shown in Figure 2-7.

Joints: The following types of joints can be used with the Tension Membrane concept:

Bellows (Fig. 2-10)

Diaphragm (Fig. 2-11)

Foam in place (Fig. 2-12)

The choice of a particular joint would depend on the variables of a specific design application.

REFERENCES

2-1 *Structures Manual*, Grumman Aerospace Corporation.

2-2 T. F. Nelson: *An Investigation of the Effects of Surrounding Structure on Sonic Fatigue*. NASA CR 1536, May 1970.

2-3 S. Timoshenko: *Vibration Problems in Engineering*. D. Van Nostrand Company, Inc., Third Edition, p. 432.

2-4 *Vertical Tail Subsystem, Orbiter, Preliminary Technical Requirements*. North American Rockwell, Specification MC 621-0004, 22 September 1972.

2-5 *INCO Cr-Ni Stainless Steels*, International Nickel Company, Bulletin A, Sect. 1, 1963.

2-6 *Structures Manual, Section E, Dynamic Loads*, Grumman Aerospace Corporation.

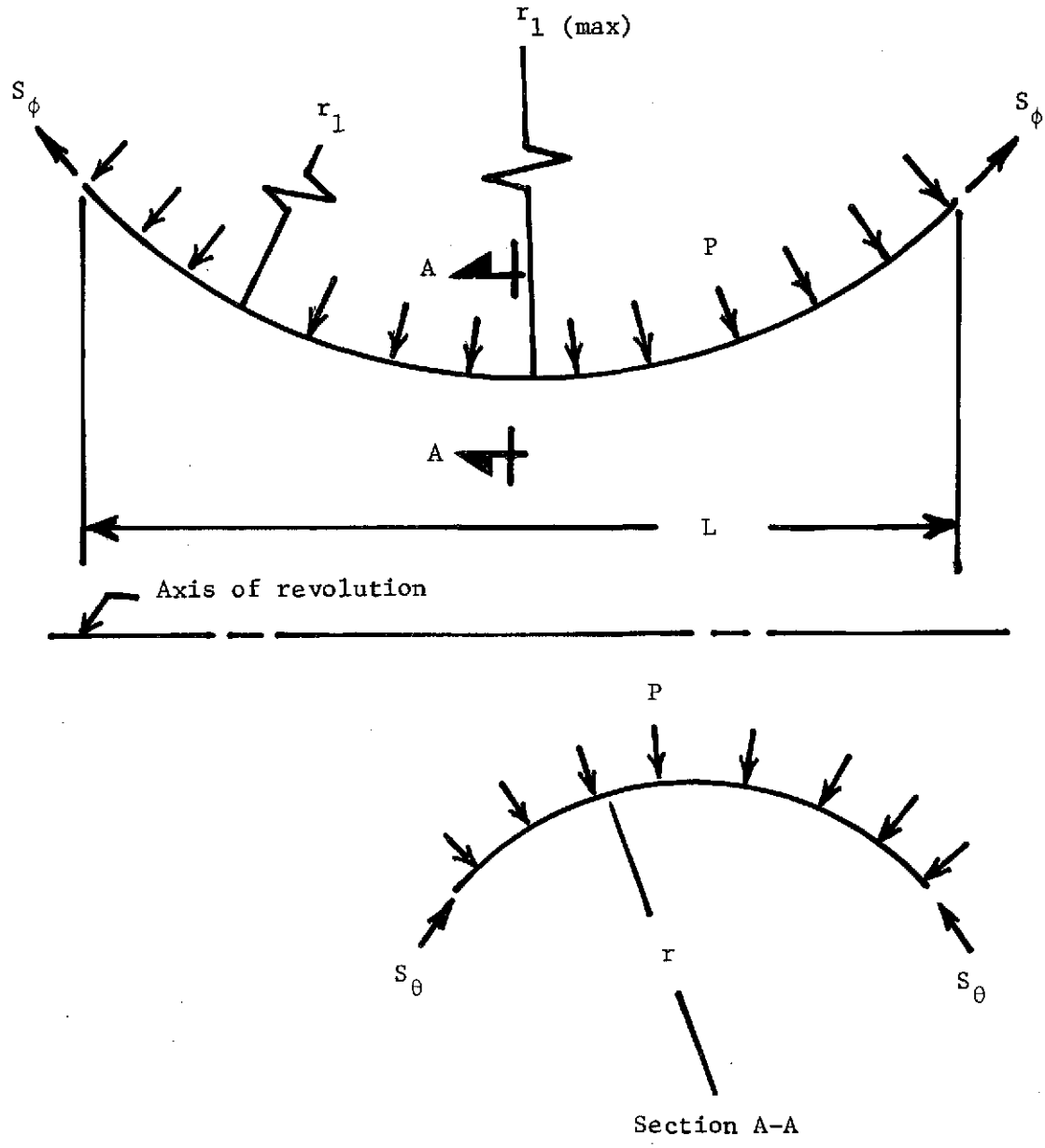

Figure 2-1. - Tension Membrane Notation

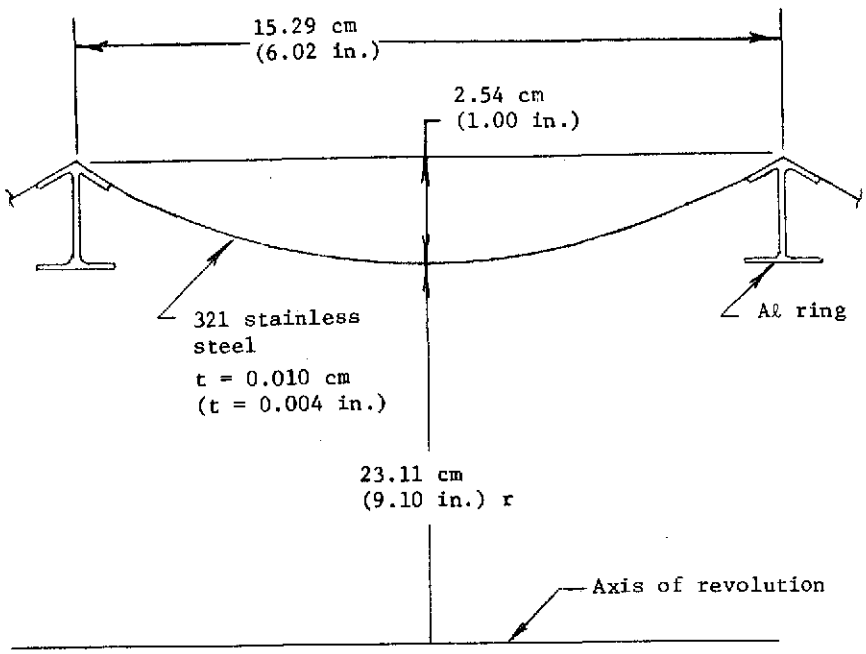

Figure 2-2. - Preliminary Tension Membrane Design

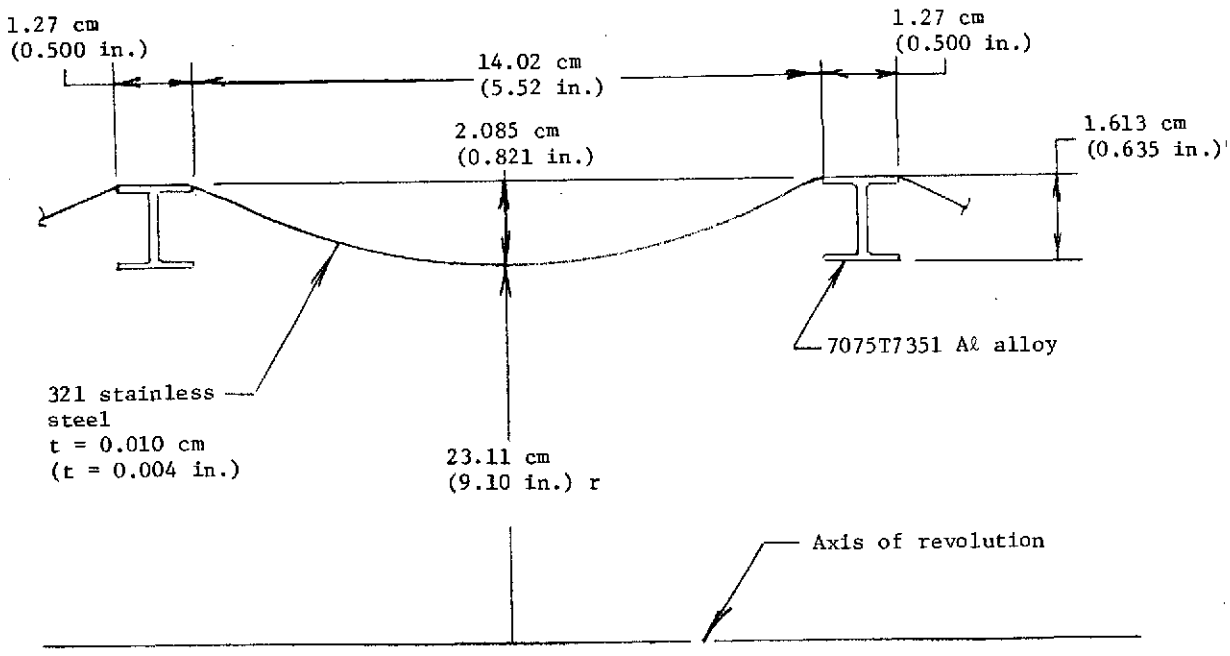

Figure 2-3. - Typical Bay Geometry, Final Model Design

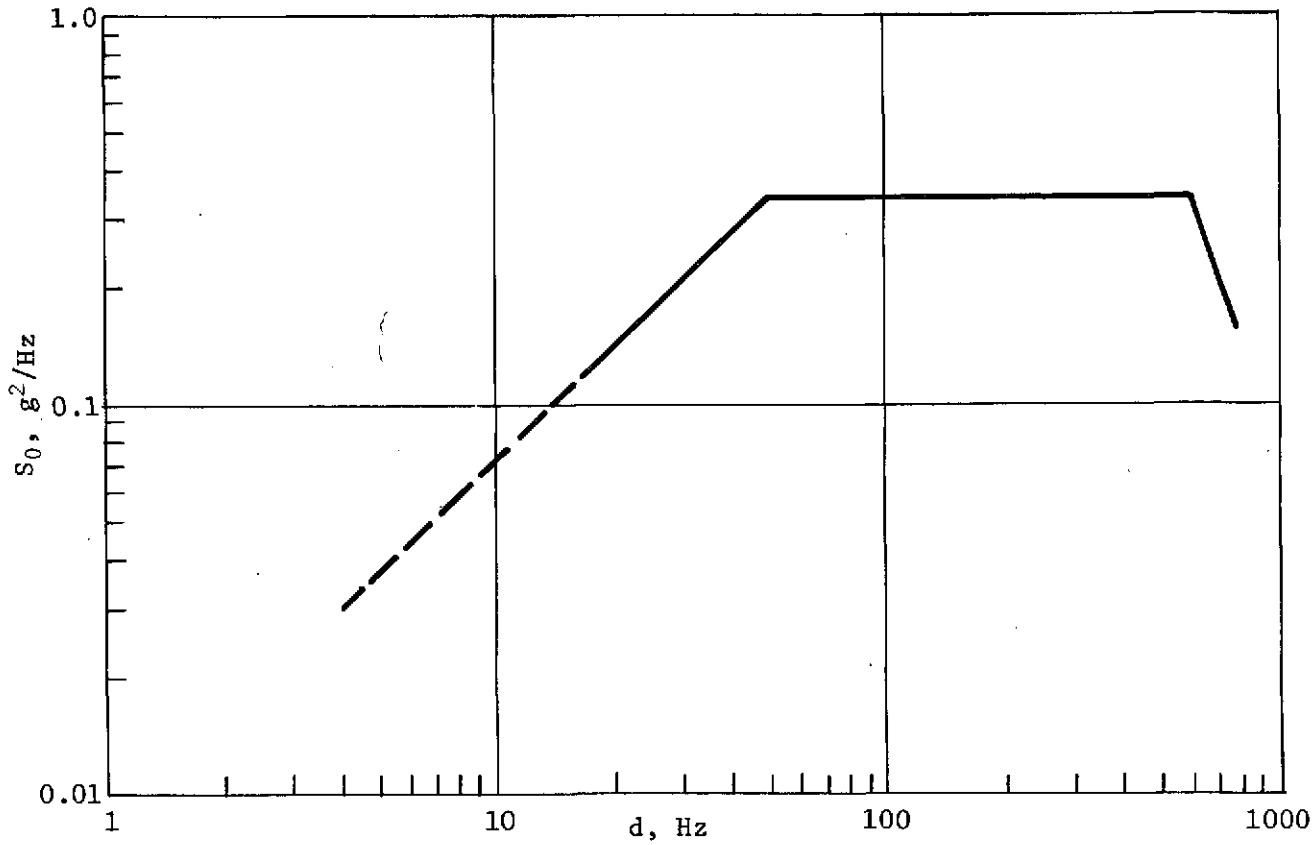

Figure 2-4. - Booster-Acceleration Spectral Density, S vs Frequency, d

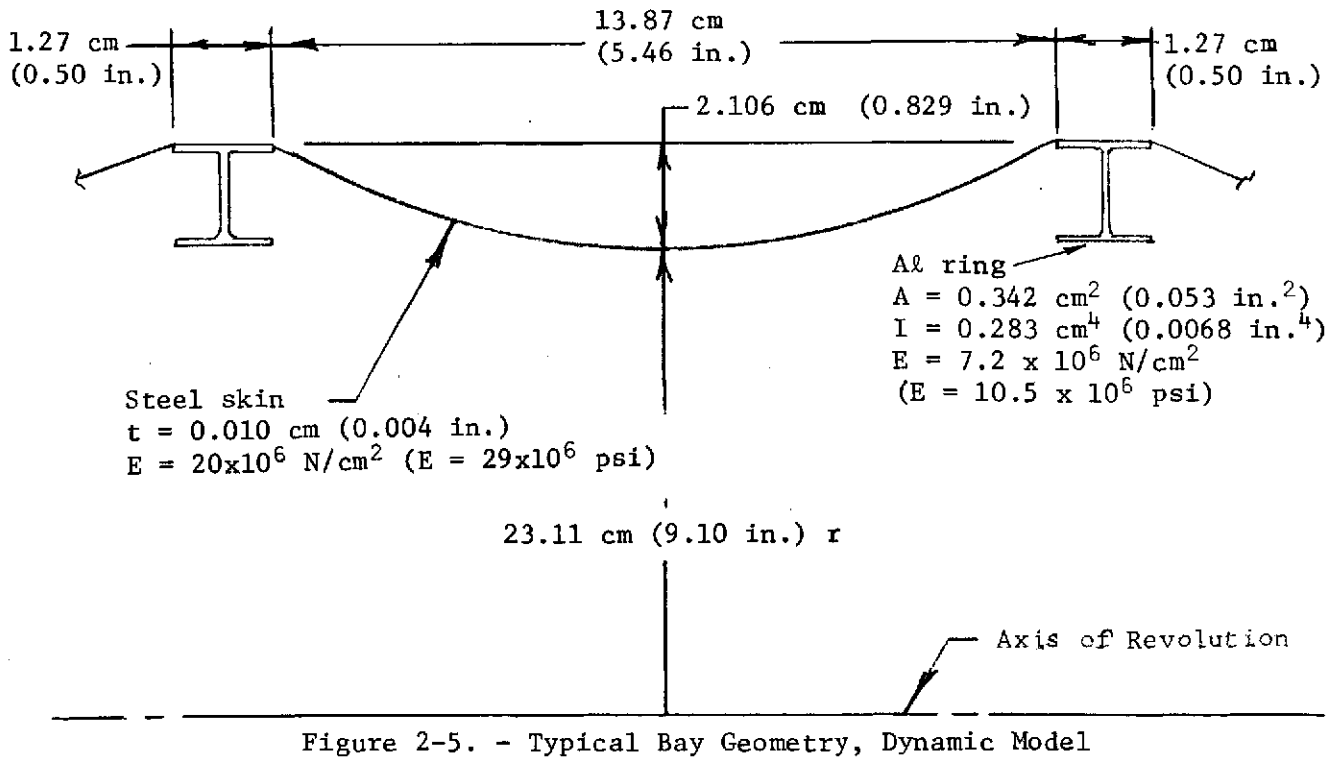

Figure 2-5. - Typical Bay Geometry, Dynamic Model

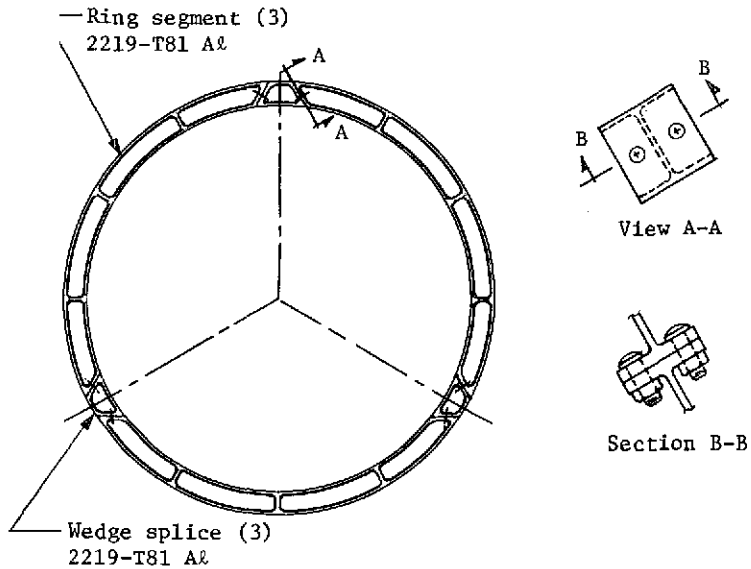

Figure 2-6. - Typical Ring Configuration Between Supports

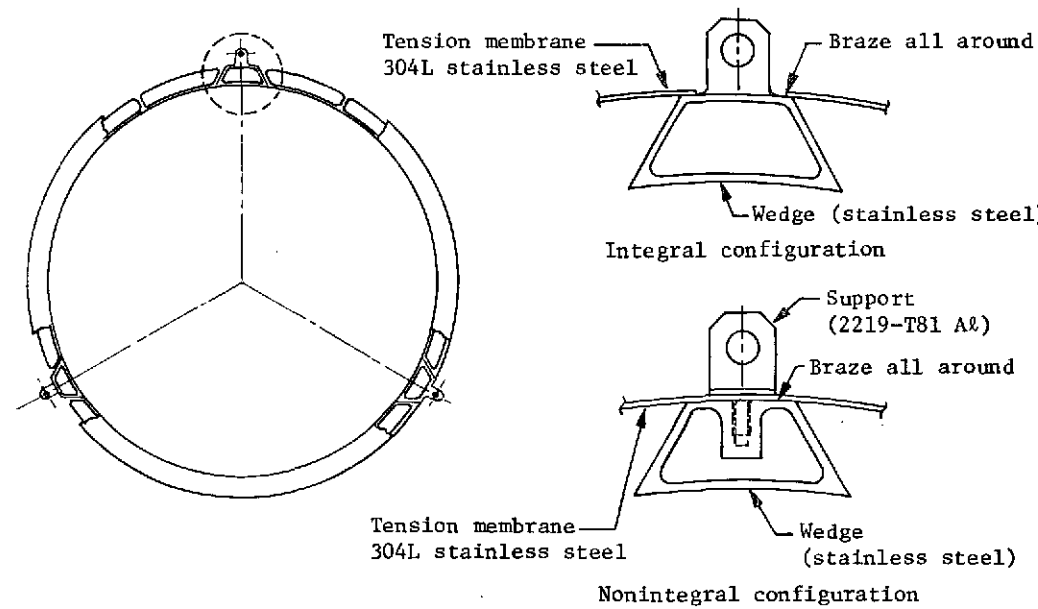

Figure 2-7. - Typical Ring Configuration at External Supports

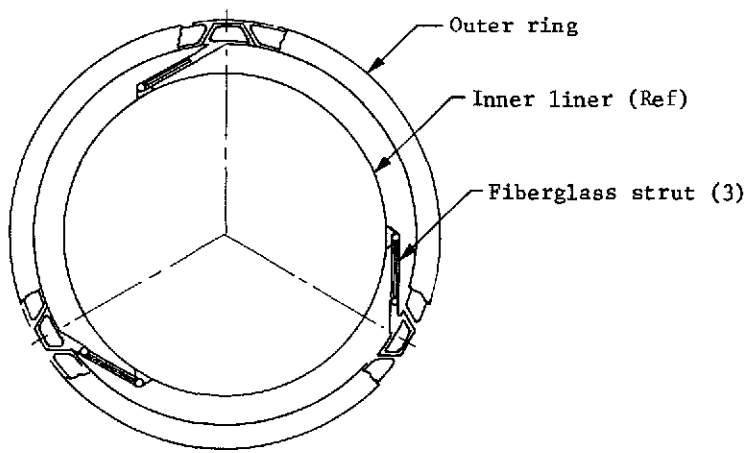

Figure 2-8. - Typical Ring Configuration at Internal Supports

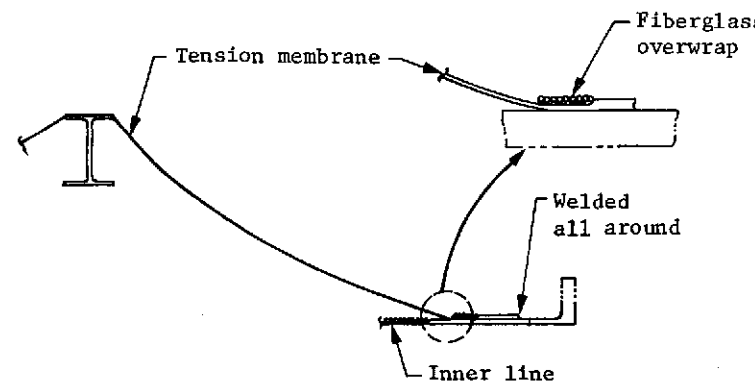

Figure 2-9. - End Fixture Configuration

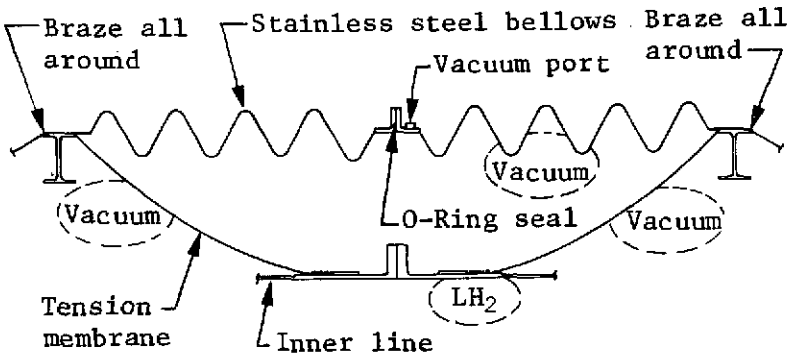

Figure 2-10. - Line Joint, Bellows Configuration

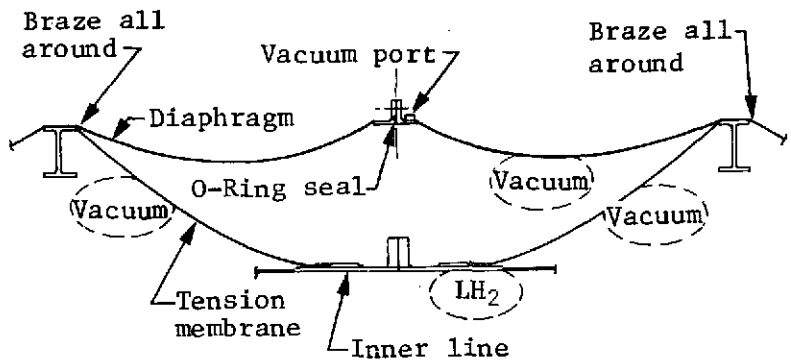

Figure 2-11 Line Joint, Diaphragm Configuration

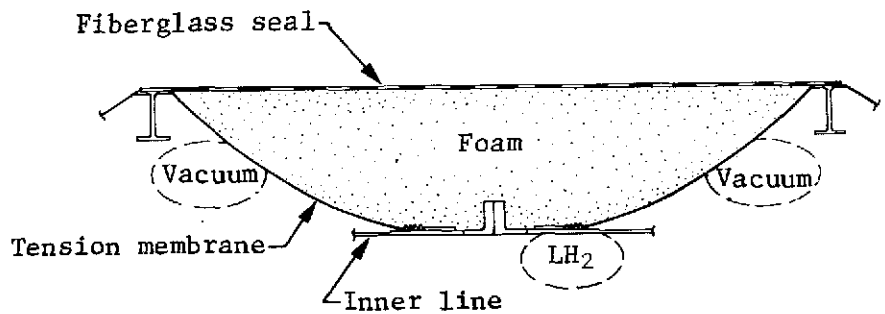

Figure 2-12. - Line Joint, Foam in Place Configuration

3. TASK II - PRELIMINARY TESTING

External pressure testing of the tension membrane concept is required to satisfy the Vacuum Shell Integrity portion of Task II of the basic NASA contract. Longitudinal and circumferential strain gages (Fig. 3-1) were applied to the tension membrane jacket at points of predicted high stress. Gages were applied back-to-back on the internal and external surfaces of the jacket. For preliminary testing, the jacket was welded to a stainless steel dummy line. An engineering vacuum was drawn on the specimen and strain readings recorded (Table 3-1). Having gages placed back-to-back, one can analytically separate the membrane stresses from the membrane-plus-bending stresses sensed by the strain gages. When the jacket was welded to the composite inner line the test was repeated and the strain readings recorded (Table 3-2).

Tension Membrane Jacket and Dummy Inner Line.- In testing the tension membrane jacket installed on a dummy inner line, the vacuum was increased incrementally and relieved until a vacuum of 711 mm Hg (28 in. Hg) was achieved. After this, the jacket was cycled between zero vacuum and 711 mm Hg (28 in. Hg) nine times to verify its structural integrity. Strain readings from the cycling portion of the data are judged to be representative of the action of the membrane and are averaged for the numerical calculations.

Using the equations of equilibrium for a circular cylinder, the strain measurements may be transformed into hoop and longitudinal stresses. Consider an element of the cylinder wall. Let x designate the longitudinal direction and h the hoop direction. The expression for strain in the x direction is:

$$e_x = \frac{1}{E}\left[S_x - \nu\left(S_h + S_z\right)\right] \qquad [3\text{-}1]$$

where

e_x = strain in the x-direction,

E = material's modulus of elasticity,

S_x = stress in the x-direction,

ν = Poisson's ratio,

S_h = stress in the hoop direction,

S_z = stress in the z-direction.

TABLE 3-1. - STRAIN INDICATOR READINGS, TENSION MEMBRANE JACKET ON DUMMY LINE, ASSEMBLY #2

Vacuum pressure, N/cm^2 (in. Hg)	Strain, μcm/cm (μin./in.)							
	Circuit							
	1	2	3	4	5	6	7	8
0	0	0	0	3	-1	-2	2	0
3.4 (10)	134	-19	33	-264	50	-174	59	-115
0	-5	6	12	-14	2	-3	-4	-4
3.4 (10)	146	-2	34	-274	52	-185	63	-121
6.8 (20)	442	324	-71	-579	64	-349	206	-194
3.4 (10)	183	71	13	-323	48	-188	82	-112
0	8	16	0	-26	1	-10	2	-4
3.4 (10)	180	42	11	-337	52	-202	84	-129
6.8 (20)	426	333	-79	-588	64	-350	206	-198
9.5 (28)	338	-234	89	-403	136	-390	302	-342
8.4 (25)	302	-171	66	-393	117	-342	259	-296
6.8 (20	262	-97	42	-367	96	-283	206	-241
5.1 (15)	212	-36	23	-315	74	-223	155	-185
3.4 (10)	169	-14	18	-262	57	-167	111	-136
1.7 (5)	101	11	15	-152	30	-82	64	-64
0	25	26	1	-31	0	-5	27	-1
9.5 (28)	328	-245	87	-398	139	-379	298	-343
0	27	23	0	-28	0	0.	29	0
9.5 (28)	323	-272	82	-399	141	-379	298	-343
0	26	12	-14	-26	0	-1	28	-2
9.5 (28)	322	-263	78	-464	140	-376	291	-346
0	25	17	-10	-35	1	-2	26	-3
9.5 (28)	323	-274	76	-404	142	-378	299	-347
0	27	9	-19	-31	-1	-3	26	-6
9.5 (28)	317	-270	67	-412	138	-380	284	-353
0	25	8	-21	-42	-5	-8	19	-13
9.5 (28)	318	-277	65	-419	136	-384	279	-359
0	20	8	-23	-50	-5	-10	16	-16
9.5 (28)	322	-290	63	-423	133	-389	298	-364
0	16	8	-25	-60	-10	-15	0	-23
9.5 (28)	315	-282	58	-430	130	-390	271	-367
0	16	6	-25	-66	-10	-18	4	-27
9.5 (28)	314	-286	55	-434	127	-395	269	-372
0	9	4	-28	-71	-14	-23	-1	-34

TABLE 3-2. - STRAIN INDICATOR READINGS, TENSION MEMBRANE JACKET ON COMPOSITE INNER LINE, ASSEMBLY #2

Vacuum pressure, N/cm^2 (in. Hg)	Strain, μcm/cm (μin./in.)							
	Circuit							
	1	2	3	4	5	6	7	8
0	0	0	0	0	0	0	0	0
3.4 (10)	50	-88	70	-190	54	-120	40	-124
1.7 (5)	18	-47	32	-94	24	-58	12	-59
0	-4	-10	0	-11	-2	-5	-3	-4
3.4 (10	54	-88	68	-189	54	-118	40	-122
6.8 (20)	136	-294	135	-355	116	-264	116	-258
5.1 (15)	92	-126	102	-272	83	-182	67	-181
3.4 (10)	58	-84	73	-196	56	-120	38	-120
1.7 (5)	28	-51	40	-118	26	-69	18	-70
0	-4	-8	0	-16	-1	-5	-1	-7
3.4 (10)	49	-82	65	-195	52	-114	41	-122
6.8 (20)	136	-212	138	-370	119	-275	126	-270
10.1 (30)	331	-361	202	0430	184	-375	208	-368
8.4 (25)	172	-258	160	-382	144	-304	148	-298
6.8 (20)	132	-201	138	-348	121	-255	116	-253
5.1 (15)	93	-134	107	0281	89	-187	77	-188
3.4 (10)	61	-83	88	-206	59	-125	44	-126
1.7 (5)	22	-41	37	-105	26	-57	16	-60
0	-4	-6	3	-19	0	-5	-1	-5
0	-2	-6	3	-12	2	-2	-2	-2
1.7 (5)	8	-22	12	-48	11	-25	8	-26
10.1 (30)	212	-362	204	0432	188	-376	209	-368
1.7 (5)	12	-28	32	-76	20	-39	12	-38
10.1 (30)	214	-359	206	-430	188	-380	211	-368
1.7 (5)	10	-20	27	-64	15	-31	13	-34
10.1 (30)	230	-370	212	-433	195	-386	220	-376
1.7 (5)	13	-28	34	-75	20	-37	13	-38
10.1 (30)	232	-374	214	-431	194	-386	220	-378
1.7 (5)	13	-28	33	-74	20	-38	12	-36
10.1 (30)	218	-345	200	-421	181	-366	201	-358
1.7 (5)	9	-24	30	-66	16	-31	11	-31
0	-3	-4	8	-19	1	-3	1	-2

If we assure that the cylinder acts in membrane fashion $S_z = 0$, then Equation [3-1] reduces to:

$$e_x = \frac{1}{E}\left[S_x - \nu\left(S_h\right)\right] \qquad [3\text{-}2]$$

Similarly, the expression for strain in the h direction is:

$$e_h = \frac{1}{E}\left[S_h - \nu\left(S_x\right)\right] \qquad [3\text{-}3]$$

Combining Equations [3-2] and [3-3]. expressions for stresses in the x and h directions in terms of the measured strains, e_x and e_y, are obtained:

$$S_x = \frac{E}{(1-\nu^2)}\left[e_x + \nu e_h\right] \qquad [3\text{-}4]$$

$$S_h = \frac{E}{(1-\nu^2)}\left[e_h + \nu e_x\right] \qquad [3\text{-}5]$$

Referring to Table 3-1 and Figure 3-1, Circuits 1 and 3 are back-to-back longitudinal gages in one location and 5 and 7 are back-to-back longitudinal gages 3.14 rad (180°) around the jacket. Circuits 2 and 4 are back-to-back hoop gages adjacent to gages 1 and 3, while circuits 6 and 8 are back-to-back hoop gages adjacent to gages 5 and 7.

The average change in strain for the four longitudinal strain gages for the nine cycles of zero to 711 mm Hg (28 in. Hg):

Gage 1 298 x 10^{-6} cm/cm (in./in.)

Gage 3 85 x 10^{-6} cm/cm (in./in.)

Gage 5 140 x 10^{-6} cm/cm (in./in.)

Gage 7 267 x 10^{-6} cm/cm (in./in.)

The membrane component is found by determining the algebraic mean of two back-to-back gages.

Gage 1, Gage 3 } membrane component = 192 x 10^{-6} cm/cm (in./in.)

Gage 5, Gage 7 } membrane component = 204 x 10^{-6} cm/cm (in./in.)

Thus, the average longitudinal membrane strain in the jacket, e_x, is 198 x 10^{-6} cm/cm (in./in.). Similarly, the average hoop membrane strain, e_h, is:

Gage 2 = -286 x 10^{-6}
Gage 4 = -379 x 10^{-6}
} -333 x 10^{-6}

Gage 6 = -376 x 10^{-6}
Gage 8 = -345 x 10^{-6}
} -361 x 10^{-6}

average = -347 x 10^{-6} cm/cm (in./in.) compression

From Equations [3-4] and [3-5], the longitudinal and hoop stresses are calculated:

$$S_x = \frac{20.0 \times 10^6}{[1-(0.3)^2]} [0.000198 + (0.3)(-0.000347)] =$$

2060 N/cm^2 (2990 psi)

$$S_h = \frac{20.0 \times 10^6}{[1-(0.3)^2]} [-0.000347 + (0.3)(0.000198)] =$$

-6320 N/cm^2 (9160 psi)

The high hoop stress indicates the unbuckled condition of the center bay (Fig. 5-25). Due to the resistance of this bay to buckling, a large proportion of the pressure load is carried hoopwise so that the longitudinal load is reduced from the load calculated based on assuming that all load is carried longitudinally, P_N = (10.13)(10.95) = 110.9 N/cm (63.5 lb/in.). The material thickness in the center bay after chem-milling was measured as approximately 0.0191 cm (0.0075 in.). If all the load were carried longitudinally, the predicted stress would be:

$$S_x = \frac{P_N}{t} = \frac{110.9}{0.0191} = 5800 \text{ N/cm}^2 \text{ (8470 psi)}$$

To meet the requirement of sustaining an ultimate load of 1.5 x one atmosphere external pressure, the shell must be able to sustain a stress of

$$S_{ULT} = 1.5(5800) = 8700 \text{ N/cm}^2 \text{ (12,700 psi)}$$

The yield stress of 321 annealed stainless steel is 24,000 to 31,000 N/cm^2 (35,000 to 45,000 psi) so that the Factor of Safety on pure membrane load is:

$$FS = \frac{24,000}{8,700} = 2.75$$

The presence of buckles on hoop segments of the membrane can be noted in photographs of the in-process testing (Fig. 5-26 through 5-30). However, when the load is relieved, the buckles almost all disappear. This indicates that the stresses are elastic (less than the yield stress) and that the Factor of Safety in these areas of local bending stress, compared to the ultimate tensile strength of annealed 321 stainless steel, 62,000 N/cm^2 (90,000 psi) is:

$$FS = \frac{62,000}{24,000} = 2.57$$

There are some few buckles that do not disappear when the pressure load is relieved. Let us assume that the stress in the area of these buckles is 34,500 H/cm^2 (50,000 psi). The strain associated with this stress is:

$$e = \frac{S}{E} = \frac{34,500}{20,000,000} = 0.00173 \text{ cm/cm (in./in.)}$$

or approximately 0.17%. The strain capability of annealed 321 stainless steel is over 40% (Ref 3-1) so that further addition of load does not increase the stress but just increases the plastic strain which may, in fact, lower the local stress. In addition, the ultimate tensile strength of 321 stainless steel is increased from 62,000 N/cm^2 (90,000 psi) to 124,00 N/cm^2 (180,000 psi) by cold working.

It is felt that the most representative assessment of the structural capability is obtained by comparing the membrane stress to the material yield stress. This is so because large membrane strains would cause the jacket to change its shape and would require a re-analysis of the jacket structure. For this reason, the Factor of Safety as determined by testing with the dummy line is calculated to be 2.75.

The vacuum tests performed earlier on the dummy line were repeated with the tension membrane jacket welded to the composite inner line. This data is reported in Table 3-2. Following the procedure described above, the longitudinal and hoop stresses were calculated for the 5 cycles from zero to 762 mm Hg (30 in. Hg). Stresses were very similar to those for the dummy line tests;

S_x = 2040 N/cm^2 (2950 psi)

S_h = -6890 N/cm^2 (-10,000 psi)

Thus, the Factor of Safety for external pressure loading on the test specimen is 2.75.

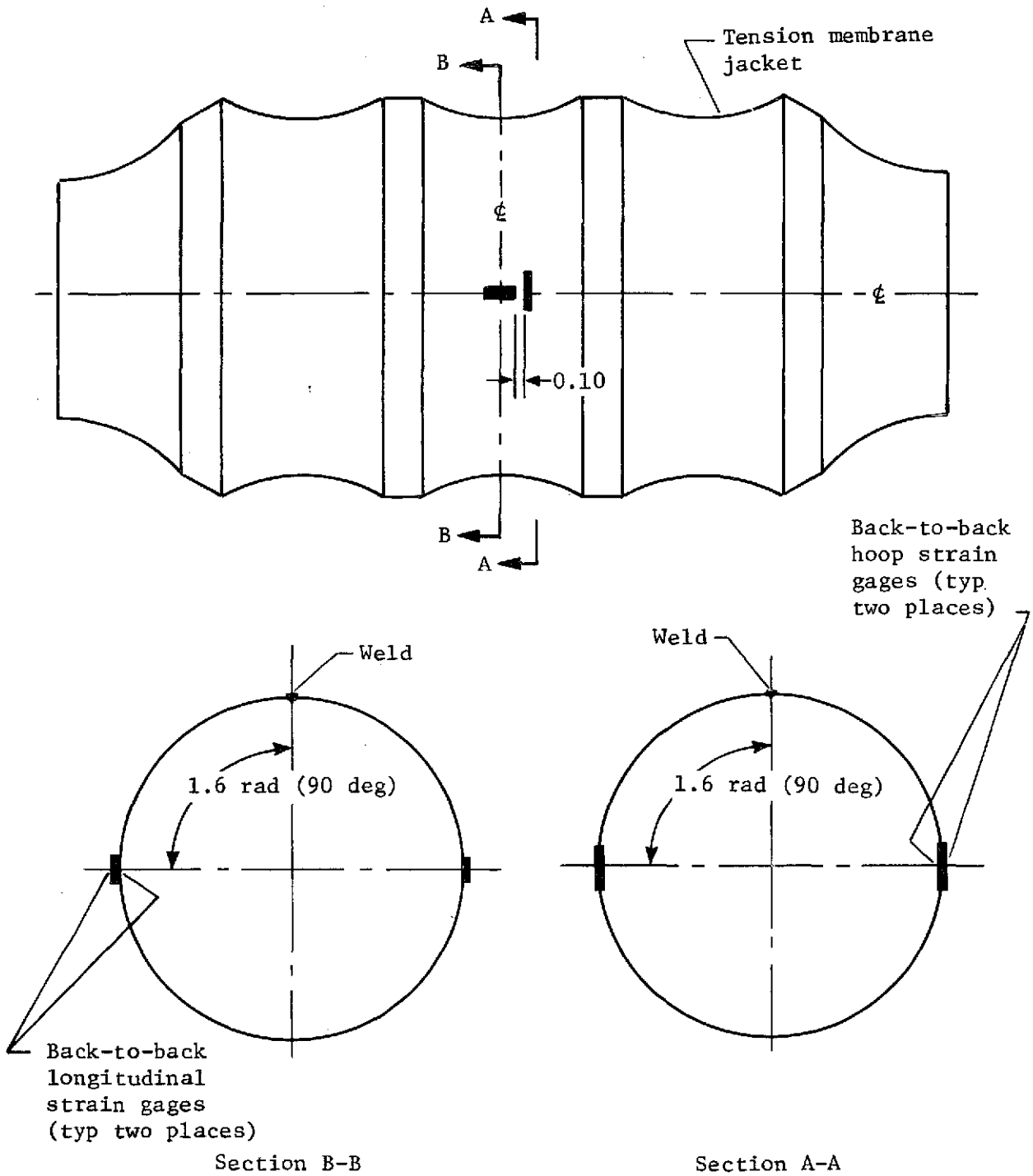

Figure 3-1. - Strain Gages Location - Tension Membrane Jacket

4. TASK III - TEST SPECIMEN DESIGN

Design conditions specified for the tension membrane specimens called for a clear distance of 3.81 cm (1.5 in.) from the inner line to the vacuum jacket and the ability to support one atmosphere of external pressure with a 1.5 Factor of Safety. The design objective is to minimize structural weight while limiting the axial load imposed on the inner line to 175 N/cm (100 lb/in.).

Membrane Shape.- The design configuration quickly came to a ring spacing of 12.70 cm (5.0 in.) and a sag between rings of 2.54 cm (1 in.). Variations around these dimensions gave the required 175 N/cm (100 lb/in.) limit load on the inner line. This design was not a minimum weight design. The final configuration selected was a ring spacing of 14.02 cm (5.52 in.) and a sag (from the theoretical cusp points) of 2.54 cm (1 in.). In the process of refining the design it became apparent that a weight saving could be achieved and local stresses decreased if the membrane shape were flattened over the ring locations. This was done, as shown in Figure 4-1. Analysis of the membrane shape assumes a true catenary curve. For ease of manufacturing, membrane segments were described using circular arcs in the engineering drawings, varying calculated loads by a small percentage.

Thickness of the membrane portions of the outer jacket is $0.0076\ ^{+0.010}_{-0.000}$ cm, ($0.003\ ^{+0.004}_{-0.000}$ in.) Calculations performed for a thickness of 0.010 cm (0.004 in.) indicated a sufficient margin of safety for the 0.0076 cm (0.003 in.) membrane. It was assumed that the final chem-milled thickness would be approximately 0.0127 cm (0.005 in.).

Support Rings.- Since the jacket will be formed first and the rings installed later, the support rings were designed as split rings. Each ring had three major segments and one small locking segment. To achieve maximum stiffness for the minimum weight, aluminum was selected for the ring material. All segments of the center rings were aluminum. The center rings are I-shaped in cross-section, and are designed for minimum weight (Figure 4-2). The end rings, at the intersection of the straight membrane and the end cone, were to provide for vacuum valves and instrumentation. Since these rings would provide access holes for adapters, they were left rectangular in section and no attempt was made to minimize their weight. The three major sections of the end rings were machined from aluminum. The access holes for the adapters were placed in the small locking sections and these sections were machined from 321 stainless steel. By making the locking segments stainless steel, it was possible to braze the adapter, vessel skin, and ring in one operation, and greatly improve the vacuum quality of the joint.

End Detail.- Balancing the axial load from the membrane and supporting the pressure load at the line closure are the tasks performed by the end cone. The attachment of the end cone to the inner line is made by welding the jacket to a thickened ring at the end of the inner line. Because of cone angle, a radially outward load component is present at the intersection of the end cone and the end collar of the tension membrane. A glass-fiber strap resists this load. After the end weld is made between the jacket and the inner line, a shallow channel shaped member is bonded around the outer surface of the end collar. The depression in the channel serves to retain the glass-fiber strap while it is being laid up. Where cured, the glass-fiber strap has the capacity to resist the vertical component of the membrane load.

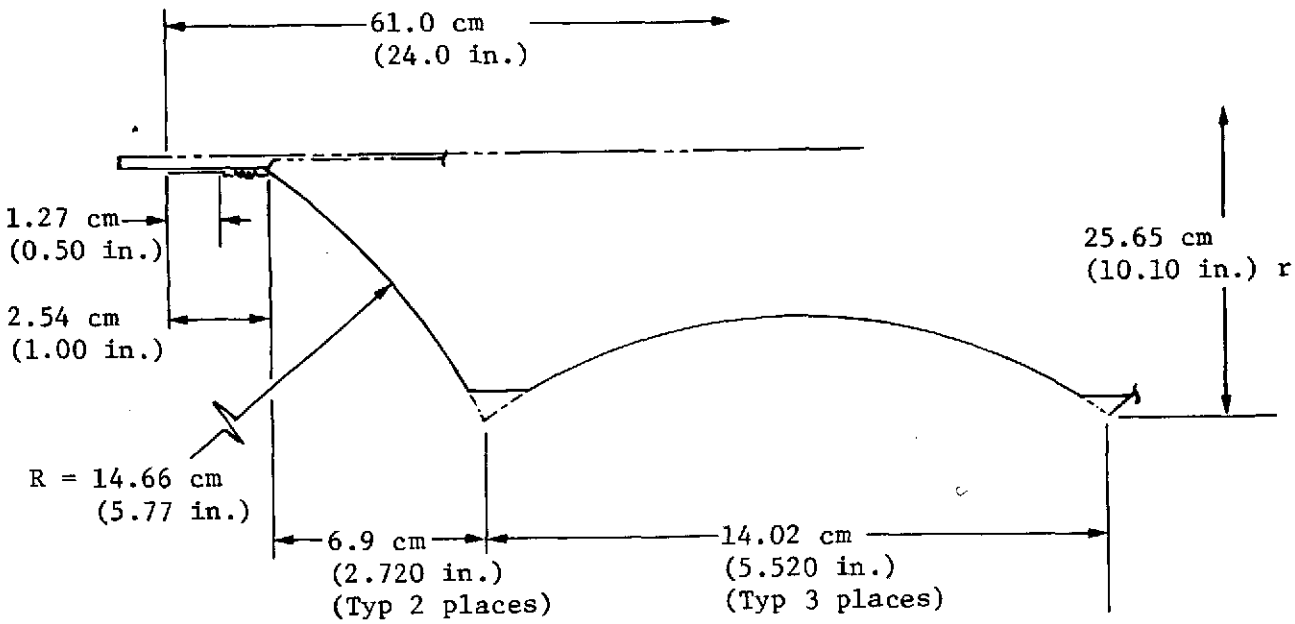

Figure 4-1. - Tension Membrane, Preliminary Configuration

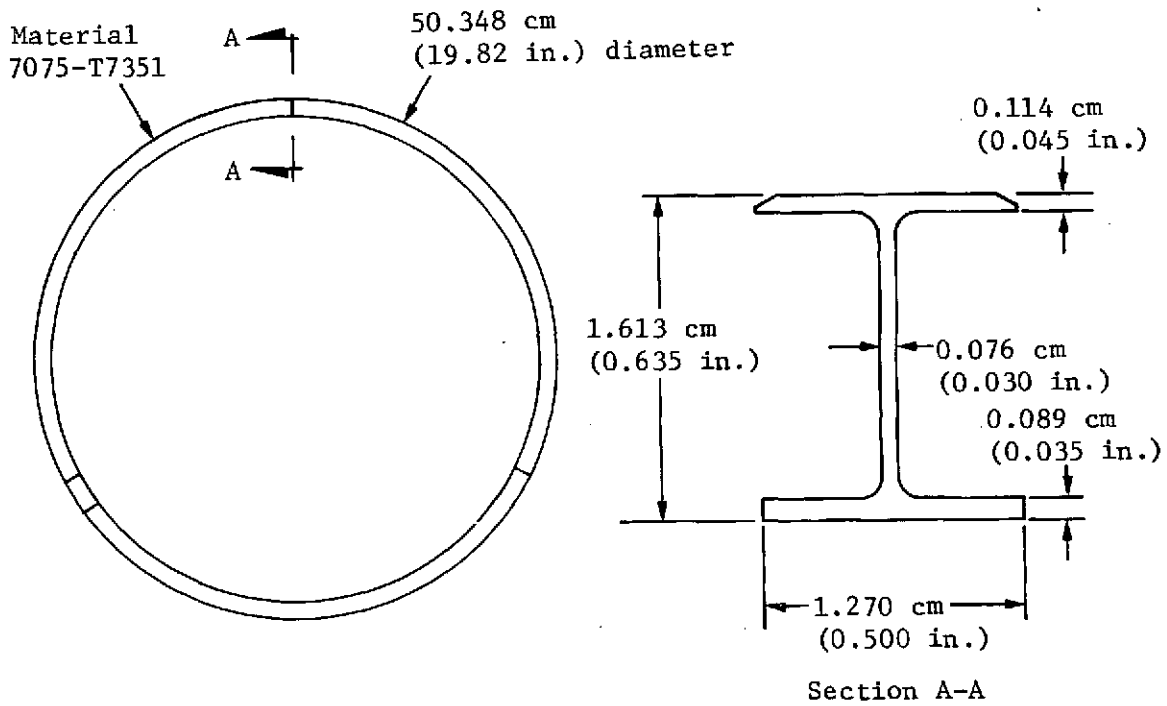

Figure 4-2. - Central Ring Configuration

5. TASK IV - TEST SPECIMEN FABRICATION

Forming of the light gage sheet to the tension membrane configuration can be accomplished in a number of ways. For designs that will operate near the tensile yield stress of the membrane material (small sag, large ring spacing), the shape can be formed by drawing a vacuum on the cylinder while at the same time applying an axial load. For designs with relatively deep sages, the stress in the membrane wall is low and forming must be done by mechanical means. In this case two options exist: (1) to make a welded cylinder of the maximum jacket diameter and form convolutions by spinning or other mechanical means, and (2) to make a welded cylinder of the minimum diameter required and expand by internal pressure against an external die to achieve the desired shape.

Grumman elected to form the tension membrane shape by expanding a minimum diameter cylinder. Two options were considered: (1) expanding a very light gage, 0.010 cm (0.004 in.) cylinder purchased from an outside vendor, or (2) welding an approximate 0.0457 cm (0.018 in.) thick cylinder, expanding it to the desired shape, and then chem-milling the forming to achieve the required wall thickness. The second approach was selected.

Element Fabrication and Assembly.- The specimen begins as an 0.0381 cm (0.015 in.) to 0.0457 cm (0.018 in.) cylinder welded by Grumman. The following major steps comprise the specimen fabrication:

1) weld 0.0381 cm (0.015 in.) to 0.0457 cm (0.018) thick stainless steel cylinders;

2) machine a solid model of the tension membrane;

3) fabricate a two-piece female die around the solid model;

4) retain the two-piece die;

5) expand the basic 38.6 cm (15.2 in.) diameter cylinder to to the tension membrane shape;

6) inspect the formed part to determine minimum wall thickness;

7) Chem-mill formed part to desired minimum wall thickness;

8) machine split support rings;

9) install support rings;

10) vacuum test using dummy inner line;

11) join tension membrane to composite inner line;

12) vacuum test assembly.

The completion of these steps proceeded in the following manner:

Preform Cylinders: Thirteen cylinders to be used as preforms in the bulge forming process were fabricated. These cylinders were made from 0.0457 cm (0.018 in.) thick stainless steel sheet, rolled to shape and butt welded. The cylinders were x-ray inspected after one weld pass and some porosity was indicated; after a second weld pass, the cylinders were accepted.

Adapter Assembly: The detail parts for the vacuum valve and vacuum gage assembly and for the Deutsch connector adapters were fabricated. The Deutsch connectors, Veeco valves and thermocouple vacuum gages were procured. Assembly of the vacuum valve/gage adapters was completed.

Dummy Line: To verify the vacuum performance of the tension membrane jacket before it is installed on the composite inner line, the jacket is vacuum tested after installation on a heavyweight dummy inner line. This setup is also used to perform the Task II test of the tension membrane jacket. The dummy line is rolled from 0.241 cm (0.095 in.) thick stainless steel sheet and butt welded. Three lines were fabricated.

Center Rings: Fabrication of the segmented center rings was completed. Four rings were machined, two per vessel for two test specimens. Each ring is made in four segments, three equal length large segments and one shorter wedge-type segment. The three large segments are placed in the jacket and expanded with a tool and then the wedge section is inserted. The weight of rings averaged 0.181 kg (0.40 lb).

End Rings: Fabrication of the segmented end rings was completed. Four rings were machined. These rings were not designed for minimum weight as were the center rings, but were left solid in cross-section to provide for the vacuum ports and instrumentation leadthroughs. Installation procedure is similar to that for the center rings.

Bulging Tool: The elements of the bulging die were completed. On assembly it was found that certain modifications were required to assure proper performance. This additional work consisted of resurfacing the end plates, opening up attachment holes, and providing additional shims. Photos of a bulging sequence showing the bulging tool in operation are given in Figures 5-1 to 5-8.

Postform: Bulge forming of cylinders to the postform configuration was completed. Seven bulging operations were carried out. In the first operation, it was attempted to bulge the postform in one bulge and the strain capability of the material was exceeded resulting in rupture of the vessel. After this, the vessels were given a preliminary bulge, annealed, and then bulged to the configuration. Five vessels were bulged to the final shape. One vessel was used for welding development, the other four were given additional work with internal tools to completely define the ring geometry. Figures 5-9 and 5-10 show the more completely defined ring shape. Table 5-1 lists the fabrication procedures for each vessel.

Chem-milling of Postforms: Three of the four completely formed postforms were shipped to Aerochem Corporation Orange, California for chem-milling to final jacket thickness. Vidigaging of the minimum gage areas of jackets #2 and #6 showed thickness measurements of 0.0147 cm (0.0058 in.) to 0.0191 cm (0.0075 in.). The third jacket, #7, was below 0.0127 cm (0.005 in.) in several areas and accurate measurements of the final thickness could not be made. It is estimated that the wall thickness is 0.0076 cm (0.003 in.) to 0.010 cm (0.004 in.) in these areas. Figure 5-11 is a photo of a chem-milled jacket.

Ring Installation: The installation of center and end rings for the two vessels was completed. Vessels #2 and #6 were chosen for the test specimens. The rings were installed as described above. No shimming or adhesive was necessary. Figure 5-12 shows the rings installed in the tension membrane jacket.

Installation of Adapters and Instrumentation: The adapters for vacuum instrumentation and strain gage instrumentation were installed on vessels #2 and #6. Before that, eight strain gages (four internal and four external) were applied to vessel #6 and wired. The eight internal strain gage wires and two thermocouple leads were attached to the Deutsch connector before it was soldered to its adapter. On vessel #2, two thermocouple leads were wired to the Deutsch connector. Figure 5-13 shows the strain gage set up on vessel #6. Figures 5-14 and 5-15 show the external and internal gage placements, respectively.

Assemble Jacket to Dummy Line: Jacket #6 and Jacket #2 were welded to a dummy inner line. The two completed assemblies are shown in Figure 5-16.

Installation of Composite Inner Line: After completing their in-process decay rate testing the jackets were cut from the dummy inner lines. The jacket design provided additional length for this intermediate step in the jacket assembly. After cutting the jacket free from the dummy line, care was taken to trim and square the vessel edges as preparation for the final weld operation.

TABLE 5-1. - TENSION MEMBRANE VACUUM JACKET FABRICATION

Cylinder serial no.	Pressure 1st bulge, N/cm^2 (psi)	Pressure 2nd bulge, N/cm^2 (psi)	Comments
5	1034 (1500)	--	Failed at 1034 N/cm^2 (1500 psi) in the weld area
3	689 (1000)	--	Used for obtaining weld parameters
10	172* (250)	1551 (2250)	Used as back up for chem-milled cylinders (was not chem-milled)
7	152* (220)	1551 (2250)	Chem-milled to 0.0076 cm (0.003 in.) - 0.0102 cm (0.004 in.), back up for cylinders 2 and 6
2	152* (220)	1551 (2250)	Selected for test assembly, chem-milled to 0.0178 cm (0.007 in.)
9	152* (220)	965 (1400)	Failed at 965 N/cm^2 (1400 psi) in the weld area
6	152* (220)	1551 (2250)	Selected for test assembly, chem-milled to 0.0178 cm (0.007 in.)

*Annealed after first bulge 1255°K (1800°F)

Before welding the jacket to the line, the jacket was worked to provide a very close fit to the line. After the jackets were sized, the thermocouples on the inner lines were wired to the Deutsch connectors in the jackets.

Thermocouples were attached to the inner surface of the composite inner line to record liner temperatures during welding. The thermocouples were placed approximately one-half inch inward of the weld location at 1.57 rad (90 deg) intervals around the inner circumference. Temperatures measured during the welding operation are shown in Table 5-2. Maximum temperature recorded during the welding was 352°K (173°F).

Bonding of the aluminum channels that are used to locate the glass-fiber support straps at the ends of the vessel, was completed. Wrapping of the glass-fiber end straps was completed on May 8. No attempt was made to pre-tension the glass-fiber during the wrapping operation.

The two test specimens were delivered to the Martin Marietta Corporation, Denver, Colorado on May 15, 1973.

In-Process Testing. Vacuum testing was done in two phases: (1) the vacuum integrity of the tension membrane jacket was demonstrated on a dummy line; (2) the vacuum integrity of the tension membrane jacket assembled to the composite inner line was demonstrated.

A block diagram illustrating the vacuum testing of the tension menbrane jacket on the dummy inner line is shown in Figure 5-17. If the required vacuum level is reached, the system is closed off and the decay rate testing is begun. If the vacuum level is not reached, the jacket is checked for leaks. In this case, the vessel is divided into zones, one zone at a time is bagged and helium leak checked. When the leak is located, it is repaired and the zone is rechecked. This is continued until each zone of the vessel has been checked. Then the vessel is ready to proceed to the decay rate test. The vessel is evacuated and sealed. If the decay rate exceeds the required rate, the vessel is again helium leak checked zone by zone. The qualification test is completed when the jacket reaches the required decay rate.

When the jacket has completed the vacuum test on the dummy line, it is cut from the dummy line and trimmed. Then the jacket, in its final configuration, is assembled to the composite inner line.

TABLE 5-2. - TEMPERATURES RECORDED ON COMPOSITE LINE DURING WELDING OF TENSION MEMBRANE JACKET

Assembly no. 1	Temperature °K (°F)							
	End no. 1				End no. 2			
	Thermocouple				Thermocouple			
	1	2	3	4	1	2	3	4
Prior to weld	296 (74)	296 (74)	296 (74)	296 (74)	300 (80)	300 (80)	300 (80)	300 (80)
Heat up & weld	304 (87)	297 (75)	297 (75)	297 (75)	303 (85)	302 (84)	299 (78)	299 (78)
Heat up & weld	311 (100)	299 (79)	297 (75)	297 (75)	307 (93)	305 (89)	300 (80)	299 (79)
Heat up & weld	316 (110)	305 (89)	297 (75)	297 (75)	310 (99)	308 (95)	303 (86)	300 (80)
Heat up & weld	316 (110)	314 (105)	300 (80)	298 (76)	313 (103)	313 (104)	312 (102)	302 (84)
Heat up & weld	316 (110)	322 (120)	303 (85)	300 (80)	314 (105)	313 (103)	318 (113)	309 (97)
Heat up & weld	316 (110)	328 (130)	311 (100)	303 (85)	314 (105)	313 (104)	320 (116)	325 (125)
Heat up & weld	315 (108)	326 (127)	323 (121)	308 (95)	319 (115)	314 (105)	320 (117)	329 (133)
Heat up & weld	315 (107)	324 (124)	325 (125)	324 (124)	325 (125)	313 (104)	318 (113)	329 (133)
Heat up & weld	318 (113)	322 (120)	324 (123)	332 (138)				
Heat up & weld	320 (117)	321 (119)	323 (121)	336 (145)				
1 minute after weld	319 (114)	320 (116)	321 (119)	333 (140)	335 (143)	312 (102)	317 (111)	329 (132)
Distance from edge, cm (in.)	6.9 (2.7)	6.9 (2.7)	6.9 (2.7)	6.9 (2.7)	6.6 (2.6)	8.4 (3.3)	7.9 (3.1)	6.9 (2.7)

Assembly no. 2	End no. 1				End no. 2			
Prior to weld	296 (74)	296 (74)	296 (74)	296 (74)	301 (82)	300 (81)	301 (82)	301 (82)
Heat up & weld	316 (110)	296 (75)	297 (75)	297 (75)	300 (80)	300 (80)	300 (80)	315 (108)
Heat up & weld	322 (120	299 (78)	297 (75)	297 (75)	305 (90)	300 (80)	300 (80)	319 (108)
Heat up & weld	325 (125)	300 (80)	298 (75)	298 (76)	319 (115)	300 (80)	300 (81)	319 (115)
Heat up & weld	328 (130)	305 (90)	298 (76)	298 (76)	336 (145)	336 (145)	301 (82)	320 (117)
Heat up & weld	329 (132)	318 (112)	299 (78)	300 (80)	341 (155)	307 (93)	303 (85)	319 (115)
Heat up & weld	328 (130)	333 (140)	303 (85)	303 (85)	338 (148)	329 (132)	305 (90)	319 (114)
Heat up & weld	325 (125)	341 (154)	309 (97)	305 (90)	333 (140)	343 (157)	311 (100)	318 (113)
Heat up & weld	325 (125)	343 (158)	324 (123)	308 (95)	330 (135)	340 (153)	319 (115)	318 (112)
Heat up & weld	325 (125)	343 (158)	339 (150)	310 (98)	326 (127)	337 (147)	333 (140)	321 (119)
Heat up & weld	325 (125)	341 (154)	346 (163)	314 (105)				
Heat up & weld	325 (125)	336 (145)	349 (168)	327 (129)				
Heat up & weld	324 (124)	335 (143)	347 (165)	344 (160)				
Heat up & weld	331 (137)	331 (137)	344 (160)	351 (173)				
1 minute after weld	332 (138)	330 (135)	343 (158)	349 (169)	326 (127)	334 (142)	338 (148)	331 (137)
Distance from edge, cm (in.)	6.1 (2.4)	6.6 (2.6)	6.1 (2.4)	6.6 (2.6)	6.9 (2.7)	6.9 (2.7)	7.1 (2.8)	7.1 (2.8)

The procedure for qualifying the test specimen assembly is outlined in Figure 5-18. The procedure is similar to that used with the dummy line. In this case, however, only two zones of the jacket are checked, at the two attachment points to the inner line, since the jacket has been checked thoroughly in the preceding test. This test is completed when the jacket/line assembly demonstrates the required decay rate.

Back-to-back hoop and longitudinal strain gages are applied to the tension membrane jacket as shown in Figure 3-1. Photos of the strain gage installation are shown in Figure 5-13, 5-14, and 5-15. Gages are placed back-to-back to allow the analytical determination of the membrane stress.

Jacket installed on dummy inner line: The two vessels were transported to the hydrostatic test area where they were evacuated and cycled to demonstrate their structural integrity. Strain gage data is reported in Section 4. Photos of assembly #2 at 0 cm (in.) Hg, 254 mm (10 in.) Hg, 381 mm (15 in.) Hg, 508 mm (20 in.) Hg, 635 mm (25 in.) Hg, and 711 mm (28 in.) Hg are included as Figures 5-19 through 5-24. Assembly #1 was not instrumented. Figures 5-25 through 5-30 show assembly #1 at various vacuum pressures from 0 cm (in.) Hg to 711 mm (28 in.) Hg.

Assembly #1 (the noninstrumented vessel) was tested first for vacuum level and decay rate. A vacuum level of approximately 2×10^{-4} torr was achieved. The vessel was locked off at 3:25 pm on April 4, 1973. At 8:30 am on April 5 the vacuum pressure was approximately 2×10^{-4} torr so that there was no measureable pressure rise.

Assembly #2 was pumped down to approximately 1×10^{-4} torr by 2:30 pm on April 5. When examined at 8:00 am on April 6 the pressure was 35×10^{-3} torr. It was felt that outgassing from the internal strain gage instrumentation was the cause of the pressure. Vacuum pumping was resumed. At 8:30 am on April 9 with a vacuum pressure of 1×10^{-4} torr the vessel was locked off. At 8:30 am on April 10 the vacuum pressure was still approximately 1×10^{-4} or essentially no vacuum decay in 24 hours.

Jacket Installed on Composite Inner Line: To ensure the structural integrity of the final test assemblies, they were vacuum cycled in the hydrostatic test area. Strain gage data from assembly #2 is given in Section 4. Both specimens were given five cycles from atmospheric pressure to approximately 762 mm Hg (30 in. Hg) vacuum pressure on April 8.

A vacuum decay check was performed at this time in the event that a weld repair was necessary. Once the glass-fiber support at the end of the vessel is installed, there is no room to apply the chill bar that would be desired for welding.

After pumping for approximately four hours on April 19, the assembly #1 vessel was locked off. A rapid pressure rise was noted. The vessel was pumped overnight, locked off the following day, and again a rapid pressure rise was noted. Gas sources were introduced around the weld and fitting areas of the vessel, but no leaks were found. Pumping was resumed and continued over the weekend. The vessel was locked off Monday morning. By this time the vessel had been pumped for 90 hours, but again a rapid pressure rise was noted when the vessel was locked off. The rate of pressure rise was increased when warm air was circulated around the inner line's inner surface, indicating that the pressure rise is caused by outgassing.

To verify that the source of the pressure rise was outgassing and not leakage, the vessel was checked with a helium leak detector having a sensitivity of 1×10^{-10} scc/sec. All weld and fitting areas of the inner and outer lines were inspected and no leaks were found. Next, the outer jacket was bagged, the bag filled with helium and allowed to sit for 30 minutes. When the vacuum annulus was pumped, no helium indications were recorded. The same procedure was followed for the inner line and again no leak indications were noted. Due to the procedure followed and the sensitivity of the instrumentation used (1×10^{-10} scc/sec), we are quite confident that there are no leaks in the outer jacket or the inner line.

It was suggested that vacuum pumping with the vessel at elevated temperature would reduce the outgassing load. Accordingly, on April 24 the vessel was placed in a Thermotron chamber set for 394°K (250°F) and a roughing pump was attached to the evacuation port. During the night the tygon tube to the roughing pump split so that while the vessel received the desired temperature exposure, the length of time that a vacuum was applied is not known. The vessel was pumped down at room temperature but the decay rate was still high.

After pumping overnight, the leak checks were repeated. No leakage was indicated. Following the leak check, the vacuum decay rate was measured. The vessel was pumped to a vacuum of 38 microns and locked off at 11:15 am. At 3:15 pm a pressure of 360 microns was measured.

Due to the pressure rises noted when pumping is stopped, thought to be caused by outgassing of the resin of the composite overwrap of the inner line or of contaminants in the wrap material, the procedure outlined in Figure 5-18 was discontinued and assembly #2 was tested in a manner similar to that used for assembly #1.

On the first check, a small leak was noted in the weld at the Deutsch connector end of the vessel, approximately 3.14 rad (180°) from the connector location. After this leak was repaired, the vessel was bagged, helium leak checked, and no leaks were found.

Following the bonding of the glass-fiber and support straps, the vessels were given a final leak check before shipping. Figures 5-31 and 5-32 show assembly #2, with the glass-fiber support straps, under full vacuum before leak checking. Figure 5-33 shows the leak check test set up with the helium leak detector. Figure 5-34 shows an assembly bagged during the test. The leak rate measured in the test was 1.4×10^{-8} scc/sec on assembly #2.

Assembly #1, shown in Figure 5-35, was then tested using the same setup. The measured leak rate for assembly #1 was 3.6×10^{-7} scc/sec.

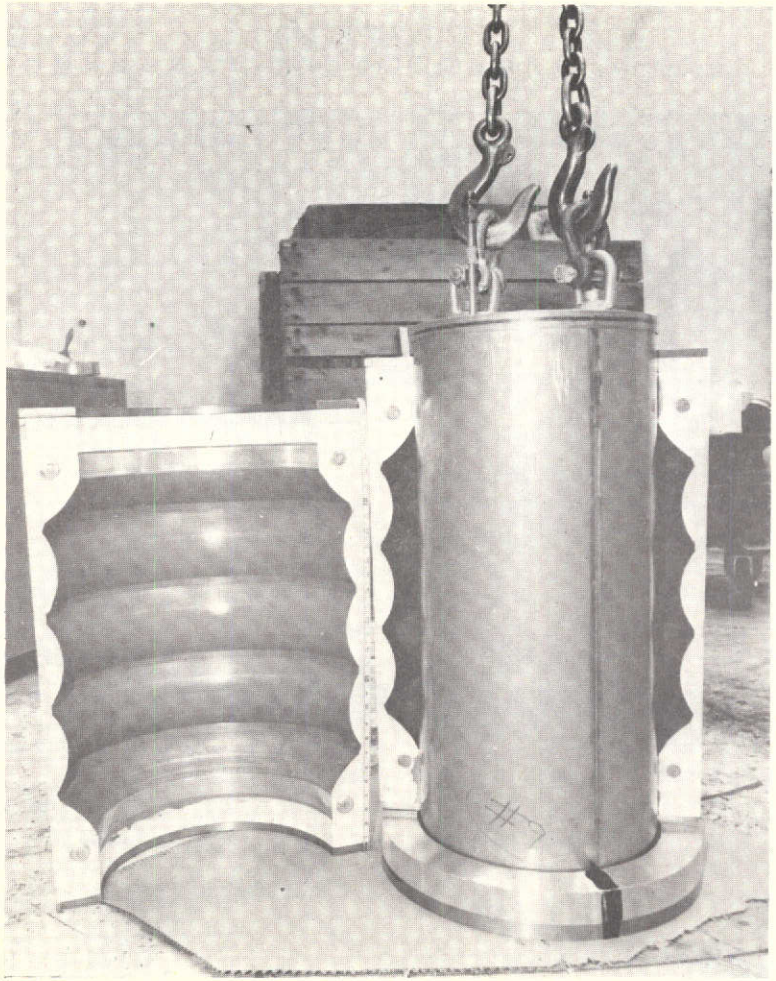

Figure 5-1. - Preform Cylinder and Partially Assembled Female Die

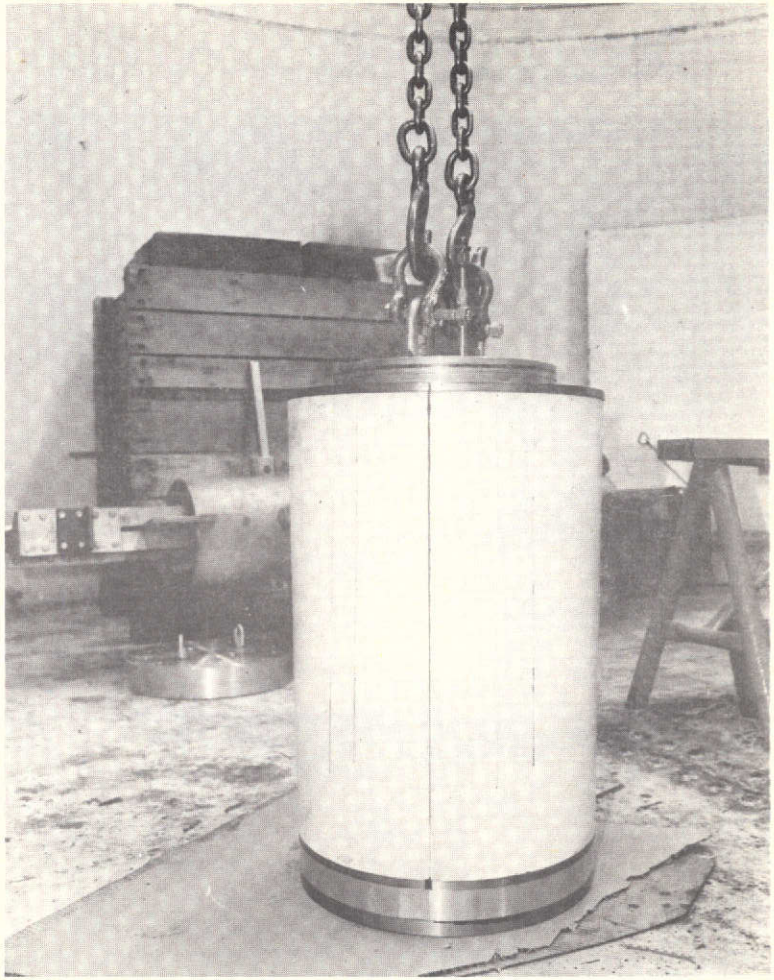

Figure 5-2. - Die Assembled Around Preform Cylinder

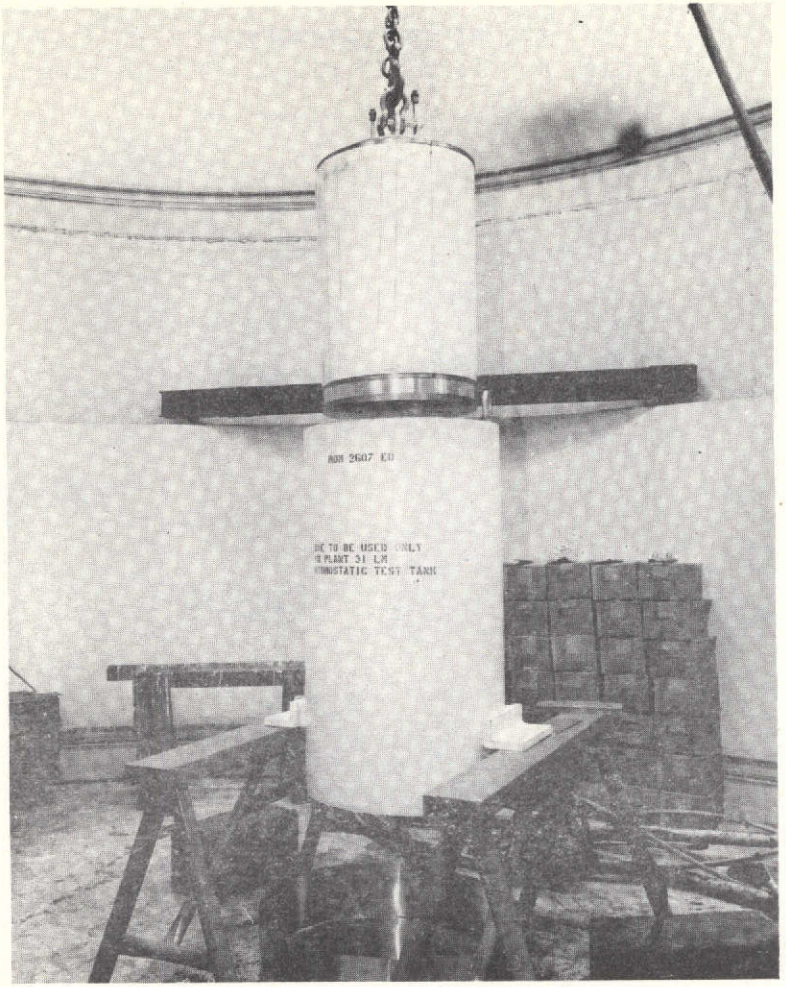

Figure 5-3. - Die Being Placed in Retaining Cylinder

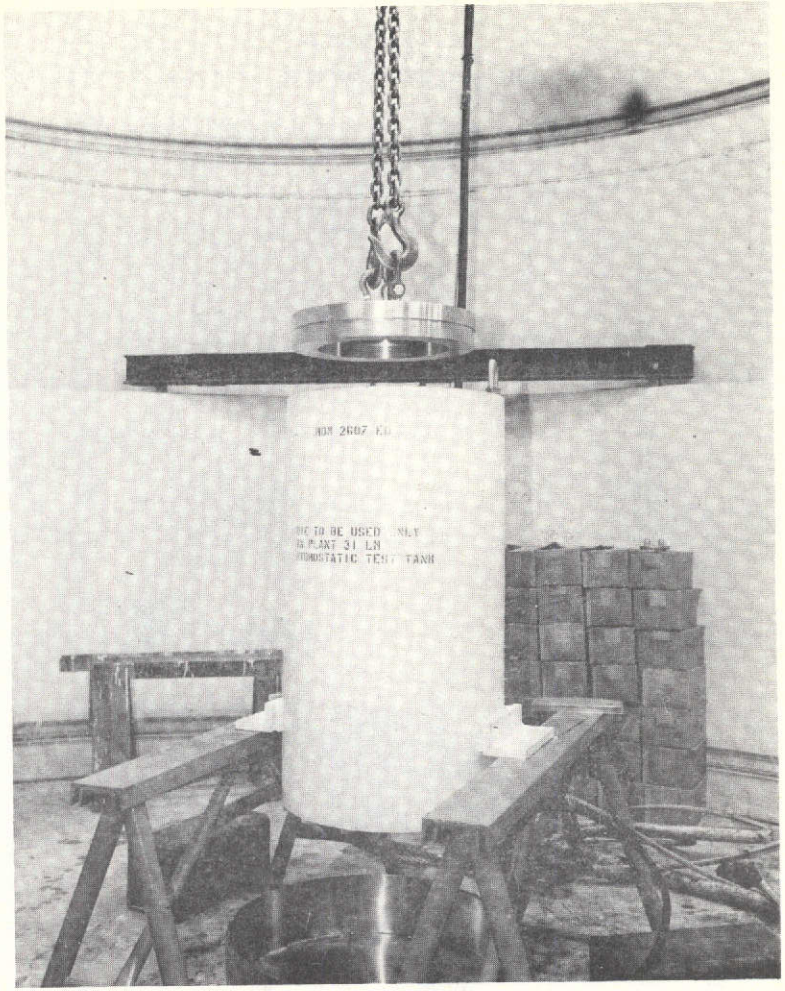

Figure 5-4. - Cover Plate Being Lowered into Place

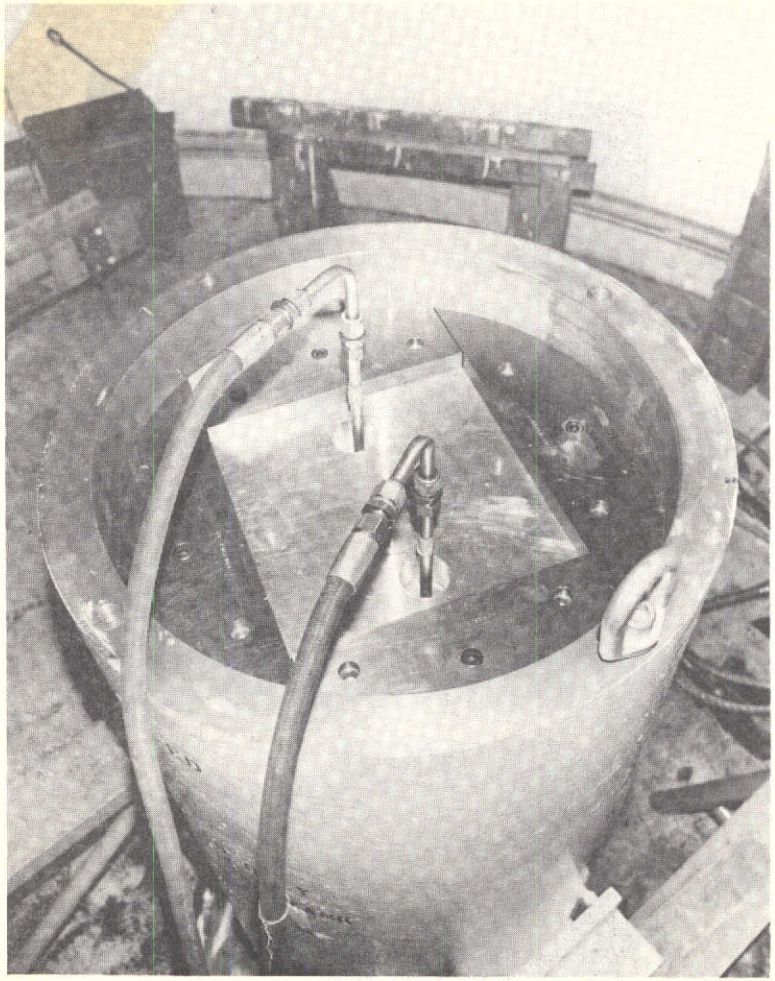

Figure 5-5. - Top View of Bulging Tool Showing Pressure Lines

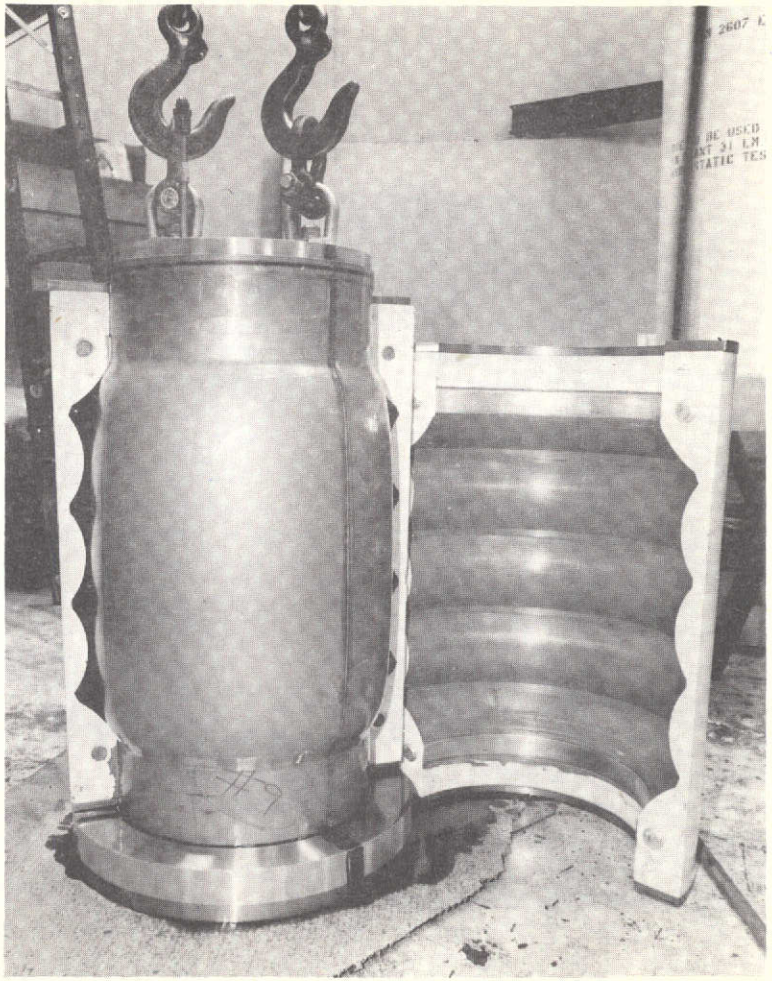

Figure 5-6. - Partially Bulged Preform (250 psi Internal Pressure)

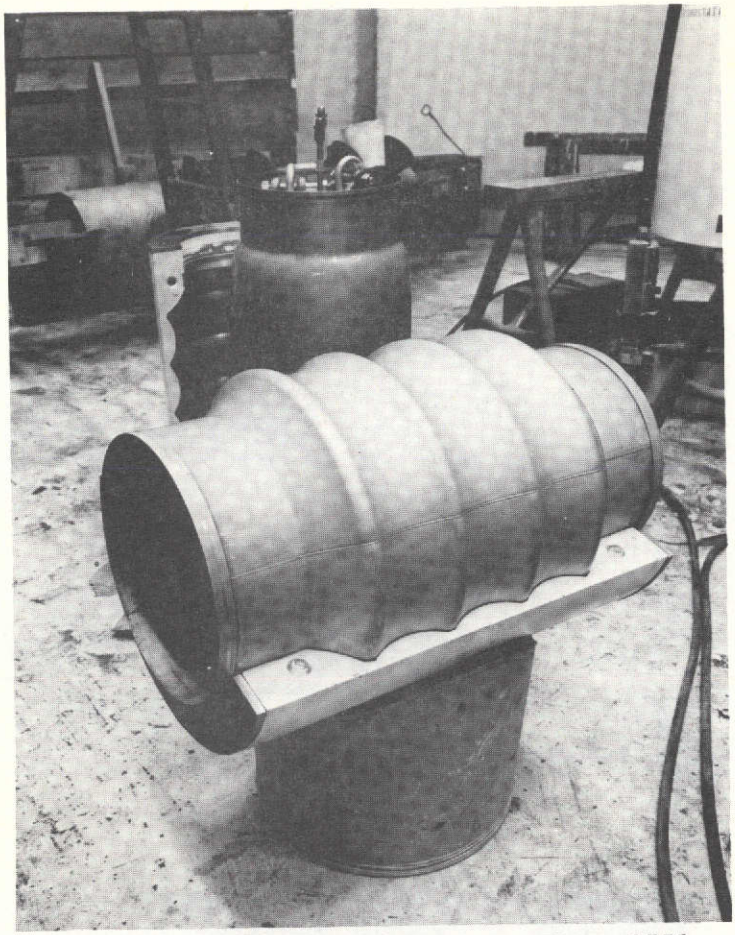

Figure 5-7. - Fully Bulged Postform 1551 N/cm^2 (2250 psi) Internal Pressure

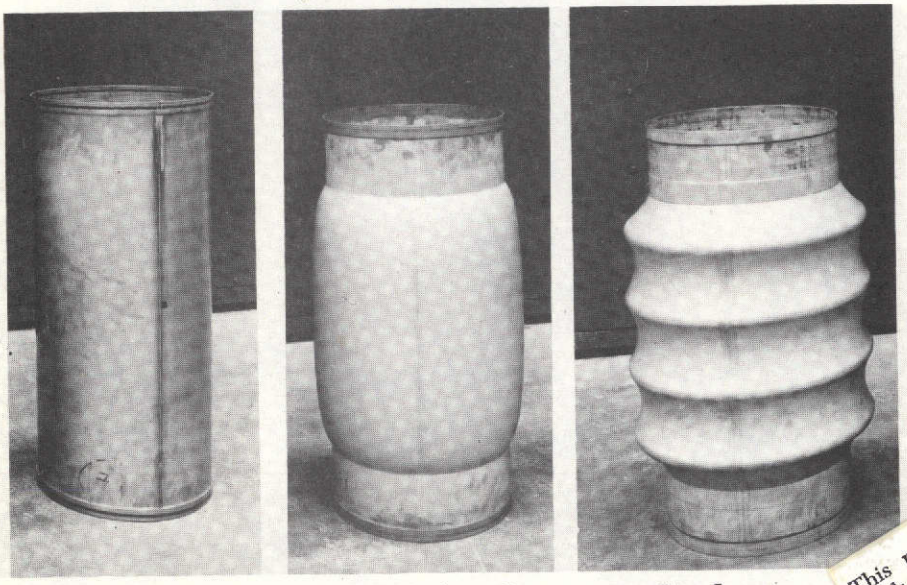

Figure 5-8. - Bulging Sequence, Preform to Postform (left to right)

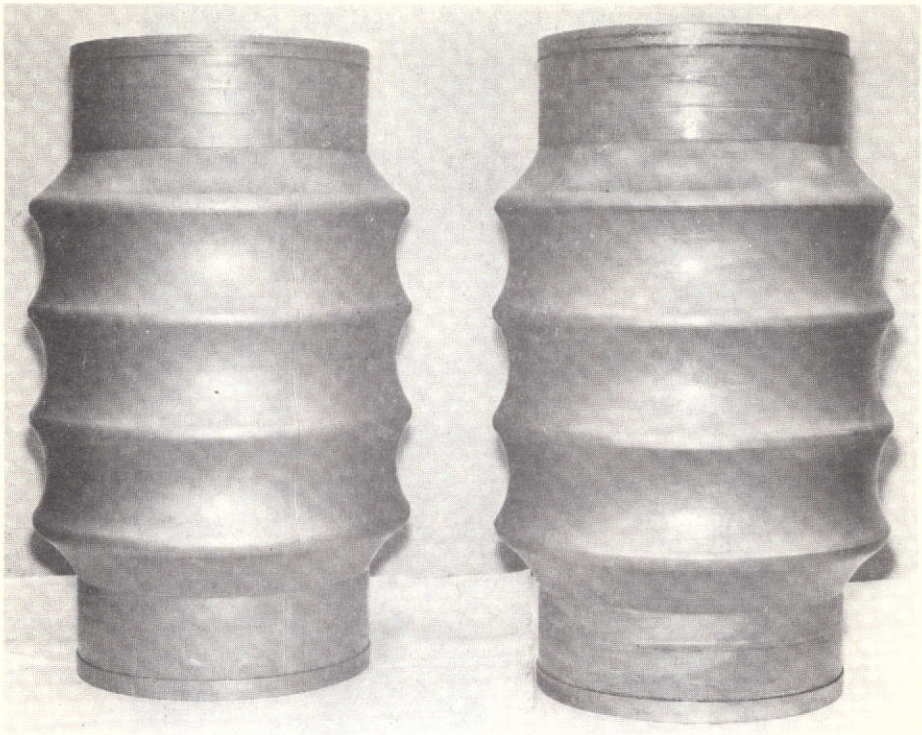

Figure 5-9. - Postform (Left) and Postform with Ring Cavity Sized Using Internal Tool (Right)

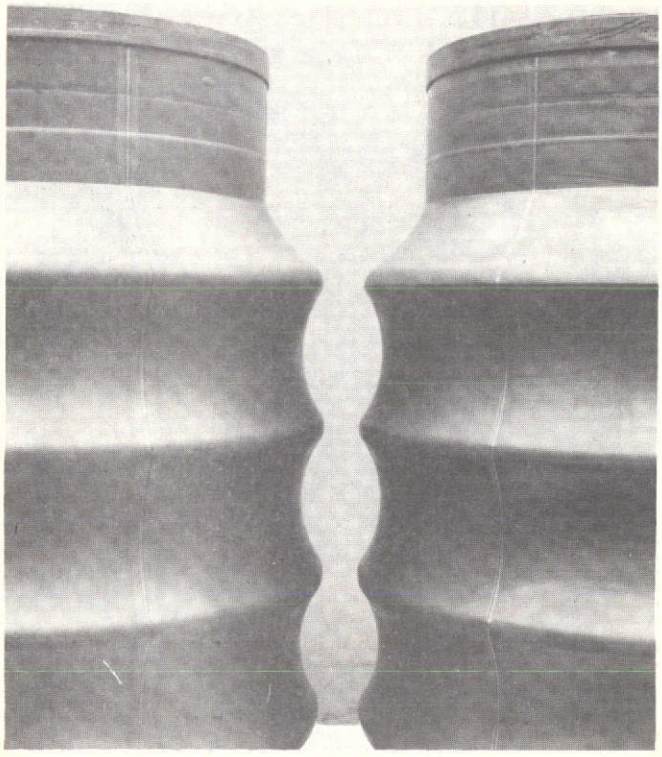

Figure 5-10. - Close Up of Sized (Right) and Unsized (Left) Postforms

This page is reproduced at the back of the report by a different reproduction method to provide better detail.

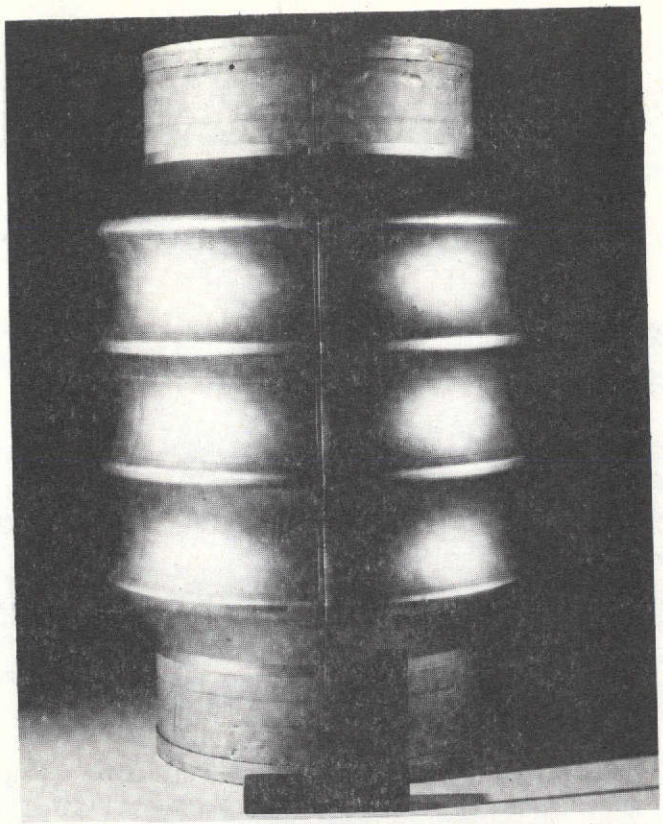

Figure 5-11. - Postform After Chem-Milling

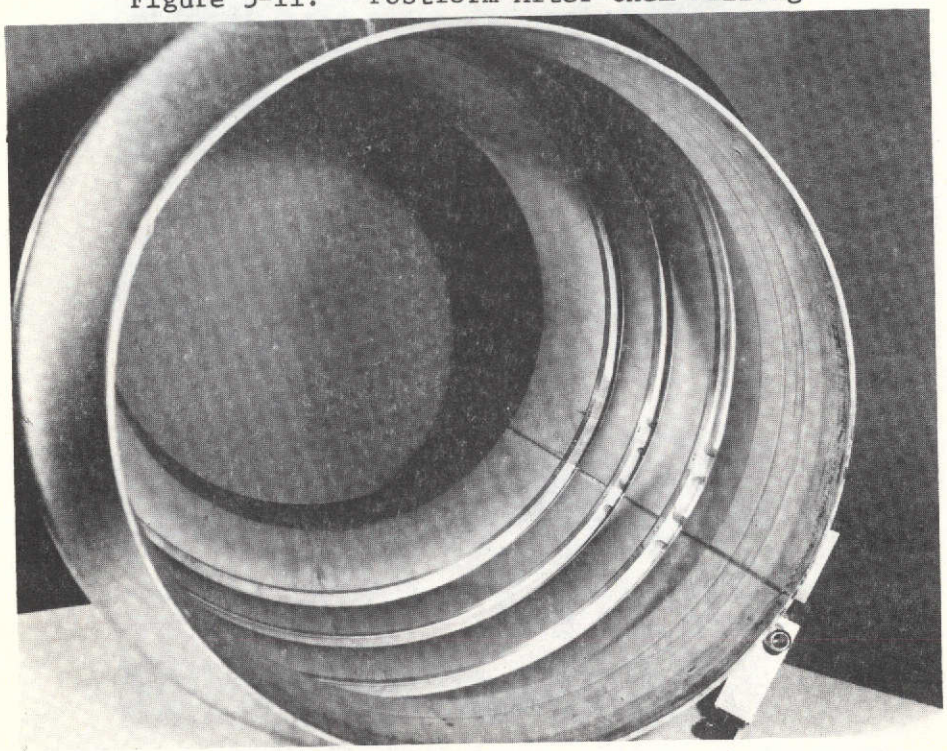

Figure 5-12. - Rings Installed in Tension Membrane Jacket

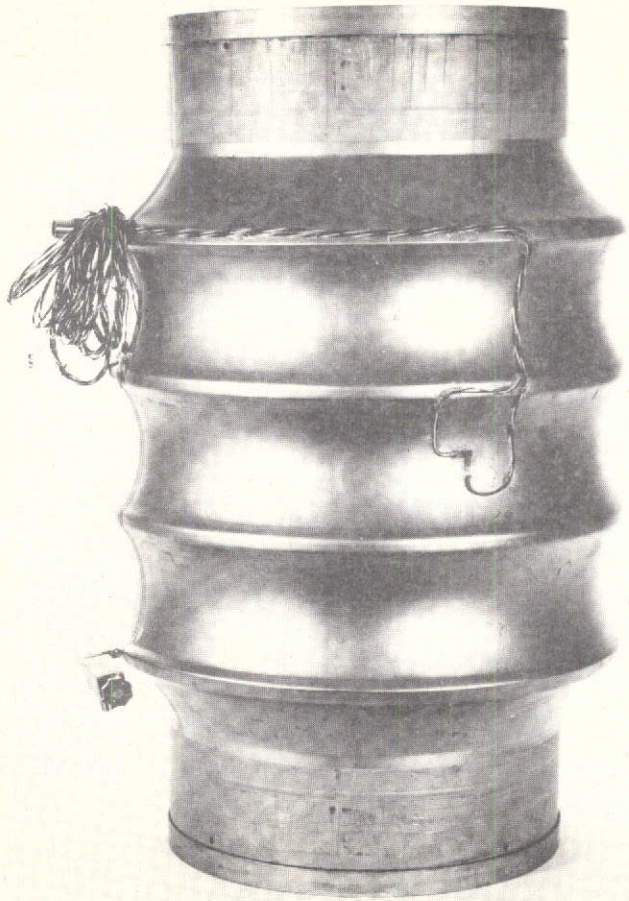

Figure 5-13. - Instrumented Tension Membrane Jacket

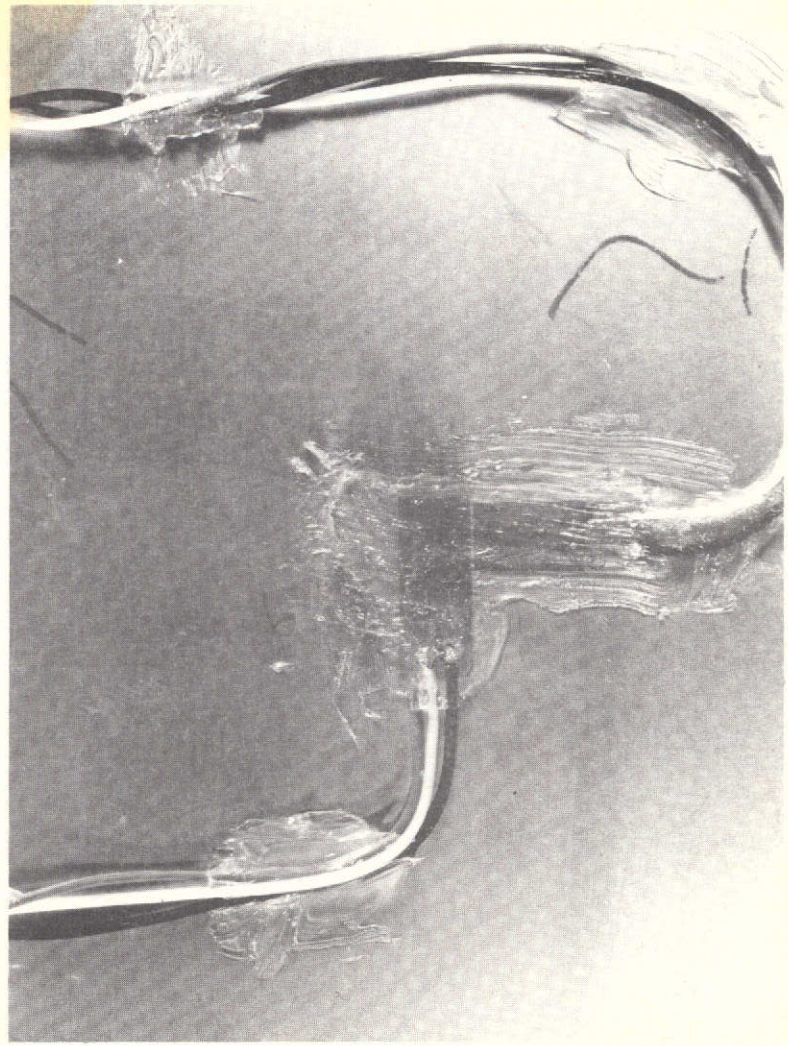

Figure 5-14. - External Strain Gage Location

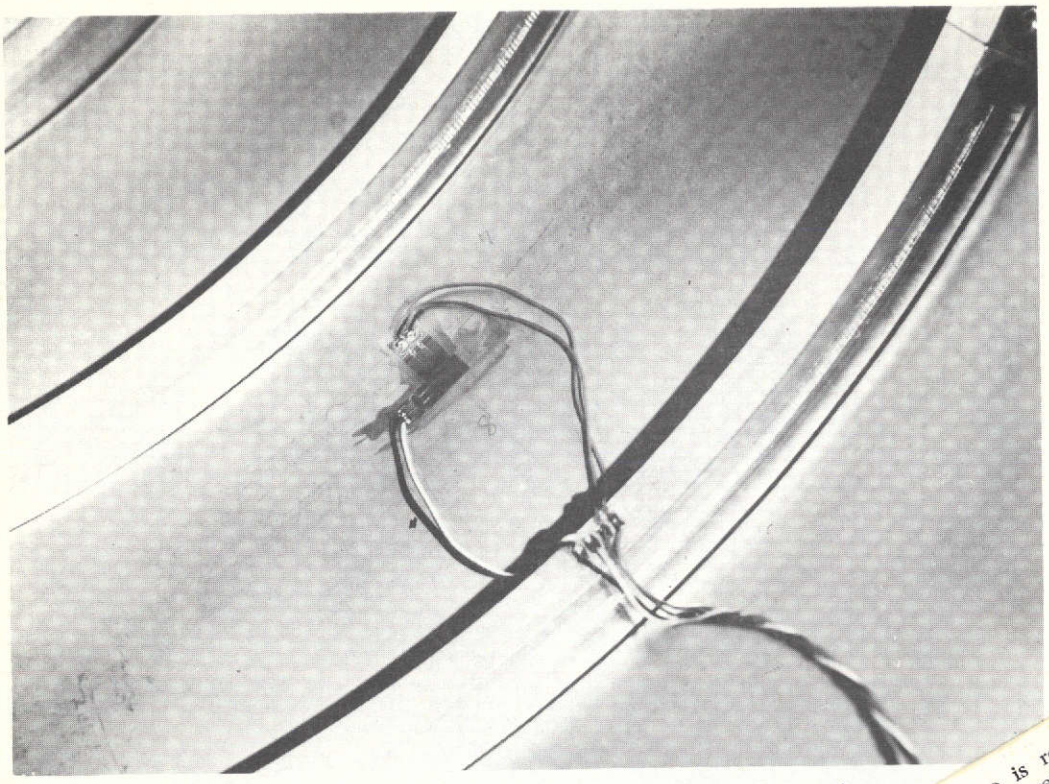

Figure 5-15. - Internal Strain Gage Location

Figure 5-16. - Tension Membrane Jackets Welded to Dummy Inner Lines

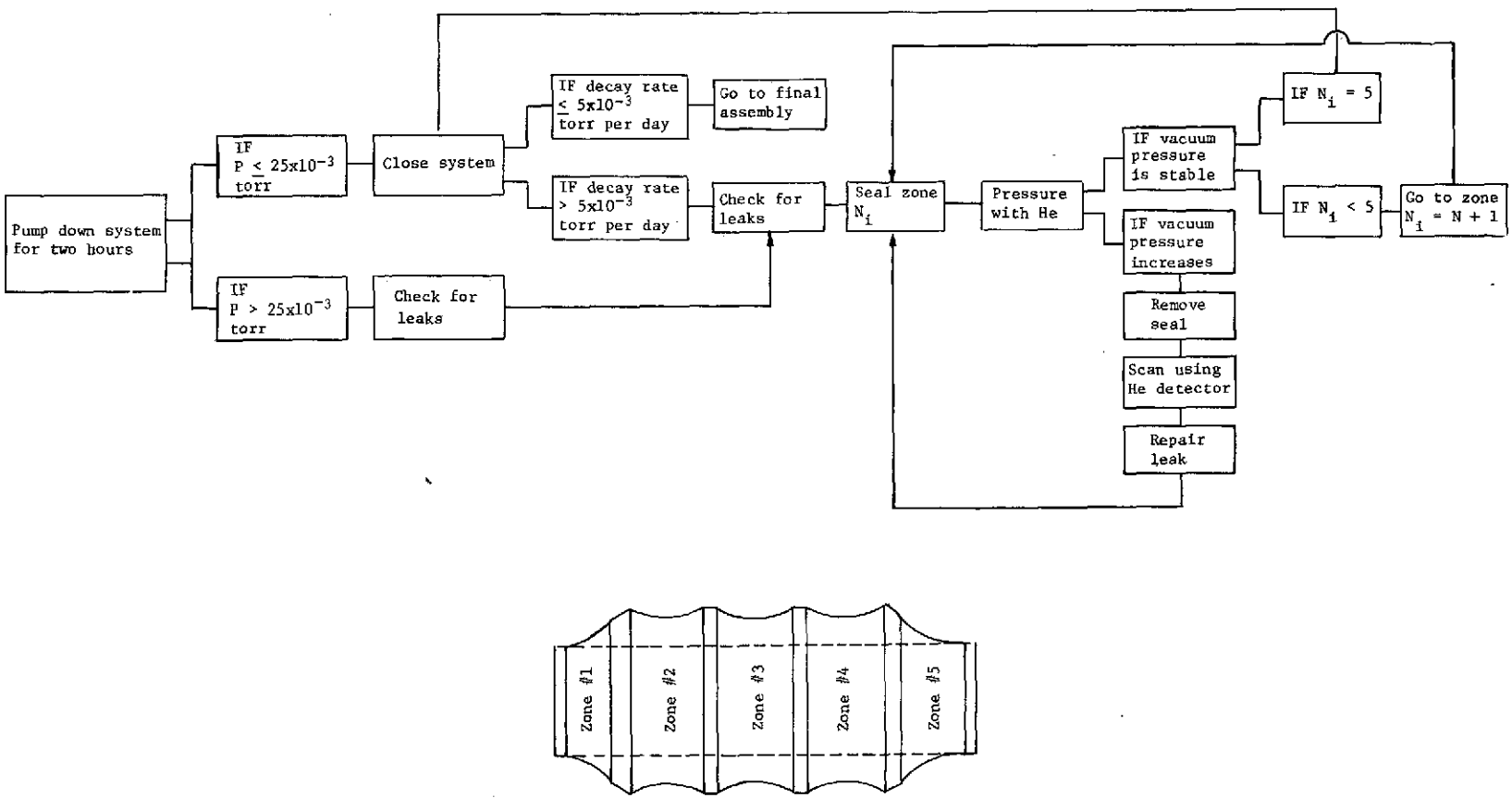

Figure 5-17. - Vacuum Qualification Test Tension Membrane Jacket

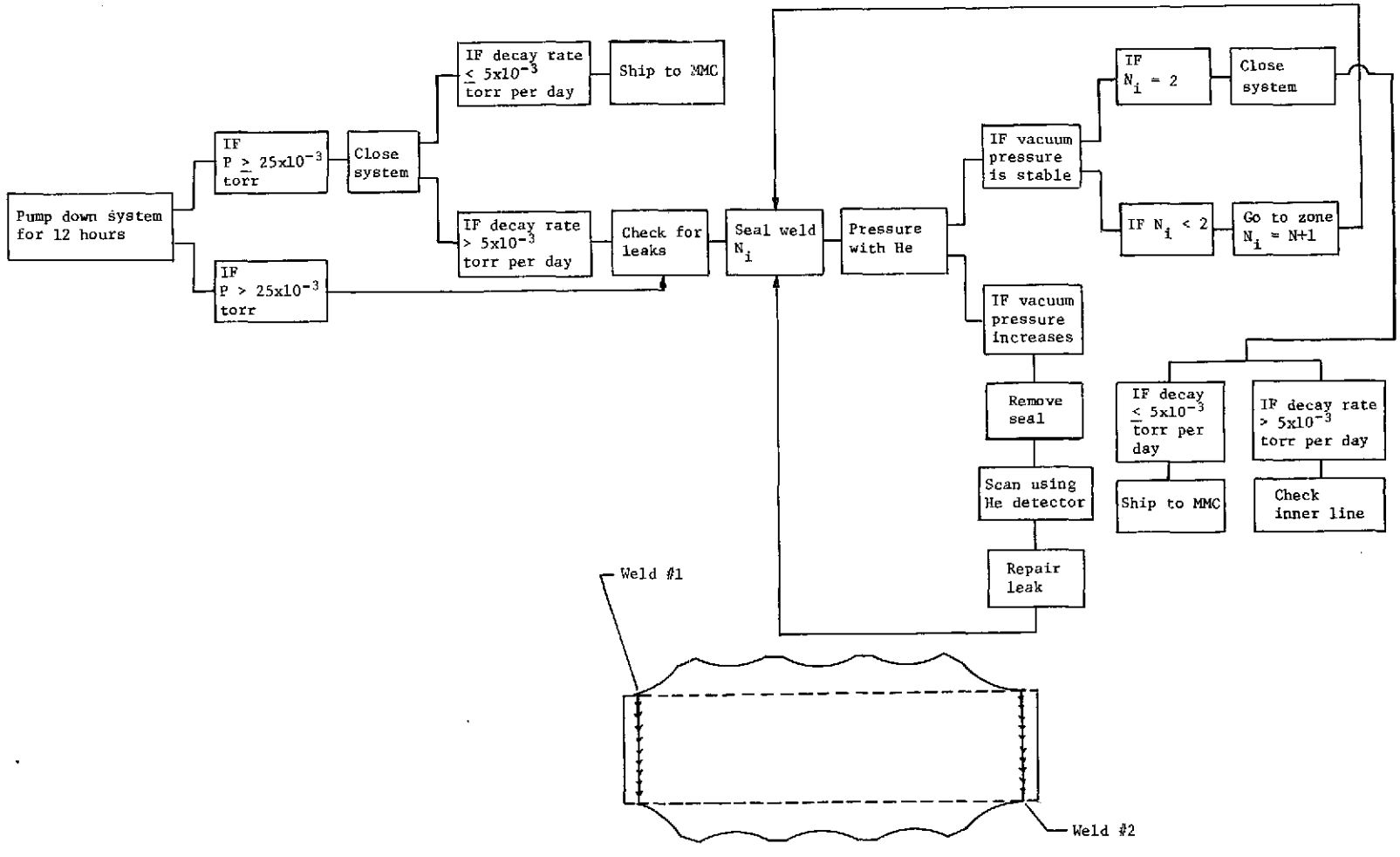

Figure 5-18. - Tension Membrane Jacket Composite Inner Line Assy Vacuum Qualification Test

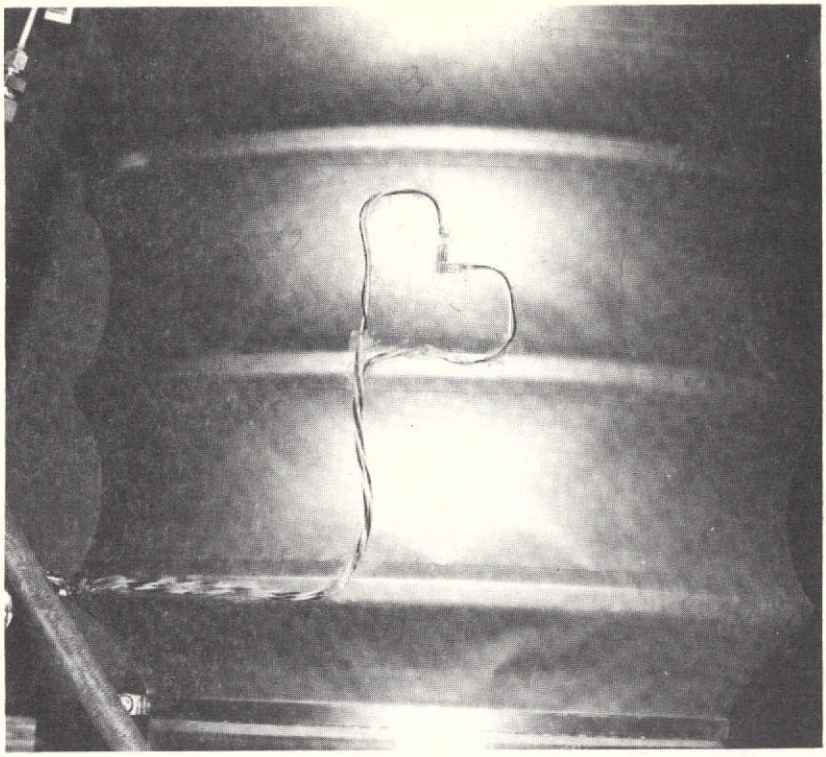

Figure 5-19. - Assembly #2, Zero Vacuum Pressure

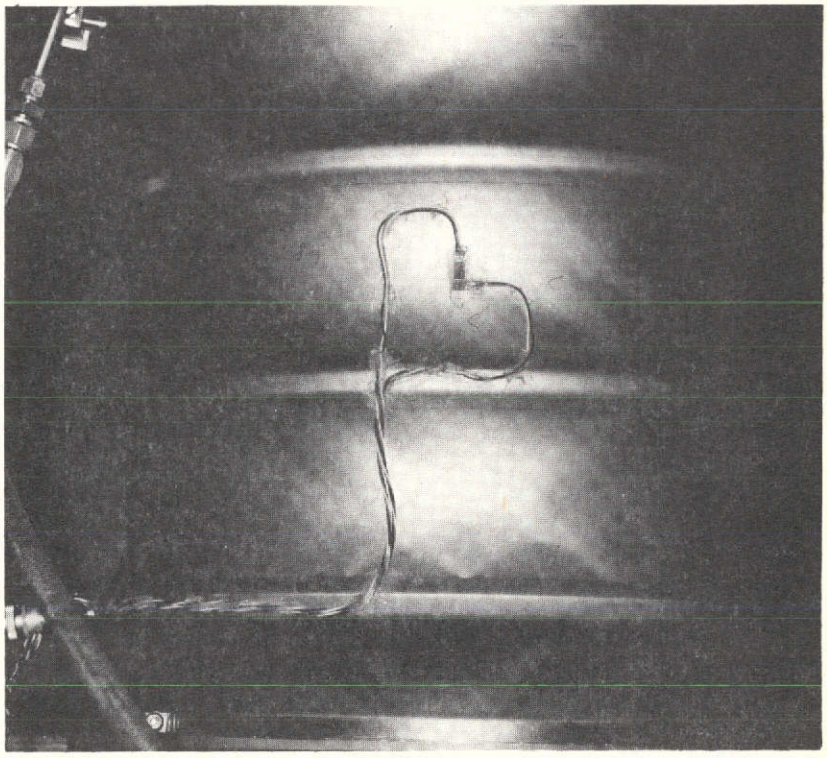

Figure 5-20. - Assembly #2, 254 mm (10 in.) Hg Vacuum Pressure

This page is reproduced at the back of the report by a different reproduction method to provide better detail.

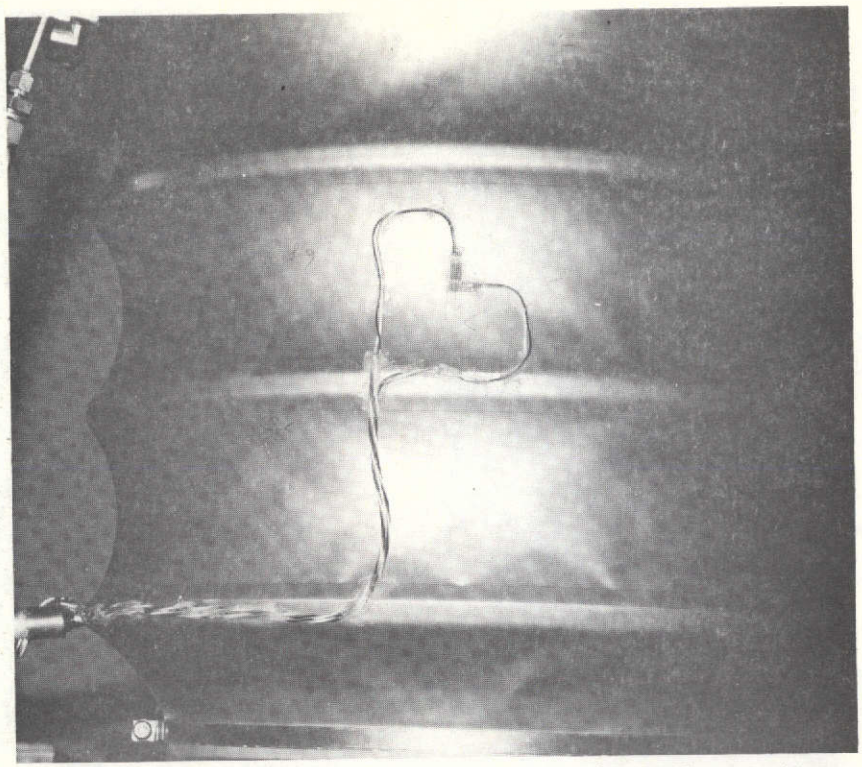

Figure 5-21. - Assembly #2, 381 mm (15 in.) Hg Vacuum Pressure

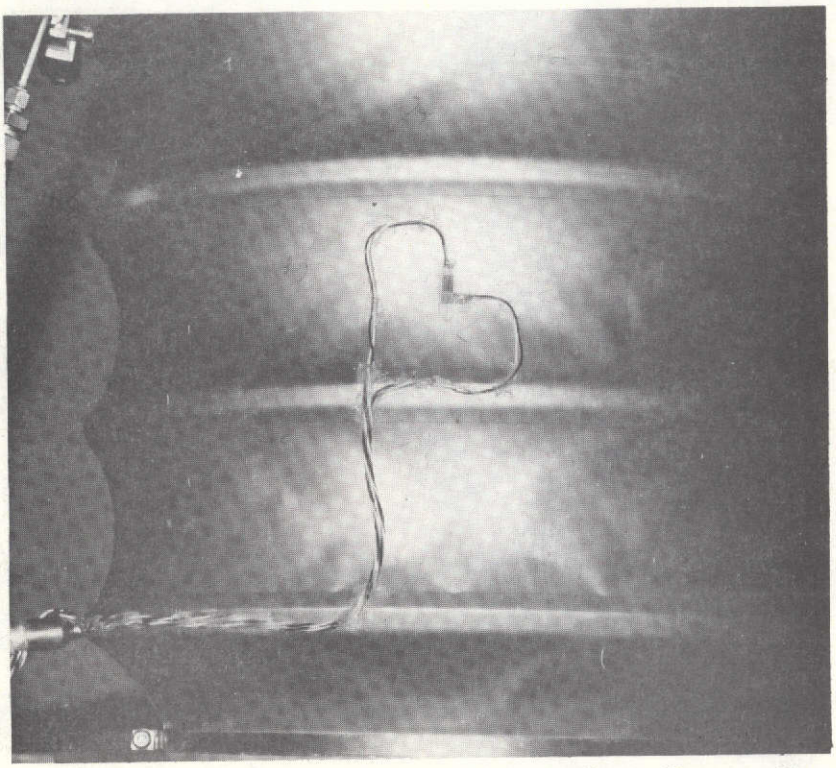

Figure 5-22. - Assembly #2, 508 mm (20 in.) Hg Vacuum Pressure

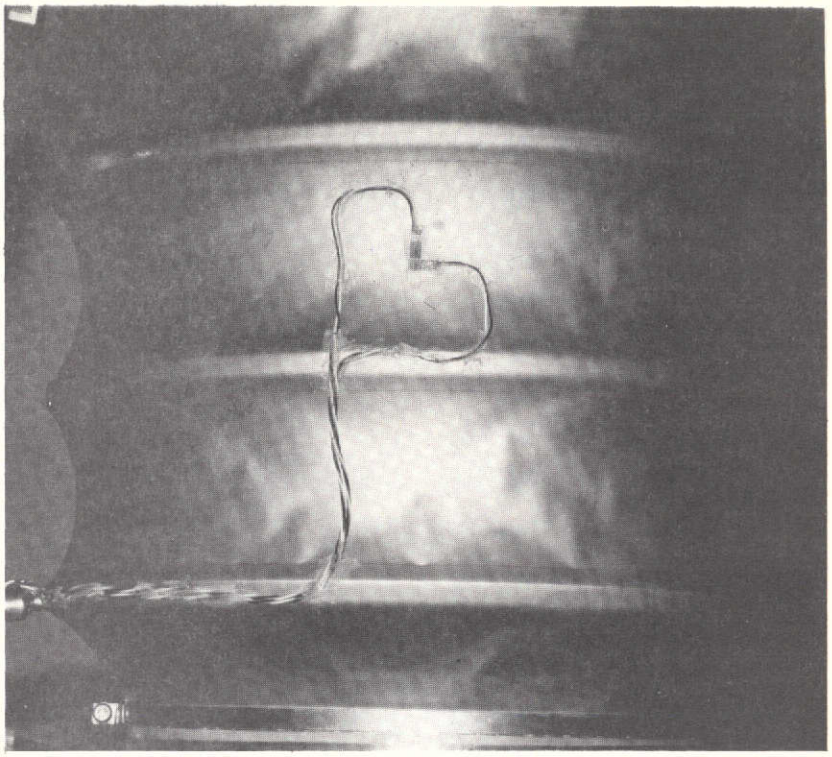

Figure 5-23. - Assembly #2, 635 mm (25 in.) Hg Vacuum Pressure

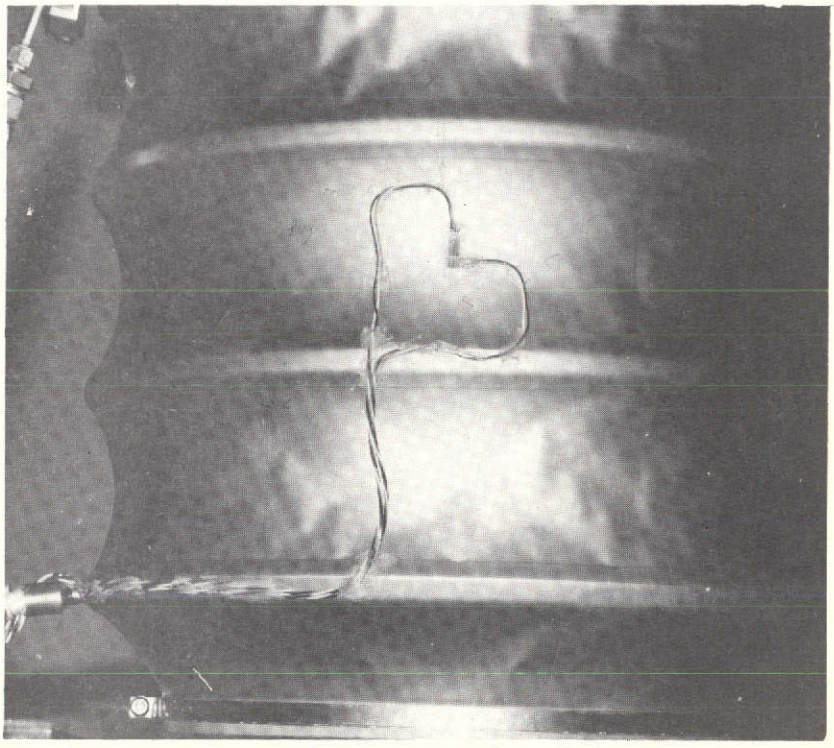

Figure 5-24. - Assembly #2, 711 mm (28 in.) Hg Vacuum Pressure

This page is reproduced at the back of the report by a different reproduction method to provide better detail.

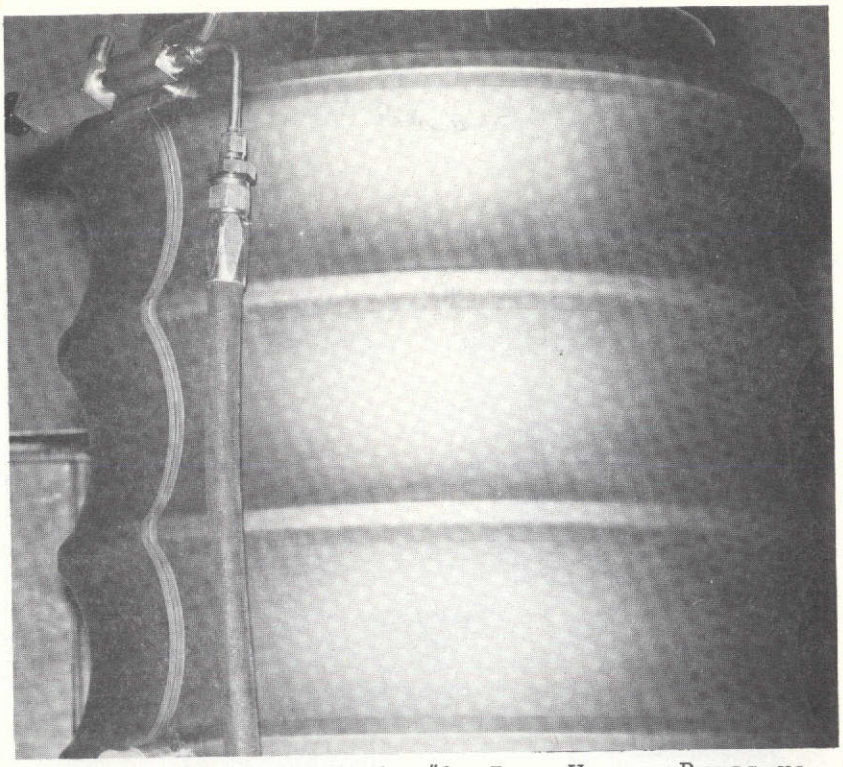

Figure 5-25. - Assembly #1, Zero Vacuum Pressure

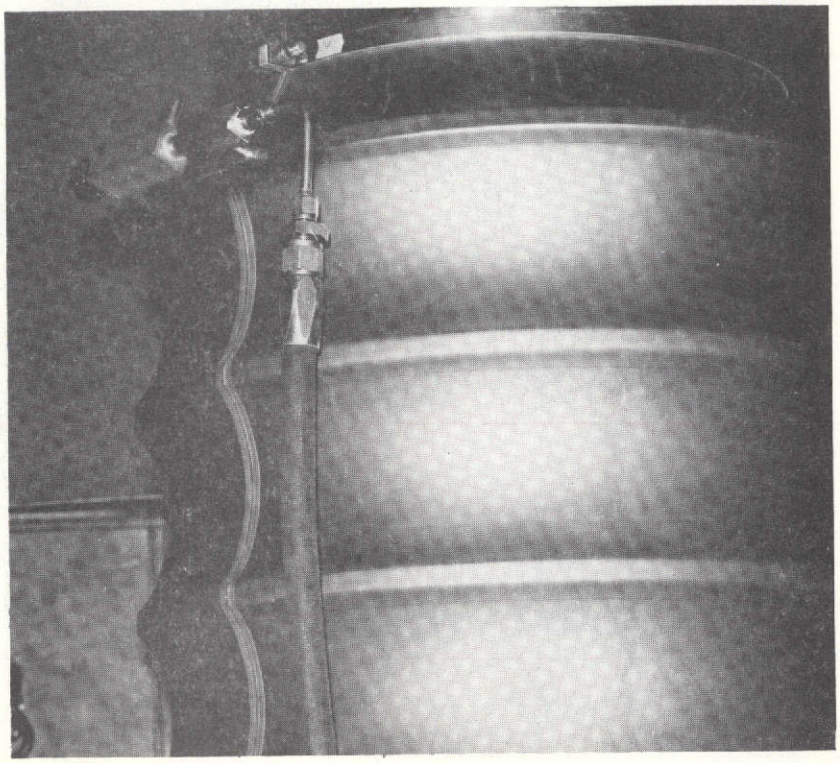

Figure 5-26. - Assembly #1, 254 mm (10 in.) Hg Vacuum Pressure

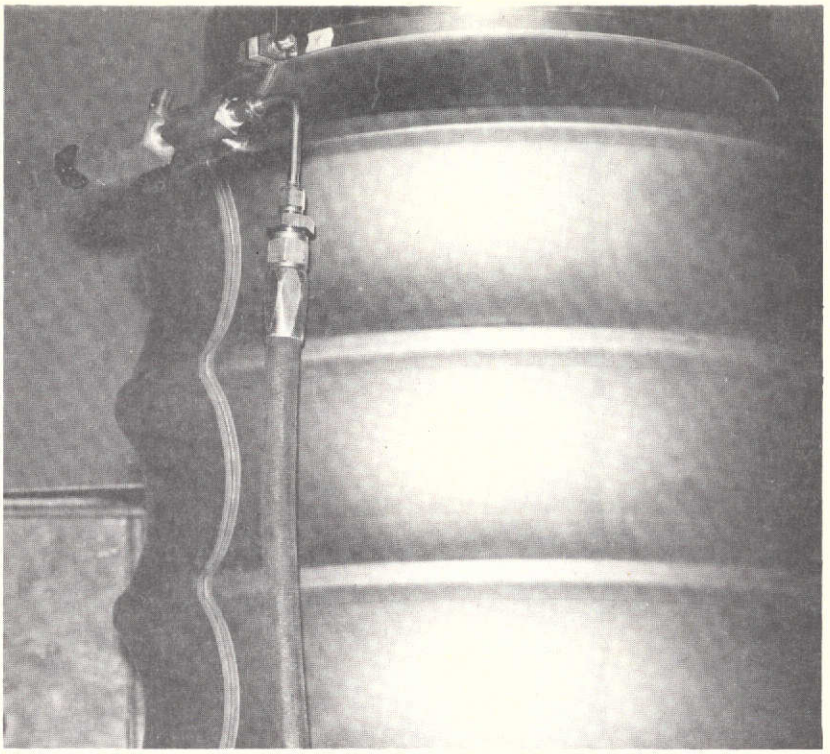

Figure 5-27. - Assembly #1, 381 mm (15 in.) Hg Vacuum Pressure

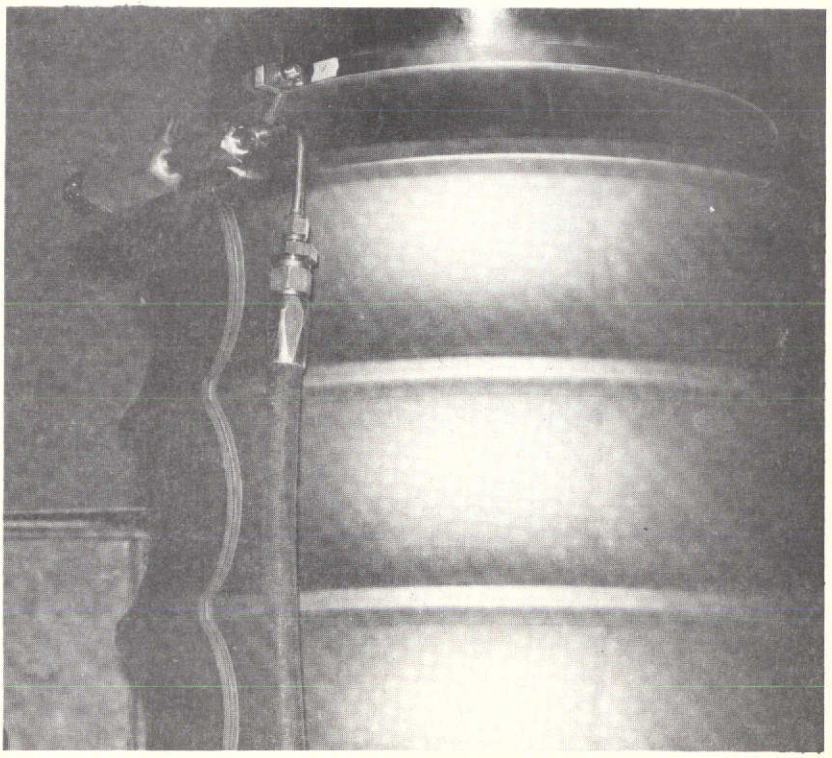

Figure 5-28. - Assembly #1, 508 mm (20 in.) Hg Vacuum Pressure

This page is reproduced at the back of the report by a different reproduction method to provide better detail.

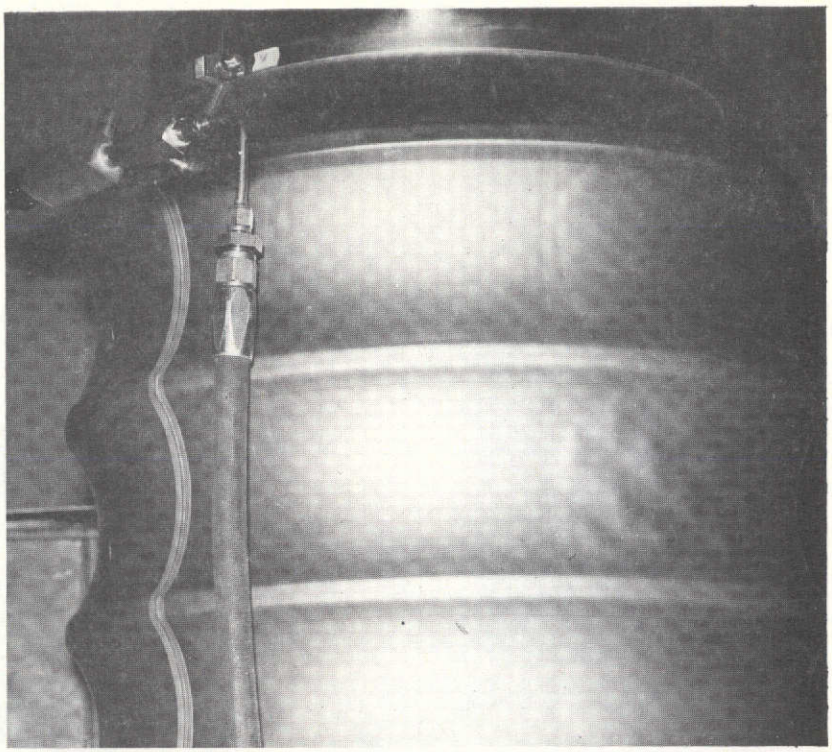

Figure 5-29. - Assembly #1, 635 mm (25 in.) Hg Vacuum Pressure

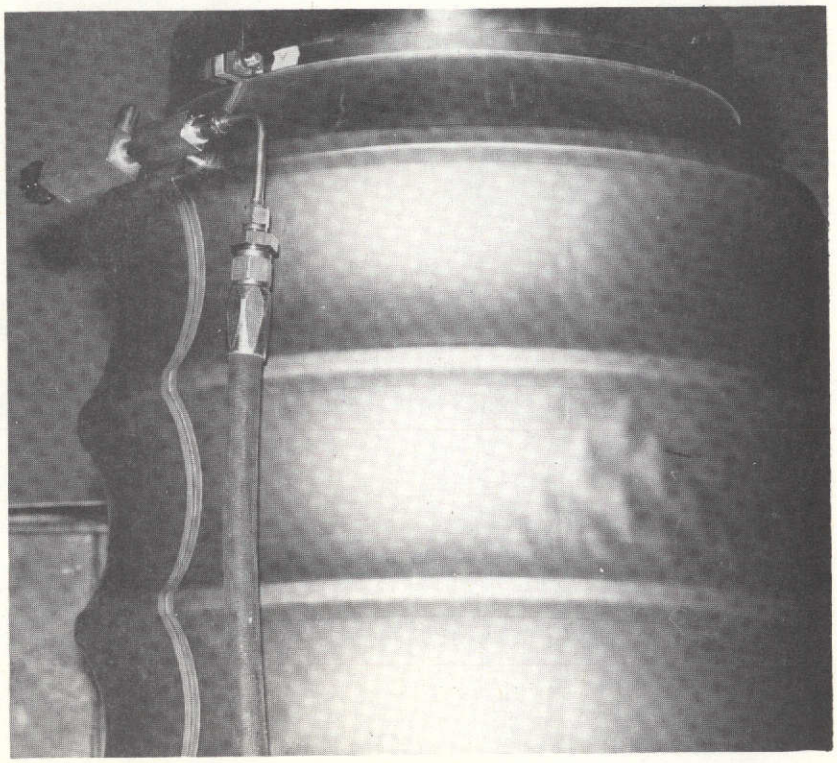

Figure 5-30. - Assembly #1, 711 mm (28 in.) Hg Vacuum Pressure

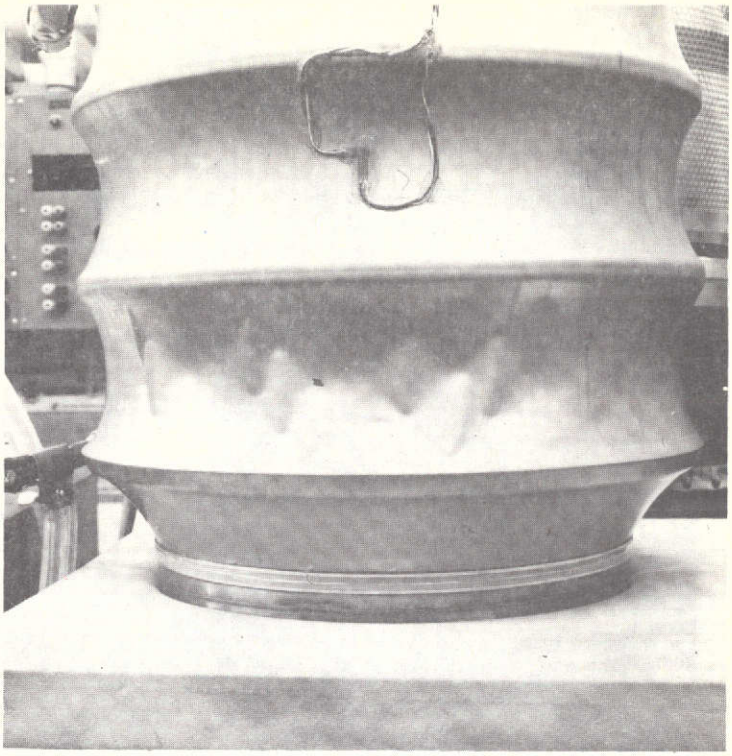

Figure 5-31. - Assembly #2, Final Configuration, Under Vacuum

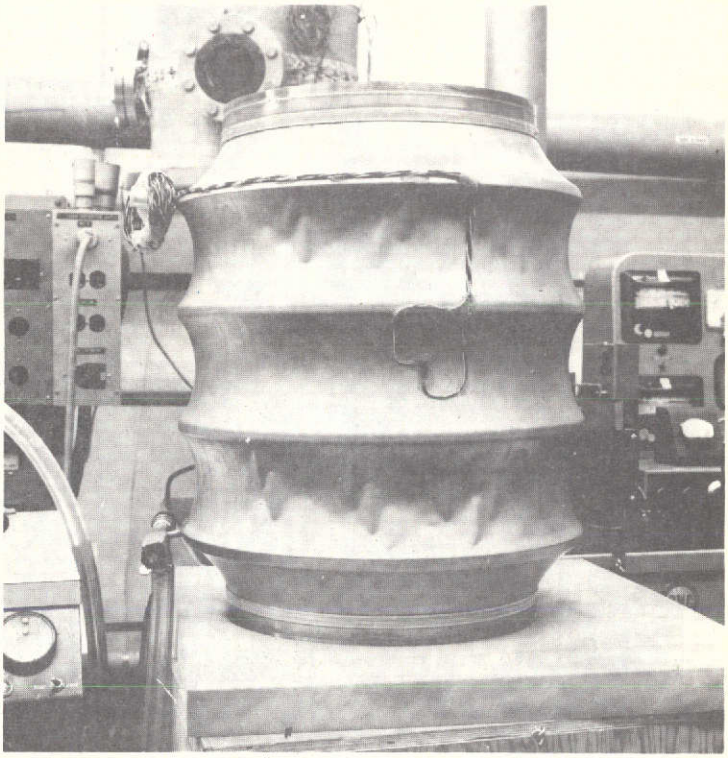

Figure 5-32. - Assembly #2, Under Full Vacuum before Leak Check

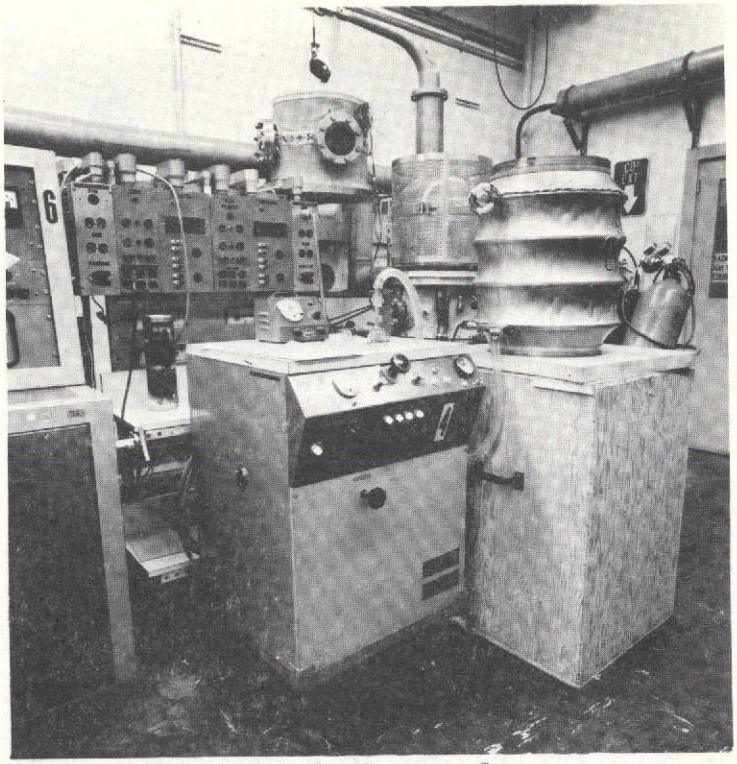

Figure 5-33. - Leak Check Test Setup

Figure 5-34. - Assembly, Bagged for Helium Leak Check

This page is reproduced at the back of the report by a different reproduction method to provide better detail.

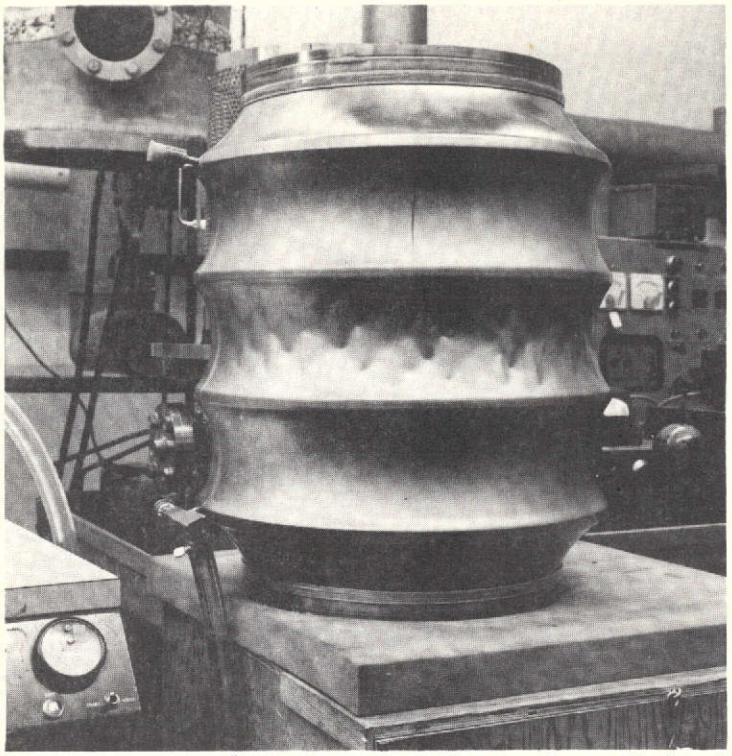

Figure 5-35. - Assembly #1, Final Configuration, Under Full Vacuum